Glasnik hemičara i tehnologa Bosne i Hercegovine
Bulletin of the Chemists and Technologists of Bosnia and Herzegovina

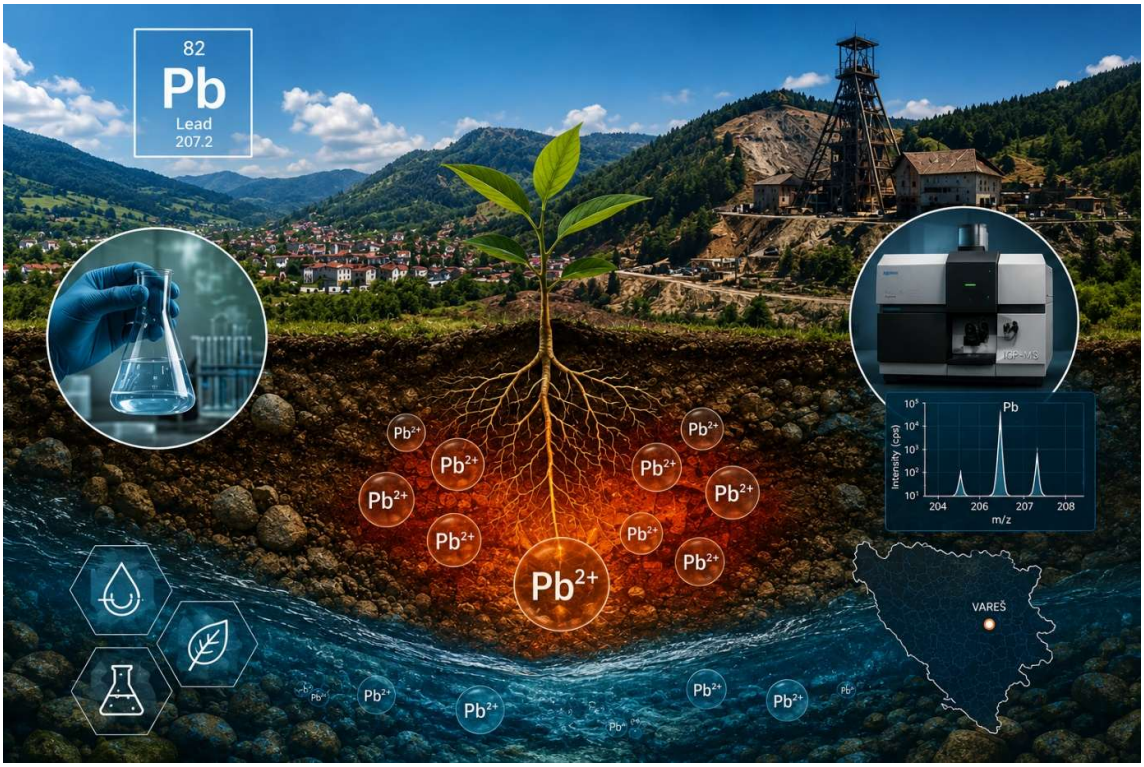

66

June 2026.

Univerzitet u Sarajevu - Prirodno-matematički fakultet, Sarajevo
University of Sarajevo - Faculty of Science, Sarajevo

Glasnik hemičara i tehnologa Bosne i Hercegovine
Bulletin of the Chemists and Technologists of Bosnia and Herzegovina

66

June 2026.

Univerzitet u Sarajevu - Prirodno-matematički fakultet, Sarajevo
University of Sarajevo - Faculty of Science, Sarajevo

Glasnik hemičara i tehnologa Bosne i Hercegovine

Print ISSN: 0367-4444
Online ISSN: 2232-7266

Bulletin of the Chemists and Technologists of Bosnia and Herzegovina

Zmaja od Bosne 33-35, BA-Sarajevo
Bosnia and Herzegovina
Phone: +387-33-279-918
Fax: +387-33-649-359
E-mail: glasnik@pmf.unsa.ba
glasnikhtbh@gmail.com

EDITORIAL BOARD

Faculty of Science Sarajevo
Zmaja od Bosne 33-35, BA-Sarajevo
Bosnia and Herzegovina
Phone: +387-33-279-904 (Administration)
+387-33-279-911 (Executive Editors)
Fax: +387-33-649-359

E-mail: glasnik@pmf.unsa.ba
glasnikhtbh@gmail.com

Dejan Milošević
Department of Physics, Faculty of Science, University of Sarajevo, Sarajevo, Bosnia and Herzegovina
Željko Jaćimović
Department of Chemical Technology, Faculty of Meallurgy and Technology, University of Montenegro, Podgorica, Montenegro
Ljudmila Benedik
Department of Environmental Sciences, "Jožef Stefan" Institute, Ljubljana, Slovenia
Meliha Zejnilagić-Hajrić
Department of Chemistry, Faculty of Science, University of Sarajevo, Sarajevo, Bosnia and Herzegovina
Tidža Muhić-Šarac
Department of Chemistry, Faculty of Science, University of Sarajevo, Sarajevo, Bosnia and Herzegovina
Sabina Gojak-Salimović
Department of Chemistry, Faculty of Science, University of Sarajevo, Sarajevo, Bosnia and Herzegovina
Ismet Tahirović
Department of Chemistry, Faculty of Science, University of Sarajevo, Sarajevo, Bosnia and Herzegovina
Danijela Vidic
Department of Chemistry, Faculty of Science, University of Sarajevo, Sarajevo, Bosnia and Herzegovina
Mustafa Memić
Department of Chemistry, Faculty of Science, University of Sarajevo, Sarajevo, Bosnia and Herzegovina
Andrea Gambaro
Department of Environmental Sciences, Informatics and Statistics, University Ca' Foscari of Venice, Venice, Italy
Institute for the Dynamics of Environmental Processes - National Research Council (CNR-IDPA), Venice, Italy
Dragana Đorđević
Centre of Chemistry - IChTM, University of Belgrade, Belgrade, Serbia
Aida Šapčanin
Department of Natural Sciences in Pharmacy, Faculty of Pharmacy, University of Sarajevo, Sarajevo, Bosnia and Herzegovina
Jože Kotnik
Department of Environmental Sciences, "Jožef Stefan" Institute, Ljubljana, Slovenia
Lucyna Samek
AGH University of Science and Technology, Faculty of Physics and Applied Computer Science, Krakow, Poland
Angela Maria Stortini
Department of Molecular Sciences and Nanosystems, University Ca' Foscari of Venice, Venice, Italy
Ivan Spanik
Institute of Analytical Chemistry, Slovak University of Technology, Bratislava, Slovakia
Mirjana Vojinović Miloradov
Department of Environmental Engineering, Faculty of Technical Sciences, University of Novi Sad, Novi Sad, Serbia
Heike Bradl
Department of Environmental Engineering, University of Applied Sciences Trier, Birkenfeld, Germany
Lea Kukoč-Modun
Department of Analytical Chemistry, Faculty of Chemistry and Technology, University of Split, Split, Croatia
Sanja Ćavar Zeljković
Centre of the Region Haná for Biotechnological and Agricultural Research, Department of Genetic Resources for Vegetables, Medicinal and Special Plants, Crop Research Institute, Šlechtitelů 29, Olomouc, Czech Republic
Centre of Region Haná for Biotechnological and Agricultural Research, Czech Advanced Technology and Research Institute, Palacky University, Šlechtitelů 27, Olomouc, Czech Republic
Igor Jerković
Department of Organic Chemisty, Faculty of Chemistry and Technology, University of Split, Split,Croatia
Roderick W. Bates
Division of Chemistry and Biological Chemistry, School of Physical and Mathematical Sciences, Nanyang Technlogical University, Singapore, Singapore
Safija Herenda
Department of Chemistry, Faculty of Science, University of Sarajevo, Sarajevo, Bosnia and Herzegovina
Muna Abu-Dalo
Department of Chemistry, Jordan University of Science and Technology, Irbid, Jordan

The journal is published semiannual, and full text version of the papers published are available free of cost at http://www.pmf.unsa.ba/hemija/glasnik.

Bulletin of the Chemists and Technologists has been licensed for indexing in:

Emerging Sources Citation Index (Web of Science, Clarivate Analytics)

CAPlus (Chemical Abstracts Plus):

Academic Search Complete (EBSCO)

Glasnik hemičara i tehnologa Bosne i Hercegovine

Bulletin of the Chemists and Technologists of Bosnia and Herzegovina

Print ISSN: 0367-4444
Online ISSN: 2232-7266

2026
Issue 66

CONTENT

Editorial I

ORIGINAL SCIENTIFIC ARTICLES

Levels of Selected Persistent Organic Pollutants in Human Milk Samples from Bosnia and Herzegovina 1-11

Lugušić Aida
Porobić Aleksandra
Muratović Samija
Djedjibegović Jasmina

Understanding MTT–Graphene Oxide Interactions for Accurate Viability Measurements 13-21

Ćetković Pećar Tamara
Haverić Anja
Haverić Sanjin
Gutić J. Sanjin

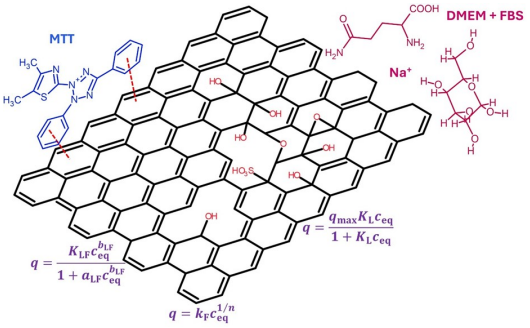

Monte Carlo Simulation of a Seeded Growth Model on a Triangular Lattice: Impact of Surface Impurities on the Final Morphology 23-30

Dijak Dijana
Karač Aleksandar

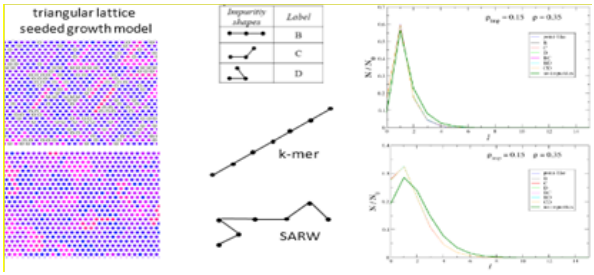

Bentonite as an adsorbent for the removal of Cr(III) ions from galvanic wastewater: equilibrium, kinetics and thermodynamics in batch and column systems 31-40

Ahmetović Melisa
Šestan Indira
Odobašić Alma
Papraćanin Edisa
Keran Husein
Junuzović Halid

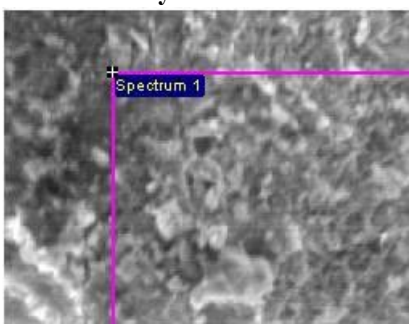

Stabilization of Waste Sludge from Municipal Wastewater Treatment Plant 41-46

Džambić Mirsada
Stuhli Vedran
Čorbić Mirnesa
Kusur Amela
Hodžić Senida
Mešanović Šejla

Characterization of zein-based core-shell microcapsules and matrix nanocapsules with encapsulated carvacrol 47-56

Spasojević Ljiljana
Rajić Danijela
Tošković, Dragan
Gojković Cvjetković Vesna
Bučko Sandra
Škrbić Jelena
Fraj Jadranka
Milinković Budinčić Jelena
Petrović Lidija
Katona Jaroslav

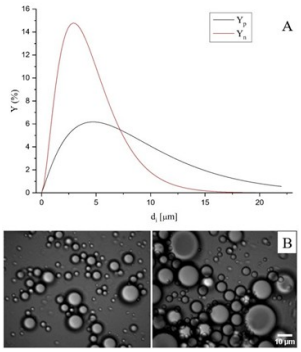

Antioxidant and Antibacterial Activity of Essential Oil of *Syzygium aromaticum* (L.) Merr. & L. M. Perry and its Application as Eco-Friendly Copper Corrosion Inhibitor 57-66

Horozić Emir
Marčetić Mirjana
Zdravković Milica
Tasić Gordana
Grekulović Vesna
Mekić Lejla
Huseinović Edina
Dedić Jasmina
Cipurković Suada
Šehić Melisa

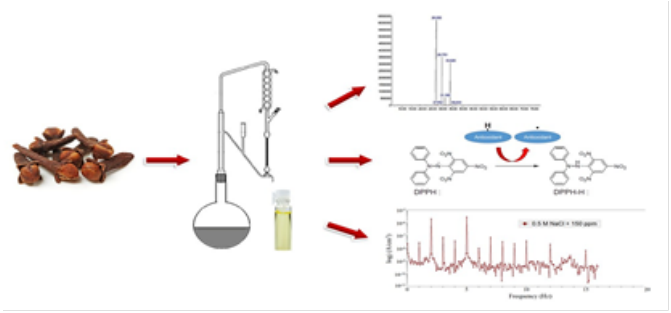

Instructions for authors 67
Sponsors 75

Editorial

Lead poisoning, also known as plumbism and saturnism. Exposure to lead can occur through contaminated air, water, dust, food or consumer products. Children are at greater risk because they are more likely to put objects in their mouths, such as those containing lead paint, and absorb a large amount of the lead they swallow. Occupational exposure is a common cause of lead poisoning in adults with certain occupations at particular risk. The diagnosis is usually made by measuring lead levels in the blood. The Centers for Disease Control and Prevention (CDC US) have set the reference level for blood lead for adults at 10 μg/dL (10 μg/100g) and for children at 3.5 μg/dL.

Classically, "acute lead poisoning" or "chronic lead poisoning" is defined as exposure to high levels of lead that are usually associated with severe health effects.

Diagnosis and treatment of lead exposure are based on the blood lead level (the amount of lead in the blood), measured in micrograms of lead per deciliter of blood (μg/dL). Urine lead levels may also be used, although less frequently. In cases of chronic exposure, lead is often sequestered in the highest concentrations first in the bones, then in the kidneys. If the provider performs a provocative excretion test, or "chelation challenge," a measurement obtained from urine rather than blood is likely to provide the healthcare provider with a more accurate representation of total lead burden.

Lead forms a wide range of compounds and exists in the environment in various forms. Organic lead poisoning is now very rare, as countries around the world have phased out the use of organic lead compounds as gasoline additives. However, such compounds are still used in industrial settings. Organic lead compounds, which readily pass through the skin and respiratory tract, primarily affect the central nervous system.

Lead poisoning is preventable. This involves individual measures such as removing lead-containing items from the home, and workplace interventions such as improved ventilation and supervision.

Lead poisoning can be acute (from intense short-term exposure) or chronic (due to repeated low-level exposure over a long period), but the latter is much more common.

Poisoning by organic lead compounds predominantly manifests with symptoms in the central nervous system, such as insomnia, delirium, cognitive deficits, tremors, hallucinations, and convulsions. In acute poisoning, typical neurological signs are pain, muscle weakness, numbness, and tingling, and rarely symptoms related to inflammation of the brain. Other acute symptoms include abdominal pain, nausea, vomiting, diarrhea, and constipation. Effects of lead on the mouth include astringency and a metallic taste. Gastrointestinal problems, such as constipation, diarrhea, poor appetite, and weight loss are common in acute poisoning.

Lead poisoning can cause a wide range of symptoms and signs that vary depending on the person affected and the duration of lead exposure. Symptoms are nonspecific and

can be subtle, and someone with elevated lead levels may not have any symptoms. Symptoms usually develop over weeks to months as lead accumulates in the body during chronic exposures, but acute symptoms also occur with short, intense exposures.

Editors

Bulletin of the Chemists and Technologists
Glasnik hemičara i tehnologa Bosne i Hercegovine
2026
66
Original Scientific Article
Print ISSN: 0367-4444
Online ISSN: 2232-7266
DOI: 10.35666/2232-7266.2026.66.01
UDK: 543[637.1:577.1](497.6)
01-11

Levels of Selected Persistent Organic Pollutants in Human Milk Samples from Bosnia and Herzegovina

Lugusic, A.*, Porobic, A., Muratovic, S., Djedjibegovic, J.

University of Sarajevo-Faculty of Pharmacy, Zmaja od Bosne 8, 71 000 Sarajevo, BiH

Article info
Received:09/12/2025
Accepted:02/02/2026

Keywords:
Human Milk
PCB
OCP
Bosnia and Herzegovina

***Corresponding author:**
Aleksandra Porobić
E-mail: aca1902@gmail.com
Phone: +387 61 709 562

Abstract: One of the greatest challenges of today is environmental pollution, which leads to serious threats to human health and the entire ecosystem. Due to their high persistence and low biodegradability, polychlorinated biphenyls (PCBs) and organochlorinated pesticides (OCPs), as the main categories of environmental pollutants of anthropogenic origin, remain present in the environment for a long period of time, continuously circulating between air, water and soil, posing a permanent risk to public health. Bosnia and Herzegovina has not previously conducted studies on the presence of environmental pollutants in breast milk, the results of which could contribute to more effective public health protection and serve as a basis for strategic planning aimed at reducing exposure to environmental pollutants. For this reason, the aim of this study was to determine the levels of selected persistent organic pollutants (PCBs and OCPs) in breast milk of lactating women (N=67) from Bosnia and Herzegovina (Federation of Bosnia and Herzegovina, Republika Srpska and Brčko District). The results presented here are the first of their kind for the territory of our country. The average values of quantified concentrations of PCB (17 congeners) and OCP (8 compounds) ranged from 1.03-162.29 ng/g l.w. and from 0.27 to 14.64 ng/g l.w., respectively. PCB congeners 52, 77, 126, and 169 were detected at higher levels compared to those reported in some of the European and Asian countries. In Brčko District and Republika Srpska, higher values were found compared to the Federation of Bosnia and Herzegovina.The measured concentrations of selected persistent pollutants in breast milk samples collected in Bosnia and Herzegovina mostly correspond to the literature data from similar studies conducted in the countries of the region and Europe.

INTRODUCTION

Environmental pollutants can arise due to numerous processes of natural and anthropogenic origin. Pollutants of anthropogenic origin include three main categories of persistent organic pollutants (POPs): industrial chemicals (e.g., polychlorinated biphenyls, PCBs), pesticides (e.g., organochlorinated pesticides, OCPs), and unintentionally produced co-products of industrial processes and combustion (dioxins and furans). The basic characteristics of POPs such as environmental persistence, semi-volatility, as well as lipophilicity allow them to accumulate over time as well as biomagnify through the food chain, resulting in their appearance in the organisms of humans and animals that are at the top of the food chain. Until the 1970s, polychlorinated biphenyls (PCBs) were widely used in various industries, in electrical equipment, transformers and capacitors, plastics, paints and pesticides. OCPs have been used in agriculture as insecticides, acaricides and fumigants in various crops, and after World War II they played a key role in the control of malaria and typhoid fever (Aktar et al., 2009; EI-Shahawi et al., 2010; Zhang et al., 2006).

Although their production has long been banned internationally, these compounds may still be released into the environment due to illegal or improper disposal of PCB-containing waste as well as continued use of OCP in agriculture. Due to their low biodegradability, they remain in the environment for a long time, circulating between air, water and land, and continue to raise major public health concerns. (ATSDR, 2000). The human body can be exposed to PCBs and OCP by respiratory, oral or dermal routes. (Fitzgerald et al., 2004; Freels et al., 2007).

Many studies show that exposure to PCBs and OCPs can be associated with various health problems affecting the nervous, immune, endocrine, and reproductive systems, as well as result in cancerous changes. (Longnecker, Rogan and Lucier, 1997; Ma and Sassoon, 2006; Vafeiadi et al., 2017; Rissato et al., 2006; Olisah et al., 2020). PCBs are also recognized as endocrine disruptors, because they can

mimic the action of endogenous hormones by binding to hormone receptors or blocking them, thus altering the normal function of the endocrine system. (Ma and Sassoon, 2006; Wang et al., 2006).

In addition, maternal contamination may serve as a source of fetal exposure prenatally and, in infants, postnatally through breast milk. (Darnerud et al., 2010; Turrio-Baldassarri et al., 2007) It is believed that infant exposure to PCBs through ingestion of contaminated breast milk may affect their growth and neurological development. (Dekoning and Karmaus, 2000; Meeker, 2012; Todaka et. al., 2010). Breast milk is considered an ideal matrix for biomonitoring due to its easy availability, non-invasive sampling method, and its high lipid content, which facilitates the accumulation of lipophilic pollutants.

Although the use of persistent pollutants in BiH and neighboring countries was banned 40 years ago or strictly regulated in recent decades, their residues are still detected in water, air, soil and food. In BiH, PCBs were used in industry and their presence was discovered in old electrical equipment and closed systems such as transformers, capacitors and switches, as well as in barrels used to store spent transformer oils. Between 2008 to 2013, according to the data of the Agency for Statistics of BiH, a certain amount of mixtures and preparations containing PCBs, polychlorinated terphenyls (PCT) or polybrominated biphenyls (PBB) were imported. (NIP, BiH) Investigations of persistent organic pollutants levels in the Neretva River revealed the presence of dichlorodiphenyltrichloroethane (DDT) and its metabolites, as well as polybrominated diphenyl ether (PBDE) congeners 47 and 99. Although the concentrations of the POPs tested in the aforementioned study were below local standards for environmental protection and human water consumption, the levels of dieldrin and total PCBs were above Environmental Protection Agency (EPA) standards for human consumption. (Djedjibegovic et al., 2010) Also, the National Implementation Plan for BiH reports incident situations of unintentional PCB releases from capacitors into the environment, as well as improper storage of old PCB- containing equipment.

All of the above highlights the importance and need for continuous monitoring of persistent organic pollutants in both the environment and food, as the primary source of exposure of the general population to these pollutants.

Long-term and repeated studies of POPs in breast milk, conducted both in the region (Krauthacker, 2000; Runkel, 2021; Vukavić et al., 2008) and globally, provide data useful for monitoring spatial and temporal trends of pollutant load in the general population, which is also one of the indicators of environmental burden. In general, these studies reported on a temporal decrease in POPs concentrations attributed to a decrease in their overall emission, but also certain geographical variations, which highlight the importance of sampling sites distribution within the monitoring process. Bosnia and Herzegovina is the only country in the region that does not have data on the content of persistent organic pollutants in breast milk, which indicates the exceptional importance of this research for the entire country.

Accordingly, the aim of this study was to determine the levels of selected persistent organic pollutants (PCBs and OCPs) in breast milk of lactating women from Bosnia and Herzegovina.

EXPERIMENTAL

Materials and methods

Research Protocol and Design

The study was designed as a cross-sectional study in which breast milk samples were collected in accordance with the guidelines of the World Health Organization (WHO) (UNEP, 2017) taking into account regional representation to ensure a nationally representative sample. The research was approved by The Ethics Committee of the University of Sarajevo-Faculty of Pharmacy for Experimental Research in the Scientific Projects (No. 0101-1267/20 of March 13, 2020). The recruitment of potential breast milk donors was carried out across Bosnia and Herzegovina (BiH) in cooperation with private and public institutions of primary and secondary health care, through social media networks, as well as by distributing information leaflets about the study. Participation in this study was entirely voluntary. A total of 130 mothers were recruited as potential breast milk donors. The main inclusion criteria were that the mother was under 40 years of age, with a normal and healthy pregnancy, with a ten-year residence in the study area, and that a breast milk sample was collected between the third and eighth week postpartum. The exclusion criteria were the mother's (child's) potential specific exposure which could significantly deviate from the national average, as well as refusal to sign the informed consent form.

Breast milk samples were collected in glass containers, previously treated at 450ºC and rinsed with an organic solvent. A minimum of 50 ml of milk sample was collected manually. Milk samples were stored at 4ºC for up to 72 hours and then frozen at -20ºC until analysis. Before laboratory analysis, frozen samples were heated to 40ºC and homogenized to ensure complete fat dissolution and distribution across the sample.

Socio-demographic characteristics of the donors such as age, level of education, occupation, place of residence, cigarette consumption, etc., as well as height and pre-pregnancy weight were collected through a questionnaire. Statistical significance of differences among groups was tested by the Mann-Whitney U test, while correlations between individual sociodemographic variables and POPs concentrations were assessed by Spearman's rank correlation. p-values lower than 0.05 were considered statistically significant.

Chemical Analysis

Chemicals and reagents hexane (from Honeywell, Germany), 2-propanol (all analytical grade), amyl alcohol (sp. gr. 0.185) and tetrabutylammonium sulphate (p.a.) were purchased from Sigma-Aldrich (Seelze, Germany). Sodium sulphite (p.a.) was purchased from Kemika (Zagreb, Croatia). Sulphuric acid (98%, p.a.) was purchased from Merck (Darmstadt, Germany) and sulphuric acid (90-91% p.a.) from Grammol, Croatia. PCB standards were purchased from Dr Ehrenstorfer GmbH (Augsburg, Germany). OCP standards were purchased from Sigma–Aldrich (Germany). Nitrogen 5.0 was supplied from Messer (Sarajevo, Bosnia and

Herzegovina). Ultrapure water (>18mΩ) was supplied by Arium® mini Lab Water System (Goettingen Germany). For fat content determination and its isolation from breast milk samples we used Gerber's method (Sabadoš D., Rajšić B., 1964), as a quick and simple method for determining the fat content in milk and dairy products of animal origin. After homogenizing the sample, the butyrometer was filled first with 10 ml of 90% sulfuric acid, then with 11 ml of breast milk and finally with 1 ml of amyl alcohol. After gentle mixing, the butyrometers were placed in a water bath for five minutes at 65ºC. Then centrifugation was performed at 1100 rpm for 5 minutes, and repeated twice. After centrifugation, the butyrometers were again placed in the water bath for 5 minutes at 65ºC. Then the percentage of isolated fat was read on the butyrometer scale. The entire fat contents were transferred into tubes with a conical bottom and ground stopper and treated with 2 ml of hexane. The tubes were vortexed for 2 minutes, placed in an ultrasonic water bath for 15 minutes and then on a shaker for 30 minutes at 80 rpm. The hexane extract was then subjected to a purification procedure with concentrated sulfuric acid, as described by Djedjibegovic et al. (2015)

Quality Control/Assurance

Quality control was carried out by analyzing a spiked breast milk sample as well as one laboratory blank of reagents for each batch of samples. All samples were analyzed in duplicate, and the content of the tested analytes was presented as an average. The values of the analytical parameters of the method used for PCB congeners and OCP components are shown in Table 1.

Table 1. Values of analytical parameters for test analytes (PCB and OCP)

Analytes of interest	R2	LD (ng/g l.w.)	LQ (ng/g l.w.)	Average RF (%)	RSD (%)
α- BHC	0.9998	0.22	0.665	89.00	4.73
β- BHC	0.9997	1.167	3.535	80.26	5.01
γ- BHC	0.9996	0.339	1.027	82.51	5.08
HEPTACHLOR	0.9958	2.324	7.042	105.56	9.04
ALDRIN	0.998	0.321	0.972	20.19	4.46
HEPTACHLORE EPOXIDE ISOMER B	0.9982	2.2	6.667	49.48	5.26
2.4' DDD	0.9993	2.704	8.193	70.18	3.73
DIELDRIN	0.9987	2.849	8.635	151.72	3.74
2.4′-DDT*	0.9988	5.134	15.556	/	/
4.4′-DDT	0.9997	3.025	9.166	3.25	5.46
PCB 28	0.9984	0.281	0.851	131.843	5.13
PCB 52	0.9995	0.322	0.976	108.324	4.69
PCB 101	0.9981	0.299	0.907	98.603	5.13
PCB 153	0.9993	0.486	1.473	102.964	4.55
PCB 138*	0.998	0.388	1.176	/	/
PCB 180	0.9981	0.3	0.908	116.609	4.07
PCB 209	0.9973	0.363	1.101	87.297	4.53
PCB 30	0.9987	0.315	0.956	ND**	24.05
PCB 123	0.9985	3.412	10.34	ND**	12.5
PCB 156	0.9995	0.315	0.956	ND**	5.2
PCB 77	0.9984	2.781	8.426	ND**	11
PCB 105	0.9991	0.349	1.058	ND**	24.8
PCB 118	0.9967	1.681	5.093	ND**	3.3
PCB 126	0.9996	0.361	1.095	ND**	3.7
PCB 157	0.9994	0.34	1.031	ND**	6.5
PCB 167	0.9963	1.767	5.355	ND**	6.86
PCB 169	0.9948	6.322	19.157	ND**	13.6
PCB 204	0.999	0.576	1.746	ND**	7.4

*2.4′-DDT and PCB 138 co-eluted so quantification was not possible

**ND – not determined (RFs were determined only for indicator PCBs mix shown in the table)

Determination of selected organic pollutants (PCBs and OCPs)

Determination of PCB and OCP compounds were performed by gas chromatography with electron capture detector (GC/ECD) using Agilent Technologies (Santa Clara, USA) 7890A GC as described in Djedjibegovic et al (2010). Briefly, the Agilent DB-5 column (60 m × 0.25 mm × 0.25 μm) with a stationary phase of 5% phenyl polysiloxane was used. Column flow rate was 1 mL min−1. The oven temperature program was the following: 90◦C (2 min), 10◦C/min to 180◦C, then 2◦C/min to 270◦C and finally 20◦C/min to 290◦C (20 min). The detector temperature was 285◦C and injection volume 1 μL. The inlet was operated in splitless mode.

Statistical analysis

Statistical analysis was performed using the SPSS Statistical Package, version 2023. Descriptive statistics, including mean, standard deviation (SD), and relative standard deviation (RSD), were calculated to evaluate the distribution of target analytes in the analyzed milk samples. Since the data were not normally distributed according to the Shapiro-Wilk test, nonparametric statistical tests were applied. Statistical significance was considered at $p < 0.05$.

RESULTS AND DISCUSSION

A total of 67 breast milk samples were collected from the area of 2 entities of BiH, Federation of BiH (FBiH, n=37) and Republika Srpska (RS, n=28), and Brčko District (BD, n=2). Out of a total of 67 donors who completed the research, 66 of them filled out a questionnaire with sociodemographic characteristics. Table 2 shows the socio-demographic characteristics of breastfeeding mothers.

Table 2 Sociodemographic characteristics of lactating mothers

	Options	Total n	% of all respondents	FBiH	RS	BD
				n (%)*	n (%)*	n (%)*
Place of residence	**Urban**	52	78.79	28 (75.68)	22 (78.57)	2
	Rural	14	21.21	8 (21.62)	6 (21.43)	/
Parity	**primiparae**	38	57.58	25 (67.57)	11 (39.29)	2
	multiparae	28	42.42	11 (29.73)	17 (60.71)	/
Level of education	**Basic**	2	3.03	/	2 (7.14)	/
	Secondary	18	27.27	10 (27.03)	8 (28.57)	/
	High	46	69.70	26 (70.27)	18 (64.29)	2
Smoking status	**Non-smokers**	46	69.70	23 (62.16)	21 (75.00)	2
	Smokers	20	30.30	13 (35.14)	7 (25.00)	/
		n (mean)	**% of all respondents**	**n (mean)**	**n (mean)**	**n (mean)**
BMI	**<18.5**	4 (18.32)	6.06	1 (18.42)	2 (18.38)	1 (18.07)
	18.5 – 24,9	47 (22.11)	71.21	29 (22.11)	17 (22.12)	1 (21.77)
	25.0 – 30.0	13 (26.74)	19.70	5 (25.95)	8 (27.23)	/
	>30.0	2 (33.59)	3.03	1 (35.29)	1 (31.89)	/

n (%)* - the number and percentage of respondents in relation to the number of respondents per entity/district

The percentage of fat isolated in breast milk samples ranged from 1.3% to 6.7% with an average value of 3.51%, which is consistent with the values recorded in the literature.

Levels of selected PCBs in human milk samples

In the analyzed breast milk samples, the average concentrations of the following PCB congeners were determined: 28, 52, 101, 153, 180, 209, 30, 77, 123, 118, 105, 126, 167, 156, 157, 204 and 169 and expressed in ng/g l.w. The indicator congener PCB 138 could not be quantified due to the same retention time as 2,4'DDT from the OCP group. The values of relative standard deviations were below 30% in most samples, which is acceptable according to the relevant guidelines (AOAC (2016), European Commission, 2021) and indicate good reproducibility of the method. The exception was a certain number of samples with concentrations close to the limits of detection and quantification with elevated RSD values,

which is expected when measured at very low concentrations.

Table 3 shows the results of descriptive statistics for selected PCB congeners (28, 52, 101, 153, 180, 209, 30, 77, 123, 118, 105, 126, 167, 156, 157, 204 and 169)

Table 3 Descriptive statistics for selected PCB Congeners

	N	Average	SE	Median	SD	Variance	Min*	Max
PCB 28	34	17.74	5.15	10.05	30.02	901.29	0.43	163.87
PCB 52	66	162.29	12.67	136.78	102.92	10591.79	16.4	495.77
PCB 101	45	9.17	1.35	6.11	9.07	82.35	0.15	49.78
PCB 153	58	3.52	0.37	3.05	2.79	7.77	0.25	15.7
PCB 180	63	3.68	0.43	2.85	3.44	11.83	0.46	23.96
PCB 209	16	6.97	2.78	2.67	11.11	123.5	0.19	40.4
PCB30	65	21.16	1.89	17.11	15.22	231.77	6.11	103.8
PCB77	22	7.32	1.76	5.72	8.26	68.27	1.89	38.79
PCB123	1	1.74	/	/	/	/	/	/
PCB118	42	4.27	0.59	2.6	3.8	14.41	0.86	16.78
PCB105	42	1.64	0.39	0.54	2.53	6.4	0.18	11.97
PCB126	49	3.21	0.28	2.87	1.96	3.86	0.18	10.96
PCB167	29	82.93	24.39	33.37	131.34	17250.66	0.9	575.21
PCB156	23	1.03	0.17	1.01	0.79	0.63	0.16	3.01
PCB157	27	2.5	0.35	2.1	1.82	3.32	0.17	8.29
PCB204	9	3.52	1.61	2.37	4.84	23.45	0.89	16.07
PCB169	31	18.63	2.73	9.77	15.18	230.54	3.22	60.96

* minimal concentrations for all congeners except PCB 52, PCB 30 where lower than LQ

PCB congeners 52, 180, and 153 are present in more than 85% of breast milk samples, indicating a wide distribution of these congeners as well as significant population exposure to them. Although all three were detected in most samples, the average concentration of PCB 52 (162 ng/g l.w.) was significantly higher than the average concentration of PCB 153 (3.52 ng/g l.w.) and PCB 180 (3.68 ng/g l.w.), which is similar to the pattern of frequency but not in concentrations of these congeners reported in studies from France, the Czech Republic and China (Brucker-Davis, 2010; Cajka, 2003; Cerná et al., 2010). These differences may be due to variations in the composition of the commercial PCB products used, including differences between lots of the same product, the analytical methods used in the studies, and ultimately the stability of the relative difference in metabolic kinetics of individual congeners in different environments. (Schulz, B., Carlson, L. M., Christensen, K., et al., 2024). High concentrations indicate the need for further identification and monitoring of active sources as well as the implementation of measures for the management of PCB-containing waste in accordance with the provisions of the Stockholm Convention (UNEP, 2012).

Lower concentrations of the multichlorinated congeners PCB 153 and PCB 180 indicate chronic exposure that can be explained by their higher stability, lower volatility and potentially increased consumption of fish as one of the exposure sources (Glynn et al., 2007).

The concentrations of PCB 180 and PCB 153 determined in this study are lower than those reported in studies conducted in Greece, Russia, Poland, Sweden, and France (Costopoulou et al., 2006; Polder et al., 2008; Jaraczewska et al., 2006.; Lignell et al., 2009, Brucker-Davis, 2010). Similar or lower levels of these congeners have been reported in Serbia, Turkey and Bulgaria (Vukavić et al, 2008; Erdogrul et al., 2004; Georgieva et al., 2023).

Comparing the results of our study with the data from the research conducted in Croatia, a slightly higher concentration of PCB28 was observed in our study. However, the concentrations of PCB52 and PCB101 were several times higher, while the values for PCB153 and PCB180 were slightly lower compared to the Croatian findings (Klinčić et al., 2014).

Concentrations of dioxin-like (dl-PCB) congeners (77, 123, 118, 105, 126, 167, 156, 157, 169) and non-dioxin-like (ndl-PCB) congeners (PCB30 and PCB 204) were also determined in the analysed milk samples. Among the ndl-PCBs, PCB30 was detected in more than 90% of the samples, while PCB204 was present in 13% of the samples. The dl-PCB congeners PCB118, PCB126 and PCB105 were present in 60% - 73% of samples, while congeners PCB77, PCB156, PCB157, PCB167 and PCB169 were present in 30% to 45% of the samples. Congener PCB123 was detected in only one sample and at a concentration below the detection limit, similar to what was reported in a study conducted in Italy (Abballe et al.,

2008), while concentrations of 0.23 ng/g l.w. were detected in Germany (Wittsiepe et al., 2007)

A similar pattern in the frequency of the detected congeners was reported in the Croatian study (Klinčić et al. 2014). In our study, low average concentrations were recorded in the range from 1.00 to 7.32 ng/g l.w. for PCB congeners 105, 156, 157, 126, 204, 118, 77, while higher average concentrations were observed for PCB congeners 30 (21.16 ng/g l.w.), 169 (18.63 ng/g l.w.) and 167 (33.4 ng/g l.w.). The concentrations for PCB congeners 105, 156 and 118 in our study (0.54 ng/g l.w., 1.01 ng/g l.w. and 2.60 ng/g l.w., respectively) are similar to the concentrations of the same congeners in the Croatian study (0.9 ng/g l.w., 0.8 ng/g l.w. and 0.9 ng/g l.w.) with slightly higher concentrations of congener 118 in our study. In Italy (Abballe et al., 2008) and Sweden (Lignell et al., 2009), the concentrations of PCB 156 and PCB 157 were relatively higher compared to our and Croatian findings. A study conducted in China between 2003 and 2005 (Zhao et al., 2007) showed concentrations of PCB 77 comparable to those in our study (5.15 ng/g l.w. vs. 5.72 ng/g l.w., respectively). However, significantly higher levels of PCBs 118 and 105 were detected in China compared to BiH and other European countries, which could be explained by intensive industrialization in certain parts of China.

In our study, the dl-PCB congeners PCB77 (5.72 ng/g fat), PCB126 (2.87 ng/g fat) and PCB169 (9.77 ng/g fat) were detected. These congeners were not detected or were detected in very low concentrations in various studies conducted across Europe between 1999 and 2011 (Abballe et al., 2008; Lignell et al., 2009; Bencko et al., 2004; Wittsiepe et al., 2007; Klinčić et al., 2014). Variation in detection can be attributed to different potential exposure sources, as well as to differences in the implementation of legal regulations on PCB use restrictions and waste management practices. Potential sources of exposure to dl-PCB congeners in BiH could be continued presence of old electrical equipment and transformers containing PCBs, industrial and post-war contamination of soil and air, frequent uncontrolled incineration of various types of waste (plastics, rubber), as well as insufficient compliance with regulations required under Stockholm and Basel Conventions, which BiH has formally committed to uphold.

Concentrations of PCB 169 were significantly higher ($Z=-2,42$; $p<0.016$) in mothers who were smokers (current or former) than in non-smokers. The sum of dl-PCB and ndl-PCB was significantly higher in the milk of mothers living in urban area comparing to those from rural areas. Significant negative correlation with mothers' parity was for PCB77 ($p=0.028$), PCB118 ($p=0.044$), and PCB156 ($p=0.048$).

Levels of selected OCPs in human milk samples

In the analyzed breast milk samples, the average concentrations of the following OCPs were determined: alpha BHC, beta BHC, gamma BHC, heptachlor, aldrin, heptachlor epoxide isomer B, 2,4'DDD, dieldrin and 4.4'DDT (Table 4). When determining RF in spiked milk samples, RF of 4.4′ DDT was low, but due to its toxicological relevance and presence in the population, it was included in further statistical processing.

Table 4 Descriptive statistics for selected OCPs (concentration in ng/g l.w.)

	N	Average	SE	Median	SD	Variance	Min	Max
αBHC	25	0.67	0.1	0.34	0.51	0.26	0.11	1.95
βBHC	26	6.98	3.96	1.8	20.22	408.73	0.6	104.22
γBHC	67	7.36	0.54	6.03	4.39	19.23	2.55	26.61
HEPTACHLOR	44	4.63	0.61	3.59	4.02	16.19	1.19	17.09
ALDRIN	6	0.27	0.07	0.16	0.17	0.03	0.16	0.5
HEPTACHLOR EPOXIDE ISOMER B	60	3.02	0.47	3.4	3.62	13.08	1.12	27.97
2.4' DDD	20	2.78	0.32	2.78	1.44	2.06	1.38	4.18
DIELDRIN	25	3.46	0.51	4.4	2.54	6.43	1.45	11.28
4.4' DDT	40	14.64	6.45	4.67	40.76	1661.54	1.54	251.62

OCP concentrations in breast milk samples from Bosnia and Herzegovina, shown in Table 4, compared to similar studies in Croatia and other European countries, indicate a moderate to elevated burden on the population. Compared to the findings in several Asian and African countries, OCP concentrations are significantly lower in our study. Regarding the concentrations of BHC isomers determined in our study, the levels of alpha BHC (0.34ng/g l.w) are similar to those reported in neighboring Croatia (0.40 ng/g l.w.) (Klinčić et al., 2014) and Poland (0.32 ng/g l.w) (Szyrwińska and Lulek, 2007). In contrast, beta BHC (1.80 ng/g l.w.) is almost twice lower than those in Croatia (3.10 ng/g l.w.), (Klinčić et al., 2014) and several times lower than the levels in the Czech Republic (57 ng/g l.w.) (Cajka and Hajslova, 2003) and Poland (17.7 ng/g l.w.) (Szyrwińska and Lulek, 2007) and significantly lower than the extremely high values recorded in China (950 ng/g l.w.) (Wong et al., 2002) and India (563 ng/g l.w.) (Bedi et

al., 2013). The detected concentration of lindane or gamma BHC (6.03 ng/g l.w) in this study is slightly higher compared to the results of the study conducted by Klinčić et al. (1.4 ng/g l.w.) and Szyrwińska et al. (0.16 ng/g l.w), similar to the values detected in Tunisia (8 ng/g l.w) (Ennaceur et. al., 2007) and several times lower than the extremely high values recorded in India (658 ng/g l.w) (Bedi et al., 2013). The concentration of 4.4' DDT of 4.67 ng/g l.w in our study is slightly higher than the level recorded in Croatia (1.5 ng/g l.w.), but several times lower than the levels recorded in China (545 ng/g l.w), Poland (70.30 ng/g l.w) and India (980 ng/g l.w) (Klinčić et al., 2014; Wong, et al., 2002; Szyrwińska and Lulek, 2007; Bedi et al., 2013). The average concentration of dieldrin detected in our study (3.46 ng/g l.w.) corresponds to the average concentrations of less than 3.8 ng/g l.w. reported by the Republic of Croatia (Fång et al., 2008) and Germany (Zietz et al., 2008). In breast milk samples from Latin American and Caribbean countries, the average concentrations of dieldrin ranged from 2.6 to 5 ng/g l.w., while in samples from African countries, the average values ranged from 1.3 to 4.1 ng/g of fat (UNEP 2009). A median concentration of 3 ng/g l.w. was reported in a study conducted in Japan and is also close to the values of dieldrin in our study. (Nagayama et al., 2007)

Heptachlor concentrations were, in most conducted studies, reported as cis-heptachlor epoxide (cis-HCL-epoxide), heptachlor epoxide (HCL-epoxide which is a mixture of A and B isomers) and heptachlor. The concentrations of heptachlor epoxide (HCL-epoxide) reported from European countries were in most cases below or close to 3 ng/g fat (UNEP 2011), which is similar to the levels of average concentrations of heptachlor and heptachlor epoxide (isomer B) recorded in our study (4.63 ng/g l.w. and 3.02 ng/g l.w. respectively). Higher concentrations of these analytes were recorded in Ukraine, 16–22 ng/g l.w. (Gladen et al., 1999 and 2003), and in the Netherlands, 30 ng/g l.w. (Albers et al., 1996).
Significantly higher concentrations of beta BHC (p=0.045), heptachlor epoxide (p=0.007), and sum of OCP (p=0.002) were found in the milk of mothers living in urban relative to mothers from rural areas.

Comparison of iPCB Sum Concentrations, Total PCB Sum and OCP Sum Between BiH Entities

A comparison of the average concentrations of the sum of selected analytes (∑iPCB, ∑totalPCB and ∑OCP between the entities of BiH is shown in Chart 1.

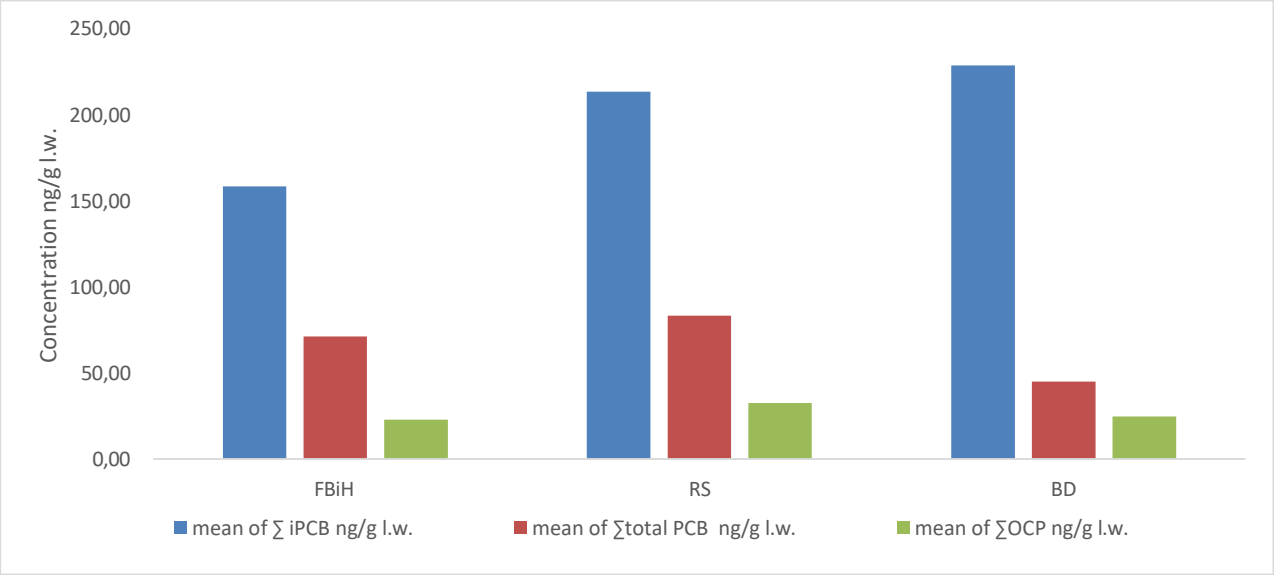

Chart 1 Average concentrations of the sum of selected analytes (∑iPCB, ∑totalPCB and ∑OCP by entities (FBiH and RS) and district of BiH (Brčko District (BD))

Graph 1 shows clear differences in average concentrations of ∑iPCB, with the highest values present in Brčko District and Republika Srpska, while lower values of ∑iPCB are observed in the Federation of BiH. The Mann-Whitney U test showed that these differences between the two entities (FBiH and RS) were statistically significant (p=0.027). Due to the limited number of samples (n=2) from the Brčko District, data from this region were not considered in the statistical significance evaluation, despite the fact that the highest concentrations were recorded there. For the average concentrations of the ∑totalPCB and ∑OCP, the results of the Mann-Whitney U test showed that there was no statistically significant difference between the entities (p>0.05), although differences for the ∑totalPCB are visible on the graph.

CONCLUSION

Due to their potential adverse effects on human health, the monitoring of POPs—particularly through breast milk—is of great importance, especially in developing countries such as Bosnia and Herzegovina. The population is exposed to these contaminants through food, water, and air, and monitoring their levels in biological samples such

as breast milk provides valuable insight into both the degree of environmental contamination and the extent of exposure of mothers and newborns, who represent the most vulnerable population group.

Longterm monitoring of environmental pollutants also enables the assessment of temporal trends in environmental contamination and the evaluation of implemented protective measures and strategies. This further emphasizes the importance of continuous research on these substances.

According to available scientific literature, this study represents the first investigation of environmental pollutants through breast milk monitoring in Bosnia and Herzegovina. It is therefore of substantial importance for the country as a whole.

The measured concentrations of selected persistent pollutants in breast milk samples from Bosnia and Herzegovina fall within the range of values reported in the literature for urban areas and are lower than typical concentrations observed in contaminated regions. However, PCB congeners 52, 77, 126, and 169 were detected at higher levels compared to those reported in some of the European and Asian countries.

Significantly higher concentrations of beta BHC, heptachlor epoxide, sum of OCPs, sum of dl-PCB and ndl-PCBs were found in the milk of mothers from urban than from rural areas. Concentration of PCB169 was significantly higher in milk from mothers who were smokers (current or former) than in non-smoking mothers.

REFERENCES

Schulz, B., Carlson, L. M., Christensen, K., Weitekamp, C. A., Marek, R. F., Martinez, A., Hornbuckle, K. C., & Lehmann, G. M. (2024). Comprehensive compilation of congener profiles to support health assessment of environmental exposures to polychlorinated biphenyl mixtures. Environmental research, 263(Pt 1), 120081. https://doi.org/10.1016/j.envres.2024.120081

Nagayama, J., Tsuji, H., Iida, T., Nakagawa, R., Matsueda, T., Hirakawa, H., Yanagawa, T., Fukushige, J., & Watanabe, T. (2007). Immunologic effects of perinatal exposure to dioxins, PCBs and organochlorine pesticides in Japanese infants. Chemosphere, 67(9), S393–S398. https://doi.org/10.1016/j.chemosphere.2006.05.134

Djedjibegović, J., Marjanović, A., Burnić, S., Omeragić, E., Dobraca, A., Čaklovica, F., & Sober, M. (2015). Polychlorinated biphenyls (PCBs) in fish from the Sana River (Bosnia and Herzegovina): A preliminary study on the health risk in sport fishermen. Journal of environmental science and health. Part. B, Pesticides, food contaminants, and agricultural wastes, 50(9), 638–644. https://doi.org/10.1080/03601234.2015.1038956

Abballe, A., Ballard, T.J., Dellatte, E., di Domenico, A., Ferri, F., Fulgenzi, A.R., Grisanti, G., Iacovella, N., Ingelido, A.M., Malisch, R., Miniero, R., Porpora, M.G., Risica, S., Ziemacki, G., De Felip, E. (2008). Persistent environmental contaminants in human milk: concentrations and time trends in Italy. Chemosphere 73, 220–227.

Aktar, M. W., Sengupta, D., Chowdhury, A. (2009). Impact of pesticides use in agriculture: their benefits and hazards. Interdisciplinary Toxicology, 2(1), 1-12.

Albers, J. M., Kreis, I. A., Liem, A. K., & van Zoonen, P. (1996). Factors that influence the level of contamination of human milk with poly-chlorinated organic compounds. Archives of environmental contamination and toxicology, 30(2), 285–291.

AOAC, (2016). Association of Analytical Chemists, guidelines for standard method performance requirements, Appendix F, 20th ed., vol.2.

ATSDR. 2000. Toxicological Profile for Polychlorinated Biphenyls (PCBs). Atlanta (GA): Agency for Toxic Substances and Disease Registry (US); CHEMICAL AND PHYSICAL INFORMATION. Available from: https://www.ncbi.nlm.nih.gov/books/NBK587431/

ATSDR. 2000. Toxicological Profile for Polychlorinated Biphenyls (PCBs). Atlanta (GA): Agency for Toxic Substances and Disease Registry (US); PRODUCTION, IMPORT/EXPORT, USE, AND DISPOSAL. Available from: https://www.ncbi.nlm.nih.gov/books/NBK587421/

ATSDR. 2000. Toxicological Profile for Polychlorinated Biphenyls (PCBs). Atlanta (GA): Agency for Toxic Substances and Disease Registry (US); 2000 Nov. 6, POTENTIAL FOR HUMAN EXPOSURE. Available from: https://www.ncbi.nlm.nih.gov/books/NBK587422/

Bedi, J. S., Gill, J. P., Aulakh, R. S., Kaur, P., Sharma, A., & Pooni, P. A. (2013). Pesticide residues in human breast milk: risk assessment for infants from Punjab, India. The Science of the total environment, 463-464, 720–726. https://doi.org/10.1016/j.scitotenv.2013.06.066

Bencko, V., Cerná, M., Jech, L., & Smíd, J. (2004). Exposure of breast-fed children in the Czech Republic to PCDDs, PCDFs, and dioxin-like PCBs. Environmental toxicology and pharmacology, 18(2), 83–90. https://doi.org/10.1016/j.etap.2004.01.009

Brucker-Davis, F., Wagner-Mahler, K., Bornebusch, L., Delattre, I., Ferrari, P., Gal, J., Boda-Buccino, M., Pacini, P., Tommasi, C., Azuar, P., Bongain, A., & Fénichel, P. (2010). Exposure to selected endocrine disruptors and neonatal outcome of 86 healthy boys from Nice area (France). Chemosphere, 81(2), 169–176. https://doi.org/10.1016/j.chemosphere.2010.06.068

Cajka, T. and Hajslová, J. (2003). Polychlorinated biphenyls and organochlorine pesticides in human milk from the Locality Prague, Czech Republic: a comparative study. Bull. Environ. Contam. Toxicol. 70, 913–919.

Cerná, M., Bencko, V., Brabec, M., Smíd, J., Krsková, A., & Jech, L. (2010). Exposure assessment of breast-fed infants in the Czech Republic to indicator PCBs and selected chlorinated pesticides: area-related differences. Chemosphere, 78(2), 160–168. https://doi.org/10.1016/j.chemosphere.2009.09.062

Costopoulou, D., Vassiliadou, I., Papadopoulos, A., Makropoulos, V., & Leondiadis, L. (2006). Levels of dioxins, furans and PCBs in human serum and milk of people living in Greece. Chemosphere, 65(9), 1462–1469. https://doi.org/10.1016/j.chemosphere.2006.04.034

Darnerud, P. O., Lignell, S., Glynn, A., Aune, M., Törnkvist, A., & Stridsberg, M. (2010). POP levels in breast milk and maternal serum and thyroid hormone levels in mother-child pairs from Uppsala, Sweden.

Environment International, 36(2), 180–187. https://doi.org/10.1016/j.envint.2009.11.001

DeKoning, E. P., & Karmaus, W. (2000). PCB exposure in utero and via breast milk. A review. Journal of exposure analysis and environmental epidemiology, 10(3), 285–293. https://doi.org/10.1038/sj.jea.7500090

Djedjibegović, J., Marjanović, A., Sober, M, Skrbo A., Sinanović, K., Larssen, T., et al., (2010) Levels of persistent organic pollutants in the Neretva River (Bosnia and Herzegovina) determined by deployment of semipermeable membrane devices (SPMD). Journal of Environmental Science and Health, Part B, 45(2), 128-136. DOI: 10.1080/03601230903472017

El-Shahawi, M. S., Hamza, A., Bashammakh, A. S., & Al-Saggaf, W. T. (2010). An overview on the accumulation, distribution, transformations, toxicity and analytical methods for the monitoring of persistent organic pollutants. Talanta, 80(5), 1587–1597. https://doi.org/10.1016/j.talanta.2009.09.055

Ennaceur, S., Gandoura, N., & Driss, M. R. (2007). Organochlorine pesticide residues in human milk of mothers living in northern Tunisia. Bulletin of Environmental Contamination and Toxicology, 78(5), 325–329. https://doi.org/10.1007/s00128-007-9185-8

European Commission, Directorate-General for Health and Food Safety. (2021). Guidance Document on Pesticide Analytical Methods for Risk Assessment and Post-approval Control and Monitoring Purposes. SANTE/2020/12830 Rev.1, European Commission. Available at: https://food.ec.europa.eu/system/files/2021-03/pesticides_mrl_guidelines_wrkdoc_2020-12830.pdf (accessed 28 March 2025)

Fång, J., Nyberg, E., Winnberg, U., Bignert, A., & Bergman, Å. (2015). Spatial and temporal trends of the Stockholm Convention POPs in mothers' milk -- a global review. Environmental science and pollution research international, 22(12), 8989–9041.https://doi.org/10.1007/s11356-015-4080-z

Fitzgerald, E. F., Hwang, S. A., Langguth, K., Cayo, M., Yang, B. Z., Bush, B., Worswick, P., & Lauzon, T. (2004). Fish consumption and other environmental exposures and their associations with serum PCB concentrations among Mohawk women at Akwesasne. Environmental research, 94(2), 160–170. https://doi.org/10.1016/s0013-9351(03)00133-6

Freels, S., Chary, L. K., Turyk, M., Piorkowski, J., Mallin, K., Dimos, J., Anderson, H., McCann, K., Burse, V., & Persky, V. (2007). Congener profiles of occupational PCB exposure versus PCB exposure from fish consumption. Chemosphere, 69(3), 435–443. https://doi.org/10.1016/j.chemosphere.2007.04.087

Georgieva, T.K., Trifonova, T. & Peteva, Z. (2023). Investigation of polychlorinated biphenyls in breast milk from two regions in Bulgaria. International Journal of Hygiene and Environmental Health, 251, p.114184. https://doi.org/10.1016/j.ijheh.2023.114184

Gladen, B. C., Monaghan, S. C., Lukyanova, E. M., Hulchiy, O. P., Shkyryak-Nyzhnyk, Z. A., Sericano, J. L., & Little, R. E. (1999). Organochlorines in breast milk from two cities in Ukraine. Environmental health perspectives, 107(6), 459–462. https://doi.org/10.1289/ehp.99107459

Gladen, B. C., Shkiryak-Nyzhnyk, Z. A., Chyslovska, N., Zadorozhnaja, T. D., & Little, R. E. (2003). Persistent organochlorine compounds and birth weight. Annals of epidemiology, 13(3), 151–157. https://doi.org/10.1016/s1047-2797(02)00268-5

Glynn, A., Aune, M., Darnerud, P. O., Cnattingius, S., Bjerselius, R., Becker, W., & Lignell, S. (2007). Determinants of serum concentrations of organochlorine compounds in Swedish pregnant women: a cross-sectional study.Environmental health : a global access science source,6, 2. https://doi.org/10.1186/1476-069X-6-2

Jaraczewska, K., Lulek, J., Covaci, A., Voorspoels, S., Kaluba-Skotarczak, A., Drews, K., & Schepens, P. (2006). Distribution of polychlorinated biphenyls, organochlorine pesticides and polybrominated diphenyl ethers in human umbilical cord serum, maternal serum and milk from Wielkopolska region, Poland. The Science of the total environment, 372(1), 20–31. https://doi.org/10.1016/j.scitotenv.2006.03.030

Klinčić, D., Herceg Romanić, S., Matek Sarić, M., Grzunov, J. and Dukić, B., (2014). Polychlorinated biphenyls and organochlorine pesticides in human milk samples from two regions in Croatia. Environmental Toxicology and Pharmacology, 37(2), pp.543-552. https://doi.org/10.1016/j.etap.2014.01.009

Krauthacker B. (2000). Organochlorine Compounds In Croatian Population. Arch Hig Rada Toxicol.; 51 Supplement: 75–87.

Lignell, S., Aune, M., Darnerud, P. O., Cnattingius, S., & Glynn, A. (2009). Persistent organochlorine and organobromine compounds in mother's milk from Sweden 1996-2006: compound-specific temporal trends. Environmental research, 109(6), 760–767. https://doi.org/10.1016/j.envres.2009.04.011

Longnecker, M. P., Rogan, W. J., & Lucier, G. (1997). The human health effects of DDT (dichlorodiphenyltrichloroethane) and PCBS (polychlorinated biphenyls) and an overview of organochlorines in public health. Annual review of public health, 18, 211–244. https://doi.org/10.1146/annurev.publhealth.18.1.211

Ma, R., & Sassoon, D. A. (2006). PCBs exert an estrogenic effect through repression of the Wnt7a signaling pathway in the female reproductive tract. Environmental health perspectives, 114(6), 898–904. https://doi.org/10.1289/ehp.8748

Meeker, J. D. (2012). Exposure to environmental endocrine disruptors and child development. Archives of Pediatrics & Adolescent Medicine, 166(6), E1–E7. https://doi.org/10.1001/archpediatrics.2012.241

National Implementation Plan for theStockholm Convention in Bosnia and Herzegovina. https://www.informea.org/sites/default/files/imported-documents/UNEP-POPS-NIP-BosniaandHerzegovina-1.English.pdf retrieved 2020-11-20.

Olisah, C., Okoh, O. O., & Okoh, A. I. (2020). Occurrence of organochlorine pesticide residues in biological and environmental matrices in Africa: A two-decade review. Heliyon, 6(3), e03518. https://doi.org/10.1016/j.heliyon.2020.e03518

Polder, A., Gabrielsen, G. W., Odland, J. Ø., Savinova, T. N., Tkachev, A., Løken, K. B., & Skaare, J. U. (2008).

Spatial and temporal changes of chlorinated pesticides, PCBs, dioxins (PCDDs/PCDFs) and brominated flame retardants in human breast milk from Northern Russia. The Science of the total environment, 391(1), 41–54. https://doi.org/10.1016/j.scitotenv.2007.10.045

Rissato, S. R., Galhiane, M. S., Ximenes, V. F., de Andrade, R. M., Talamoni, J. L., Libânio, M., de Almeida, M. V., Apon, B. M., & Cavalari, A. A. (2006). Organochlorine pesticides and polychlorinated biphenyls in soil and water samples in the Northeastern part of São Paulo State, Brazil. Chemosphere, 65(11), 1949–1958. https://doi.org/10.1016/j.chemosphere.2006.07.011

Runkel, A. A., Križanec, B., Lipičar, E., Baskar, M., Hrženjak, V., Kodba, Z. C., Kononenko, L., Kanduč, T., Mazej, D., Tratnik, J. S., & Horvat, M. (2021). Organohalogens: A persisting burden in Slovenia?. Environmental research, 198, 111224. https://doi.org/10.1016/j.envres.2021.111224

Sabadoš D., Rajšić B. (1964) Determination of fat content in milk according to Gerber method, Mljekarstvo14(9): 193-208.

Szyrwińska, K., & Lulek, J. (2007). Exposure to specific polychlorinated biphenyls and some chlorinated pesticides via breast milk in Poland. Chemosphere, 66(10), 1895–1903. https://doi.org/10.1016/j.chemosphere.2006.08.010

Todaka, T., Hirakawa, H., Kajiwara, J., Hori, T., Tobiishi, K., Yasutake, D., Onozuka, D., Sasaki, S., Miyashita, C., Yoshioka, E., Yuasa, M., Kishi, R., Iida, T., & Furue, M. (2010). Relationship between the concentrations of polychlorinated dibenzo-p-dioxins, polychlorinated dibenzofurans, and polychlorinated biphenyls in maternal blood and those in breast milk. Chemosphere, 78(2), 185–192. https://doi.org/10.1016/j.chemosphere.2009.09.047

Turrio-Baldassarri, L., Abate, V., Alivernini, S., Battistelli, C. L., Carasi, S., Casella, M., Iacovella, N., Iamiceli, A. L., Indelicato, A., Scarcella, C., & La Rocca, C. (2007). A study on PCB, PCDD/PCDF industrial contamination in a mixed urban-agricultural area significantly affecting the food chain and the human exposure. Part I: soil and feed. Chemosphere, 67(9), 1822–1830. https://doi.org/10.1016/j.chemosphere.2006.05.124

UNEP. 2009. Status report on the human milk survey conducted jointly by the Secretariat of the Stockholm Convention and the World Health Organization. Geneva

UNEP. 2011. Regional monitoring reports under the global monitoring plan for effectiveness evaluation: additional tissue data from the human milk survey. Geneva

UNEP. 2012. National Implementation Plan for the Stockholm Convention on Persistent Organic Pollutants – Bosnia and Herzegovina. United Nations Environment Programme.

https://www.pops.int/ accessed on 13/12/2020.

UNEP. 2017. United Nations Environment Programme. Guidelines for Organizations, Sampling and Analysis of Human Milk on Persistent Organic Pollutants. Available at: https://wedocs.unep.org/20.500.11822/27639 Retrieved 10/10/2019.

Vafeiadi, M., Roumeliotaki, T., Chalkiadaki, G., Rantakokko, P., Kiviranta, H., Fthenou, E., Kyrtopoulos, S. A., Kogevinas, M., & Chatzi, L. (2017). Persistent organic pollutants in early pregnancy and risk of gestational diabetes mellitus. Environment International, 98, 89–95. https://doi.org/10.1016/j.envint.2016.10.005

Vukavić, T., Miloradov, M. V., Ristivojević, A., & Hlpka, J. (2008). PCB pollution of early milk in the Province of Vojvodina. Environmental Toxicology and Pharmacology, 25(2), 176–178. https://doi.org/10.1016/j.etap.2007.10.012

Wang, S. L., Chang, Y. C., Chao, H. R., Li, C. M., Li, L. A., Lin, L. Y., & Päpke, O. (2006). Body burdens of polychlorinated dibenzo-p-dioxins, dibenzofurans, and biphenyls and their relations to estrogen metabolism in pregnant women. Environmental health perspectives, 114(5), 740–745. https://doi.org/10.1289/ehp.8809

Wittsiepe, J., Fürst, P., Schrey, P., Lemm, F., Kraft, M., Eberwein, G., Winneke, G., & Wilhelm, M. (2007). PCDD/F and dioxin-like PCB in human blood and milk from German mothers. Chemosphere, 67(9), S286–S294. https://doi.org/10.1016/j.chemosphere.2006.05.118

Wong, C. K., Leung, K. M., Poon, B. H., Lan, C. Y., & Wong, M. H. (2002). Organochlorine hydrocarbons in human breast milk collected in Hong Kong and Guangzhou. Archives of Environmental Contamination and Toxicology, 43(3), 364–372. https://doi.org/10.1007/s00244-002-1210-7

Zhang, H. B., Luo, Y. M., Zhao, Q. G., Wong, M. H., & Zhang, G. L. (2006). Residues of organochlorine pesticides in Hong Kong soils. Chemosphere, 63(4), 633–641. https://doi.org/10.1016/j.chemosphere.2005.08.006

Zhao, G., Xu, Y., Li, W., Han, G., & Ling, B. (2007). PCBs and OCPs in human milk and selected foods from Luqiao and Pingqiao in Zhejiang, China. The Science of the total environment, 378(3), 281–292. https://doi.org/10.1016/j.scitotenv.2007.03.008

Zietz, B. P., Hoopmann, M., Funcke, M., Huppmann, R., Suchenwirth, R., & Gierden, E. (2008). Long-term biomonitoring of polychlorinated biphenyls and organochlorine pesticides in human milk from mothers living in northern Germany. International Journal of Hygiene and Environmental Health, 211(5-6), 624–638. https://doi.org/10.1016/j.ijheh.2008.04.001

Summary/Sažetak

Jedan od najvećih izazova današnjice je zagađenje okoliša, koje dovodi do ozbiljnih prijetnji ljudskom zdravlju i cjelokupnom ekosistemu. Zbog svoje visoke postojanosti i slabe biorazgradivosti, polihlorirani bifenili (PCB) i organohlorirani pesticidi (OCP), kao glavne kategorije okolišnih zagađivača antropogenog porijekla, ostaju prisutni u okolišu duži vremenski period, kontinuirano kružeći između zraka, vode i tla, te predstavljaju trajni rizik za javno zdravlje. Bosna i Hercegovina ranije nije provodila studije o prisutnosti okolišnih zagađivača u majčinom mlijeku, čiji bi rezultati mogli doprinijeti efikasnijoj zaštiti javnog zdravlja i poslužiti kao osnova za strateško planiranje usmjereno na smanjenje izloženosti ovim zagađivačima. Iz tog razloga, cilj ove studije bio je utvrditi nivoe odabranih postojanih organskih polutanata (PCB i OCP) u majčinom mlijeku dojilja (N=67) iz Bosne i Hercegovine (Federacija Bosne i Hercegovine, Republika Srpska i Brčko Distrikt). Ovdje prikazani rezultati prvi su te vrste na teritoriji naše zemlje. Prosječne vrijednosti kvantificiranih koncentracija PCB (17 kongenera) i OCP (8 spojeva) kretale su se u rasponu od 1.03 do 162.29 ng/g l.w., odnosno od 0.27 do 14.64 ng/g l.w. PCB kongeneri 52, 77, 126 i 169 su kvantificirani u višim koncentracijama u usporedbi s onima zabilježenim u nekim europskim i azijskim zemljama. U Brčko Distriktu i Republici Srpskoj pronađene su više vrijednosti u usporedbi s Federacijom Bosne i Hercegovine. Izmjerene koncentracije odabranih postojanih polutanata u uzorcima majčinog mlijeka prikupljenih u Bosni i Hercegovini uglavnom odgovaraju literaturnim podacima iz sličnih studija provedenih u zemljama regije i Evrope.

Bulletin of the Chemists and Technologists
Glasnik hemičara i tehnologa Bosne i Hercegovine
2026
66
13-21
Original Scientific Article
Print ISSN: 0367-4444
Online ISSN: 2232-7266
DOI: 10.35666/2232-7266.2026.66.02
UDK: 543[547.79:547.78]

Understanding MTT–Graphene Oxide Interactions for Accurate Viability Measurements

Ćetković Pećar, T.[a], Haverić, A.[a], Haverić, S.[a], Gutić, S.J.[b,*]

[a]*University of Sarajevo – Institute for Genetic Engineering and Biotechnology, Zmaja od Bosne 8, Sarajevo, Bosnia and Herzegovina*

[b] *University of Sarajevo – Faculty of Science, Zmaja od Bosne 33-35, Sarajevo, Bosnia and Herzegovina*

Article info
Received: 03/12/2025
Accepted: 04/02/2026

Keywords:
Colorimetric assay
MTT assay
Graphene oxide
Adsorption
Nanomaterial interference

***Corresponding author:**
E-mail: sgutic@pmf.unsa.ba
Phone: +-387-61-337636

Abstract: Large surface enriched with oxygen-containing groups, enabling interactions with various molecules, makes graphene oxide (GO) valuable in sensing, imaging, and therapy but complicates cytotoxicity assessment using standard colorimetric assays. In this study we examined adsorption of tetrazolium (MTT) ion, used as a dye in colorimetric assay, on GO. Using a cell-free system, adsorption behavior was modelled with Freundlich, Langmuir, and Langmuir–Freundlich (Sips) isotherms. Satisfactory fits were obtained by all models. However, the Sips model provided the best nonlinear regression performance, while Langmuir fit best under linear regression. π–π interactions between MTT and the GO aromatic rings were discussed as the most probable driving force for the adsorption. Interactions between GO and components of the culture medium (DMEM) and serum (FBS) were indirectly observed by comparing MTT monolayer capacity values with the values obtained in aqueous MTT solutions. The results confirm that GO interactions with MTT, responsible for the interferences, can be described quantitatively in the presence of cell supporting medium and that corrective adjustments of the colorimetric assay results may be required, yet the question remains whether such corrections can be applied in practice. The present study provides an initial foundation for assessing their feasibility.

INTRODUCTION

Growing interest for the application of graphene nanomaterials (GNMs) in the biotechnological and biomedical fields has been evident (Kumar et al., 2023). Accordingly, accurate *in vitro* assessment of their potential cytotoxicity, oxidative stress induction, genotoxicity, and inflammatory effects, along with determination of the mechanisms of action of GNMs in cell membrane and cellular components damage is crucial (Gurunathan S et al., 2019; Frontiñan-Rubio et al., 2022).

Classical methods for cytotoxicity investigation are based on colorimetric tests with organic tetrazolium dyes, such as 3-(4,5-di methyl thiazol-2-yl)-2,5-diphenyltetrazolium bromide (MTT) (van Meerloo et al., 2011). Despite the large number of studies reporting the use of the MTT assay for the toxicological evaluation of graphene oxide nanomaterials (Seabra et al., 2014), several have also highlighted specific limitations that may affect the accuracy and reliability of cytotoxicity assessments of namely carbon-nanotubes (Wörle-Knirsch et al. 2006; Casey et al. 2007a, Ali-Boucetta et al., 2011), graphene (Jiao et al., 2015) and graphene oxide (Liao et al., 2011). Challenges in cytotoxicity assessment of nanoparticles in general are related to diverse potential interactions between nanoparticles and dye molecules, or their reduced forms (formazans), and those interactions can be very specific (Jiao et al., 2015; Monteiro-Riviere et al., 2009; Belyanskaya et al., 2007; Wörle-Knirsch et al., 2006). The study by Wörle-Knirsch et al. (2006) demonstrated that single-walled carbon nanotubes (SWCNTs) interact with MTT formazan crystals, leading to inaccurate assay results. Additionally, Casey et al. (2007a) showed that dispersing (SWCNTs) in cell culture medium induces color changes due to molecular interactions with medium components, as confirmed by spectroscopic analysis. Moreover, they demonstrated that SWCNTs interfered with several viability assays, including MTT, by interacting with indicator dyes and reducing their absorbance in a concentration-dependent manner (Casey et al., 2007b).

Under the "graphene" umbrella one can find various materials (eg. graphene oxide, reduced graphene oxide, quantum dots, etc.) with a variety of physical and chemical features including specific shape and size, crystalline structure and presence of various functional groups and structural defects, which makes generalization of their impact on the reliability of cytotoxicity assessment practically impossible.

Graphene oxide (GO) nanomaterials possess the ability to adsorb biomolecules via multiple interaction mechanisms, including hydrogen bonding, hydrophobic interactions, π-π stacking, and both electrostatic and van der Waals forces (Nel et al., 2009). Such interactions facilitate the adsorption of proteins from fetal bovine serum onto the GO surface, leading to the formation of a protein corona that further alters the nanomaterial's physicochemical properties and biological interactions (Cedervall et al., 2007; Hu et al., 2011; Wei et al., 2015). Optical characteristics of graphene can present additional challenges for *in vitro* tests, particularly due to absorption and reflection effects. Some studies have shown that absorption increases with the thickness of the graphene layer, with each additional graphene layer contributing to a 2.3% rise in absorption intensity (Nair et al., 2008; Bonaccorso et al., 2010). As a result, the optical properties of graphene may lead to the loss of light signals during *in vitro* studies (Jiao et al., 2015).

In this work we investigated interactions of MTT with commercially available GO material in simple aqueous solutions as well as in the presence of Dulbecco's Modified Eagle Medium (DMEM) and Fetal Bovine Serum (FBS). Experimentally obtained adsorption data was modelled with Freundlich, Langmuir, and Langmuir-Freundlich isotherms by both linear and nonlinear regression. Specific interactions between MTT and GO, as well as the differences in the values of adsorption constants for simple aqueous solutions and solutions containing cell supporting medium were discussed in accordance with structural features obtained from the detailed GO characterization.

Perspective was given on the feasibility of the introduction of experimental correction in the MTT assay, based on the knowledge on the adsorption behavior.

EXPERIMENTAL

Materials and chemicals

All materials used in this study, including commercially available graphene oxide (4 mg mL^{-1} suspension)[1], Dulbecco's Modified Eagle Medium (DMEM), fetal bovine serum (FBS), and the MTT reagent, were obtained from Sigma-Aldrich (St. Louis, MO, USA).

Material characterization

Graphene oxide was characterized by Fourier transform infrared spectroscopy (FTIR), Raman spectroscopy, X-ray diffraction (XRD), and cyclic voltammetry (CV).

Fourier-transform infrared (FTIR) spectra were recorded in attenuated total reflectance (ATR) mode using a PerkinElmer UATR Two spectrometer. Aqueous suspensions were drop-casted directly onto the ATR crystal and dried at room temperature. Spectra were collected at room temperature over the range of 400 to 4000 cm^{-1}, with a resolution of 1 cm^{-1}.

Raman spectra were obtained with a DXR Raman microscope (Thermo Scientific, USA) equipped with an Olympus optical microscope and a CCD detector. The sample was prepared by drop-casting of aqueous suspension onto a gold surface. Raman spectra were collected for dry GO sample, by excitation with a HeNe gas laser (excitation wavelength 532 nm) beam focused using magnification 50×. The scattered photons were analyzed by the spectrograph with a grating of 900 lines mm^{-1}. Laser power on the sample was kept at 2 mW.

X-ray diffraction (XRD) patterns were collected for the sample suspended in water, using a Bruker D8 Advance diffractometer with Cu Kα1,2 radiation source. Generator voltage and current were 40.0 kV and 40.0 mA, respectively.

Cyclic voltammetry was performed using a three-electrode setup with Ag/AgCl/KClsat as the reference and a platinum wire as the counter electrode. Working electrode was prepared by drop-casting 10 μL of sample suspension (1 mg mL^{-1}) onto a clean glassy carbon disc (d = 5 mm). Measurements were conducted in 0.1 M KNO_3 over the reduction potential range (from open circuit to hydrogen evolution onset) at a sweep rate of 15 mV s^{-1}.

Spectrophotometric measurements

To investigate interactions of the graphene oxides with the MTT dye, each GO was incubated with a series of MTT dilutions in cell-free systems (Jiao et al., 2015), using two different adsorption media: (i) deionized water, denoted as W; (ii) deionized water with Dulbecco's Modified Eagle Medium (DMEM) supplemented with fetal bovine serum (FBS), denoted as WMS. In both cases MTT concentrations were 0.01, 0.02, 0.05, 0.07, 0.1, and 0.2 mg mL^{-1}. Each dilution contained 1 mg (0.44 mg mL^{-1}) of graphene oxide. Calibration curve was recorded by measuring the aqueous solutions of MTT without graphene oxide. All adsorption series were corrected with the corresponding blank – deionized water for W, and deionized water with DMEM and FBS for WMS samples. After 24 hours of incubation at 37°C with continuous mixing, a series of MTT reagent dilutions were added to each mixture, followed by an additional 3-hour incubation under the same conditions. Following MTT incubation, all samples were centrifuged at 16000 rpm for 10 minutes. Clear supernatants were transferred to 96 well plate in duplicate, and their absorbance was measured at 380 nm with the ThermoFisher Scientific Multiskan SkyHigh Microplate Spectrophotometer.

[1] https://www.sigmaaldrich.com/BA/en/product/aldrich/777676?context=product

RESULTS AND DISCUSSION

Characterization of graphene oxide

Typical absorption peaks expected for graphene oxides prepared by Hummers method can be observed in the infrared spectra of GO (Fig. 1). Adsorbed water molecules are responsible for the strong overlapping absorptions in the region between 2400 and 3700 cm^{-1}, as well as at 1620 cm^{-1} (Brusko et al., 2024). Although not observed for highly oxidized graphene oxides, peak at 1585 cm^{-1} is clearly observed for the GO sample. This absorption is connected to C=C stretching in the graphene lattice, and usually appears for partially reduced graphene oxides. Absorption at 1725 cm^{-1} is typical spectral feature of graphene oxide, originating from stretching of C=O bond from carboxylic groups, as well as any other carbonyl groups (Eigler and Dimiev, 2017) while shoulder at 1815 cm^{-1} probably originates of the C=O bond stretch in the ketone group. The band with the highest intensity in the fingerprint region of the spectra, observed at 1073 cm^{-1}, arise probably from the C-O vibrations in alcohol functional groups. Other two prominent bands from the fingerprint region, at 1411 and 1233 cm^{-1}, originate from covalently attached sulfate groups, which are present due to the preparation method (Brusko et al., 2024), although the latter can also be connected to epoxy groups (C-O-C), vibrations of which are responsible for the shoulder at 980 cm^{-1}.

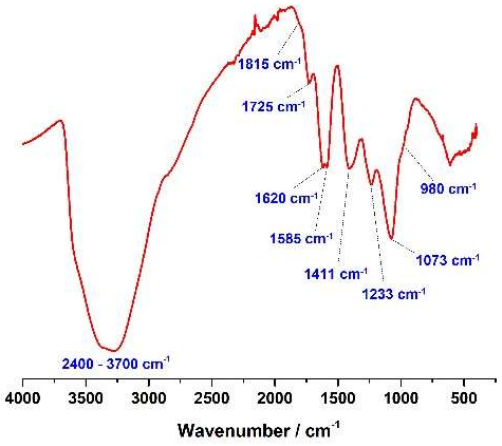

Figure 1. ATR-FTIR spectrum of dry graphene oxide

First and second order Raman spectra of dry GO sample, shown in Figure 2, were deconvoluted and with several characteristic peaks, as shown in Figure 2 (b. and c.). Although five peaks were used to fit the first-order spectrum of the sample, only four of them, namely D, D'', G, and D' have physical significance (López-Díaz et al., 2020). The shoulder arising from the D* peak, usually positioned around 1150 cm^{-1}, was not observed for this GO sample. Position of the nondispersive G peak was red-shifted to 1573 cm^{-1} (from 1585 cm^{-1} usually observed for graphene oxide), which may be an indication of AB stacking of graphene layers. The peaks arising from structural and chemical defects, denoted by D' and D, appear at 1610 cm^{-1} and 1355 cm^{-1}, respectively. Intensity ratio of these peaks, $A_{D'}/A_D$, can be used for the estimation of the dominant type of defects. In our case $A_{D'}/A_D$ was 0.082, indicating prevalence of sp^3 defects, caused by sulfate and oxygen-containing functional groups covalently attached to graphene basal plane. Position of another peak from the deconvoluted first-order spectrum, designated as D" and observed at 1500 cm^{-1}, reveals that oxygen content should be below 20 at% (Lopez-Díaz et al., 2017; Claramunt et al., 2015). Second-order part of the spectra was fitted with four Gaussian peaks designated as G*, 2D, D+D', and 2D'. Positions of the 2D and D+D' bands can be used for the estimation of percentage of sp^2-hybridized C atoms in graphene. For the GO sample wide 2D band appears at 2736 cm^{-1}, while D+D' band appears at 2932 cm^{-1}. FWHM value of 149 cm^{-1} for the former (six-fold the value for the pristine graphene) indicates that "2D" peak in fact consists of several overlapping peaks, which are not studied in detail in this work, thus position of wide "2D" peak cannot be used for the same estimation. However, position of the D+D' corresponds to the 51.7 % of sp^2 carbon atoms (López-Díaz et al., 2020), compared with the 63.1 %, estimated from the I_D/I_G ratio of 1.505 (Lopez-Díaz et al., 2017).

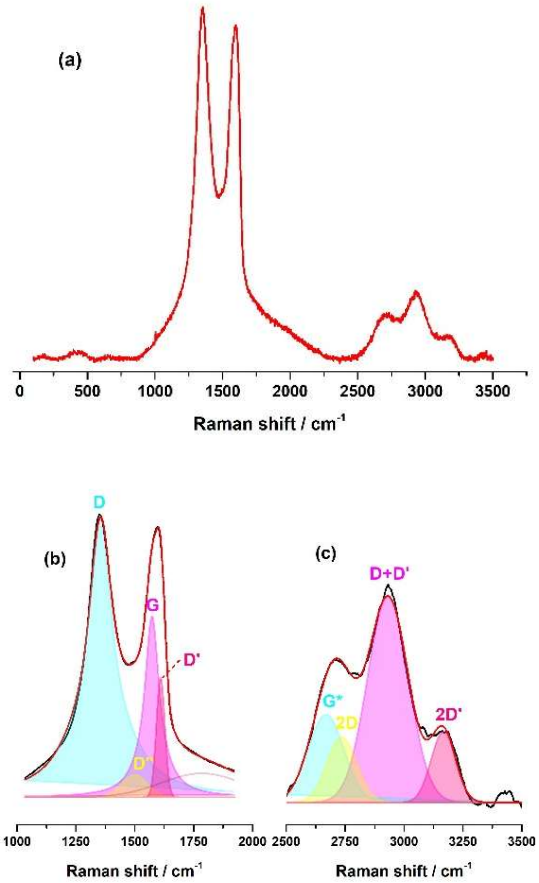

Figure 2. (a) Raman spectrum of dry graphene oxide; (b) First order Raman peaks; (c) second order Raman peaks.

XRD pattern of the GO sample (Figure 3) reveals weak and diffuse (002) graphite reflection around $2\theta = 25°$, while the characteristic graphene-oxide reflection at 2θ = 11.8°, arising from the larger distance between graphene-oxide

sheets (around 8 Å) compared to those of graphite, is not observed. Absence of this characteristic diffraction indicates high level of graphitization, which is in accordance with some features observed in Raman spectrum.

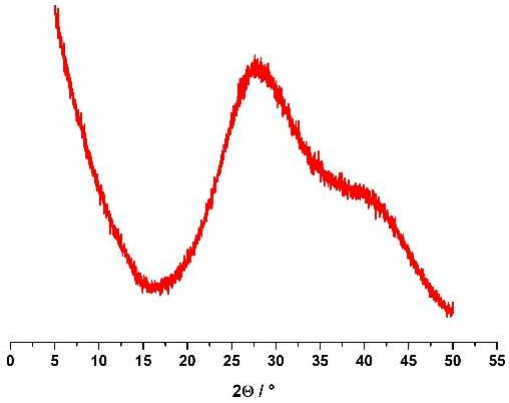

Figure 3. X-ray diffraction pattern of suspended graphene oxide

Redox behavior, estimated by cyclic voltammetry (Figure 4), is in accordance with the structural features observed from FTIR and Raman spectroscopies. First potential scan in negative direction leads to typical cathodic current peak at -1.4 V vs. Ag/AgCl reference, arising from the irreversible GO reduction, evident from the absence of corresponding oxidation peak on the backward scan, as well as the absence of reduction/oxidation peaks in the second scan. Specific charge consumed for the reduction of GO is 4.2 mC μg^{-1}, which gives a rough estimation of 52 % of sp^3 carbons with covalently attached reducible functional groups.

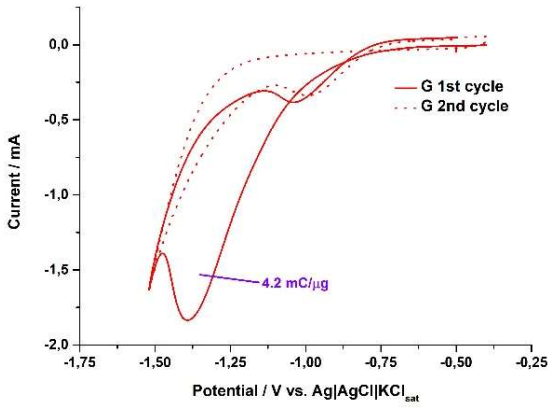

Figure 4. Cyclic voltammograms of graphene oxide film reduction in inert electrolyte

Adsorption of MTT

Nanomaterials introduced into complex culture media, especially those supplemented with FBS, undergo various physicochemical interactions that can significantly alter their surface properties and biological behavior. In particular, the rapid formation of a protein corona modifies their biological identity, affecting interactions with cells, medium components, and assay outcomes, as pointed in the literature (Cedervall et al., 2007; Hu et al., 2011; Wei et al., 2015). To try to elucidate the contribution of different components present during the colorimetric testing of viability, adsorption behavior of MTT dye was determined from two different adsorption media: (i) aqueous MTT solutions without additional components (denoted as "W"), and (ii) aqueous solutions containing constant concentration of Dulbecco's Modified Eagle Medium (DMEM) and Fetal Bovine Serum (FBS) (denoted as "WMS").

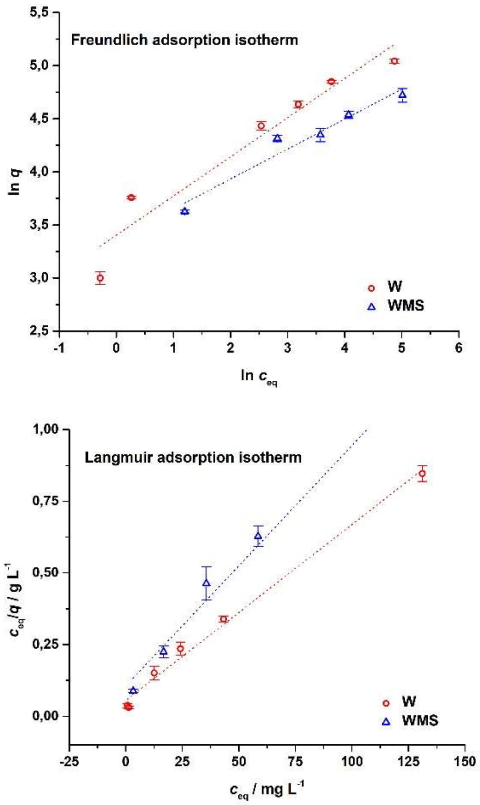

Figure 5. Adsorption of MTT on graphene oxide: linear fits of experimental results with Freundlich and Langmuir isotherm.

Three adsorption isotherms were used for fitting of the experimentally obtained results:

(i) Freundlich adsorption isotherm

$$q = k_F c_{eq}^{1/n} \quad (1)$$

(ii) Langmuir adsorption isotherm

$$q = \frac{q_{max} K_L c_{eq}}{1 + K_L c_{eq}} \quad (2)$$

(iii) Langmuir-Freundlich (Sips) adsorption isotherm

$$q = \frac{K_{LF} c_{eq}^{b_{LF}}}{1 + a_{LF} c_{eq}^{b_{LF}}} \quad (3)$$

where q / mg g^{-1} is the mass of the adsorbed MTT per unit mass of the adsorbent, c_{eq} / mg L^{-1} equilibrium concentration of MTT, and k_F, n, K_L, q_m, K_{LF}, a_{LF}, and b_{LF} constants for a particular isotherm. Data fitting was

performed by two approaches: (i) in MS Excel, using linear forms of Freundlich and Langmuir isotherms, and (ii) in online Desmos Graphing Calculator (https://www.desmos.com/), by nonlinear regressions for all three isotherms.

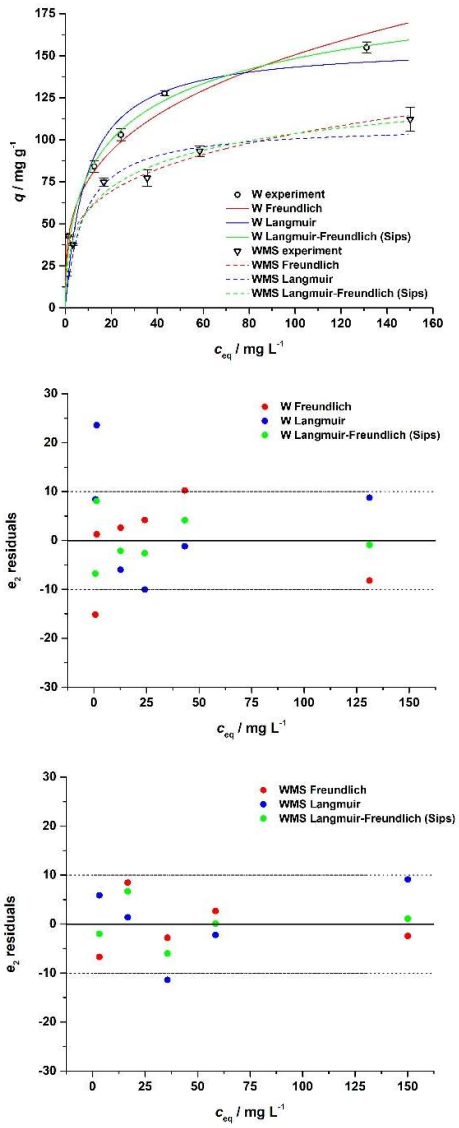

Figure 6. Nonlinear fits of experimental results with Freundlich, Langmuir and Langmuir-Freundlich (Sips) isotherms with corresponding e_2 residuals

Correlation coefficients for linear fitting of the experimental results have higher values when Langmuir model is applied, compared to the values obtained from the Freundlich model, for both adsorption media (Table 1, Figure 5). However, in nonlinear approach (Table 1, Figure 6) the correlation coefficients decrease in the order Langmuir-Freundlich (Sips) > Freundlich > Langmuir for both adsorption media. Comparing the linear and nonlinear regression for Freundlich and Langmuir models reveals that nonlinear approach leads to a better fit for Freundlich model, while linear approach gives better correlation for Langmuir model. It is also important to note that in the case of Freundlich model nonlinear fit leads to higher values of constants, compared to the linear fit, while the opposite is true for Langmuir model. Differences between parameter values obtained by linear and nonlinear regression arise from distortions in the error distribution caused by data transformation during linearization (Hu et al., 2023). Although linearization is straightforward and commonly used, isotherm parameters derived in this manner are presented here only to highlight the bias introduced by linearization. In the following discussion parameters obtained from nonlinear regression will be considered, particularly because of the application of the multi-parameter Langmuir–Freundlich (Sips) model.

Table 1: Adsorption isotherm parameters

Freundlich adsorption isotherm

Medium	W		WMS	
Fitting	Linear	Nonlinear	Linear	Nonlinear
k_F [*1]	30±2	38±1	29±1	32.9±0.1
n	2.7±0.1	3.4±0.1	3.6±0.3	4.0±0.2
R^2	0.9346	0.9670	0.9500	0.9550

Langmuir adsorption isotherm

Medium	W		WMS	
Fitting	Linear	Nonlinear	Linear	Nonlinear
K_L [*2]	0.11±0.02	0.109±0.007	0.079±0.005	0.13±0.02
q_{max} [*3]	163±4	156±1	120±8	109±9
R^2	0.9927	0.9350	0.9922	0.9169

Langmuir-Freundlich (Sips) adsorption isotherm

Medium	W		WMS	
Fitting	Linear	Nonlinear	Linear	Nonlinear
K_{LF} [*4]	-	36±2	-	29±3
a_{LF} [*5]	-	0.15±0.01	-	0.18±0.02
b_{LF}	-	0.531±0.008	-	0.50±0.06
R^2	-	0.9891	-	0.9718

[*1] / (mg/g)/(L/mg)^n; [*2] / L/mg; [*3] / mg/g; [*4] / L/g; [*5] / L/mg

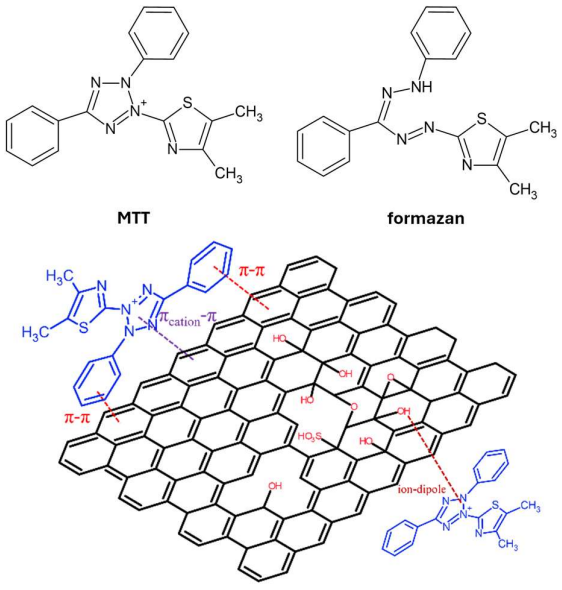

Figure 7. Structures of MTT, formazan and graphene oxides, and some of the possible interactions between the MTT molecule and graphene oxide.

Characterization of the sample, as discussed earlier, revealed some basic features of the graphene oxide structure, which are responsible for interactions with MTT dye, as well as with other components of the medium. Between 50 and 60 % of the carbon atoms from the GO sample structure are sp^3-hybridized and covalently connected to polar functional groups such as alcohol, epoxy, carbonyl or sulfate, that enable interaction with the adsorbate species via dipole-dipole or dipole-ion interactions. The difference between the percentage of sp^3-hybridized C atoms and the estimated oxygen content (less than 20 %) is potentially related to the high content of epoxy groups, compared to other functionalities. In any case, the rest of the C atoms (40 – 50 % of sp^2-hybridized) form aromatic graphene structure which enables π-π interactions with the species containing aromatic rings.

Both MTT and the corresponding formazan molecule (Fig. 7), contain aromatic rings that can interact with the graphene via π-π interactions (Fig. 7). Furthermore, MTT dye is aromatic cation available and applied in a form of bromide salt, which opens up the possibility for a different types of interactions, including π_{cation}-π, dipole-ion or even ionic interactions with anionic groups on graphene at the higher pH values (Fig. 7). Interaction energies drop several orders of magnitude in the series ion-ion > dipole-ion > π_{cation}-π > π-π (Georgakilas et al., 2012), implying that the former will be thermodynamically favorable. However, the positive charge of the MTT ion is located in the aromatic ring, with the two exposed benzene rings, which significantly increases contribution of π_{cation}-π and π-π interactions in bulk adsorption (Georgakilas et al., 2012). Furthermore, in aqueous solution dominant functional groups attached to the graphene surface are either unable to dissociate (epoxy groups) or are very weak acids (alcohol groups) (Lu et al., 2021), which leaves a small fraction of acidic groups (sulfate and carboxylic) for the ion-ion interaction. Variety of the possible interactions is in the agreement with the values of the constants n and b_{LF} (Table 1.) obtained from fitting with Freundlich and Langmuir-Frenudlich (Sips) model respectively, which point to the heterogeneous adsorption (Murphy et al., 2023).

The MTT assay is based on a spectrophotometric measurement of formazan, a colored product formed through the reduction of the yellow, water-soluble tetrazolium salt (MTT) by mitochondrial dehydrogenases, cytoplasmic NAD(P)H-dependent oxidoreductases and other reducing agents in metabolically active cells. The reduction of MTT yields a violet-blue, water-insoluble formazan that accumulates in lipid droplets and can be solubilized with organic solvents for spectrophotometric quantification of cell viability. It is important to note that adsorption studies performed in cell-free systems capture only part of the complexity of cytotoxicity assays. While they provide valuable information on physicochemical interactions between graphene nanomaterials and assay components (Monteiro-Riviere et al., 2009), real cellular environments introduce additional layers of complexity, including membrane dynamics, metabolic activity, intracellular trafficking, and signaling cascades. These processes can modulate both the extent and the biological consequences of adsorption, meaning that results obtained in simplified systems should be interpreted as complementary to cellular assays. This distinction is crucial for accurate evaluation of the biological impact of graphene nanomaterials.

Since the reduction product (formazan) is the species quantified in the assay, it is necessary to consider whether adsorption of its precursor (MTT) alone is sufficient to evaluate the impact of interactions with the material studied on assay outcomes. Given that the graphene oxide particles used here have size distributions of D90 = 5–7 µm, D50 = 2–4 µm, and D10 = 1–2 µm (https://www.sigmaaldrich.com/BA/en/product/aldrich/777676?srsltid=AfmBOopH5rtQ6uspqC8TFsQ_1N6ru6UvIOYDsiFd66a1hsFRCe733lUg, accessed 29/12/2025), comparable to the size of cells typically analyzed by the MTT assay, internalization of GO particles carrying adsorbed MTT is limited, thereby preventing intracellular formazan formation. Consequently, measurements of MTT adsorption are sufficient for assessing assay interference in cytotoxicity studies involving cells of comparable dimensions. Under these conditions, measurements of MTT adsorption may provide a reasonable approximation for evaluating assay interference in cytotoxicity studies involving cells of comparable dimensions.

Based on its molecular structure, we hypothesize that the corresponding formazan may also interact with graphene oxide, predominantly through π–π interactions, as it is an electrically neutral molecule with weak dipole moments. This raises the possibility that, even if MTT–GO complexes are internalized and MTT is subsequently reduced within viable cells, the resulting formazan may remain susceptible to adsorption onto graphene oxide. Such interactions could reduce the fraction of free formazan available for optical detection, thereby potentially compromising the reliability of absorbance-based cytotoxicity measurements.

Adsorption of proteins and other components of the fetal bovine serum, described in the literature (Cedervall et al., 2007; Hu et al., 2011; Wei et al., 2015), is evident from the decrease in the Langmuir's monolayer adsorption capacity, q_{max}. For the adsorption of MTT from pure aqueous solution q_{max} has a value of 156 mg g^{-1}, while the same parameter dropped to 109 mg g^{-1} for the adsorption of MTT from a solution containing DMEM and FBS. Influence of DMEM and FBS on the adsorption strength of MTT is also observable from the lower Freundlich constant (k_F) values, compared to values obtained from the simple aqueous solution of MTT, indicating weaker MTT-GO interactions when other adsorbates are present. DMEM and FBS components – soluble proteins and salts – compete with the MTT molecules for the hydrophilic and ionic adsorption sites, leaving aromatic sites for the exclusive adsorption of MTT through weaker π-π interactions. Another noteworthy observation is that values of a_{LF} and b_{LF} did not differ significantly for simple aqueous solutions and solutions containing DMEM and FBS, while the K_{LF} value reduced from 36 to 29 L g^{-1}. Since ratio K_{LF}/a_{LF} represents the monolayer adsorption capacity (Wang and Guo, 2020) obtained from Langmuir-Freundlich model values of 240 and 161 mg g^{-1} were calculated for adsorption of MTT from simple aqueous solution and solution with DMEM and FBS, respectively. As in the case for the q_{max} values determined from

Langmuir model, monolayer capacity for MTT is higher in aqueous solution without DMEM and FBS. However, Langmuir isotherm describes homogenous monolayer adsorption, while Langmuir-Freundlich (Sips) model assumes several different absorption sites with distinct adsorption energies, which makes the latter more relevant for quantitative description when graphene oxide acts as adsorbent for MTT. Although the Freundlich adsorption isotherm is one of the most widely used empirical models, while Langmuir adsorption isotherm is the most famous theoretical model, neither model alone adequately describes the heterogeneous nature of the present system, involving both the adsorbent (graphene oxide) and the adsorbates (MTT and other medium components) over a wide concentration range. While Freundlich isotherm provides satisfactory fits over medium concentration ranges and does not predict a saturation plateau at high concentrations, the applicability of the Langmuir isotherm is restricted to the adsorption of non-interacting adsorbate molecules on energetically equivalent sites (Hu et al., 2023; Al-Ghouti and Da'ana 2020). These limitations are evident from the residuals obtained by nonlinear fitting (Fig. 6). In contrast, satisfactory fits across the entire concentration range are achieved using the Sips adsorption isotherm, which combines features of the Langmuir and Freundlich models.

CONCLUSIONS

The results suggest that the affinity between graphene oxide and MTT arises from multiple possible interaction mechanisms, including π–π, dipole–dipole, and limited dipole–ion interactions. Structural characterization indicates that both sp^2-hybridized aromatic domains and oxygen-containing functional groups bonded to sp^3 carbon atoms contribute to these interactions, which aligns with isotherm parameters indicating a heterogeneous adsorption environment. The exposed aromatic rings of MTT favour π–π interactions with aromatic graphene regions, while the sterically shielded ionic center limits stronger ion–ion and ion-dipol contributions. According to these considerations the corresponding formazan product is also expected to adsorb strongly and remain non-desorbed under assay conditions.

Quantitative modelling further supports these mechanistic insights. Although linear regression suggests better performance of the Langmuir model, nonlinear fitting reveals that the Langmuir–Freundlich (Sips) model most accurately describes the adsorption behaviour, reflecting the heterogeneity of GO surface sites. The competition between MTT and supporting medium components is evident from reduced adsorption parameters in DMEM/FBS-containing solutions, indicating that proteins and salts occupy hydrophilic or ionic adsorption sites while leaving aromatic π-domains available for weaker interactions with MTT. This effect is consistently reflected in decreases in both Langmuir monolayer capacity and Langmuir–Freundlich model parameters.

Taken together, these findings provide a description of graphene oxide interactions with MTT under conditions relevant to cytotoxicity testing. The results quantitatively demonstrate that medium constituents significantly modulate adsorption behaviour and that both MTT and formazan can remain bound to GO with limited desorption. These mechanistic and modelling insights form a necessary foundation for evaluating how such interactions affect spectrophotometric readouts and represent an important first step toward assessing the broader implications for the reliability of colorimetric cell viability assays involving graphene-based nanomaterials.

Since the graphene oxide used in this study represents a highly specific material within the graphene family, the findings presented here cannot be directly extrapolated to other materials, even within the "graphene oxide" subcategory. To generalize the impact of graphene oxide on the reliability of cytotoxicity assessments, further studies employing multiple, thoroughly characterized GO materials are required. In contrast, generalization of the behavior across the entire graphene family appears impractical due to the extensive diversity of structural and chemical characteristics. Also, further investigation of formazan adsorption to graphene oxide is essential to clarify its contribution to assay interference and to improve the reliability of absorbance-based cytotoxicity assessments involving graphene-derived materials.

REFERENCES

Al-Ghouti, M. A., Da'ana, D. A. (2020). Guidelines for the use and interpretation of adsorption isotherm models: A review. *Journal of Hazardous Materials*, 393, 122383.

Ali Boucetta, H., Al Jamal, K. T., Müller, K. H., Li, S., Porter, A. E., Eddaoudi, A., Prato, M., Bianco, A., & Kostarelos, K. (2011). Cellular uptake and cytotoxic impact of chemically functionalized and polymer coated carbon nanotubes. *Small*, 7(22), 3230–3238.

Belyanskaya, L., Manser, P., Spohn, P., Bruinink, A., & Wick, P. (2007). The reliability and limits of the MTT reduction assay for carbon nanotubes–cell interaction. *Carbon*, 45(13), 2643–2648.

Bonaccorso, F., Sun, Z., Hasan, T., & Ferrari, A. C. (2010). Graphene photonics and optoelectronics. *Nature Photonics, 4*(9), 611–622.

Brusko, V., Khannanov, A., Rakhmatullin, A., Dimiev, A. M. (2024). Unraveling the infrared spectrum of graphene oxide. *Carbon*, 229.

Casey, A., Davoren, M., Herzog, E., Lyng, F. M., Byrne, H. J., & Chambers, G. (2007a). Probing the interaction of single-walled carbon nanotubes within cell culture medium as a precursor to toxicity testing. Carbon, 45, 34–40.

Casey, A., Herzog, E., Davoren, M., Lyng, F. M., Byrne, H. J., & Chambers, G. (2007b). Spectroscopic analysis confirms the interactions between single walled carbon nanotubes and various dyes commonly used to assess cytotoxicity. *Carbon*, 45, 1425–1432.

Cedervall, T., Lynch, I., Lindman, S., Berggård, T., Thulin, E., Nilsson, H., … & Linse, S. (2007). Understanding the nanoparticle–protein corona using methods to quantify exchange rates and affinities of proteins for nanoparticles. *Proceedings of the National Academy of Sciences*, 104(7), 2050–2055.

Claramunt, S., Varea, A., Lopez-Díaz, D., Velázquez, M. M., Cornet, A., Cirera, A. (2015). The importance of interbands on the interpretation of the Raman spectrum of graphene oxide. *The Journal of Physical Chemistry C*, 119, 10123–10129.

Eigler, S., Dimiev, A. M. (2017). Characterization techniques. In A. M. Dimiev & S. Eigler (Eds.), *Graphene oxide: Fundamentals and applications* (pp. 85–120). John Wiley & Sons.

Frontiñan Rubio, J., González, V. J., Vázquez, E., & Durán Prado, M. (2022). Rapid and efficient testing of the toxicity of graphene related materials in primary human lung cells. *Scientific Reports*, 12(1), 7664.

Geograkilas, V., Otyepka, M., Bourlinos, A. B., Chandra, V., Kim, N., Kemp, K. C., Hobza, P., Zboril, R., Kim, K. S., (2012). Functionalization of Graphene: Covalent and Non-Covalent Approaches, Derivatives and Applications. *Chemical Reviews*, 112, 6156–6214.

Gurunathan, S., Arsalan Iqbal, M., Qasim, M., Park, C. H., Yoo, H., Hwang, J. H., … & Hong, K. (2019). Evaluation of graphene oxide induced cellular toxicity and transcriptome analysis in human embryonic kidney cells. *Nanomaterials*, 9(7), 969.

Hu, W., Peng, C., Lv, M., Li, X., Zhang, Y., Chen, N., Fan, C., & Huang, Q. (2011). Protein corona-mediated mitigation of cytotoxicity of graphene oxide. *ACS Nano*, 5(5), 3693–3700.

Hu, Q., Lan, R., He, L., Liu, H., Pei, X. (2023). A critical review of adsorption isotherm models for aqueous contaminants: Curve characteristics, site energy distribution and common controversies. *Journal of Environmental Management*, 329, 117104

Jiao, G., He, X., Li, X., Qiu, J., Xu, H., Zhang, N., & Liu, S. (2015). Limitations of MTT and CCK-8 assay for evaluation of graphene cytotoxicity. *RSC Advances*, 5(66), 53240–53244.

Kumar, R., Singh, D. P., Muñoz, R., Amami, M., Singh, R. K., Singh, S., & Kumar, V. (2023). Graphene based materials for biotechnological and biomedical applications: Drug delivery, bioimaging and biosensing. Materials Today Chemistry, 33, 101750.

Liao, K. H., Lin, Y. S., Macosko, C. W., & Haynes, C. L. (2011). Cytotoxicity of graphene oxide and graphene in human erythrocytes and skin fibroblasts. *ACS Applied Materials & Interfaces*, 3, 2607–2615.

López-Díaz, D., Delgado-Notario, J. A., Clericò, V., Diez, E., Merchán, M. D., Velázquez, M. M. (2020). Towards understanding the Raman spectrum of graphene oxide: The effect of the chemical composition. *Coatings*, 10(6), 524.

Lopez-Díaz, D., Lopez Holgado, M., García-Fierro, J. L., Velázquez, M. M. (2017). Evolution of the Raman spectrum with the chemical composition of graphene oxide. *The Journal of Physical Chemistry C*, 121, 20489–20497.

Lu, Y., Huang, L., Guo, Y., Yang, X. (2021). Theoretical insights into origin of graphene oxide acidity and relating behavior of oxygen-containing groups in water. *Carbon*, 183, 355–361.

Monteiro Riviere, N. A., Inman, A. O., & Zhang, L. W. (2009). Limitations and relative utility of screening assays to assess engineered nanoparticle toxicity in a human cell line. *Toxicology and Applied Pharmacology*, 234(2), 222–235.

Murphy, O. P., Vashishtha, M., Palanisamy, P., Kumar, K. V. (2023). A review on the adsorption isotherms and design calculations for the optimization of adsorbent mass and contact time. *ACS Omega*, 8(20), 17407–17430.

Nair, R. R., Blake, P., Grigorenko, A. N., Novoselov, K. S., Booth, T. J., Stauber, T., Peres, N. M., & Geim, A. K. (2008). Fine structure constant defines visual transparency of graphene. *Science, 320*(5881), 1308.

Nel, A. E., Mädler, L., Velegol, D., Xia, T., Hoek, E. M., Somasundaran, P., Klaessig, F., Castranova, V., & Thompson, M. (2009). Understanding biophysicochemical interactions at the nano-bio interface. *Nature Materials*, 8(7), 543–557.

Seabra, A. B., Paula, A. J., De Lima, R., Alves, O. L., & Durán, N. (2014). Nanotoxicity of graphene and graphene oxide. *Chemical Research in Toxicology*, 27(2), 159–168.

van Meerloo, J., Kaspers, G. J., & Cloos, J. (2011). Cell sensitivity assays: The MTT assay. *Methods in Molecular Biology*, 731, 237–245.

Wang, J., Guo, X. (2020). Adsorption isotherm models: Classification, physical meaning, application and solving method. *Chemosphere*, 258, 127279.

Wei, X. Q., Hao, L. Y., Shao, X. R., Zhang, Q., Jia, X. Q., Zhang, Z. R., Lin, Y. F., & Peng, Q. (2015). Insight into the interaction of graphene oxide with serum proteins and the impact of the degree of reduction and concentration. *ACS Applied Materials & Interfaces, 7*(24), 13367–13374.

Wörle-Knirsch, J. M., Pulskamp, K., & Krug, H. F. (2006). Oops they did it again! Carbon nanotubes hoax scientists in viability assays. *Nano Letters*, 6(6), 1261–1268.

Aknowledgements

This work has been supported by the Ministry of Science, Higher Education, and Youth of Sarajevo Canton (grant No: 27-02-11-41250-2/21).

Summary/Sažetak

Velika geometrijska površina bogata kiseoničnim funkcionalnim grupama, zaslužna za interakcije sa različitim molekulama, čini grafen oksid (GO) pogodnim za primjenu u senzorima, imidžingu i terapijama, ali istovremeno komplikuje procjenu citotoksičnosti primjenom standardnih kolorimetrijskih testova. U ovom radu je ispitana adsorpcija tetrazolijum (MTT) jona, koji se koristi u kolorimetrijskim testovima, na GO. Koristeći sistem bez ćelija, adsorpciono ponašanje je opisano pomoću Frojdlihove, Lengmirove i Lengmir-Frojndlihove (Sipsove) izoterme. Zadovoljavajuće korelacije su dobijene pomoću svih modela, pri čemu je Sipsov model pokazao najbolje rezultate za nelinearnu regresiju, dok je Lengmirov model najviše odgovarao za linearnu regresiju. π–π interakcije između MTT i aromatskih prstenova GO najvjerovatnije predstavljaju glavni uzrok adsorpcije. Interakcije između GO i komponenti medija za ćelijske kulture (DMEM) i seruma (FBS) su opažene indirektno, poređenjem vrijednosti za kapacitet monosloja. Rezultati potvrđuju da interakcije između GO i MTT, odgovorne za interferencije, mogu biti kvantitativno opisane u prisustvu medija za ćelijske kulture i da je potrebno uvesti korekcije rezultata kolorimetrijskih testova. Međutim, još uvijek nije jasno da li se ove korekcije mogu jednostavno upotrijebiti u praksi. Ova studija predstavlja podlogu za procjenu isplativosti uvođenja korekcija.

Glasnik hemičara i tehnologa Bosne i Hercegovine

Bulletin of the Chemists and Technologists of Bosnia and Herzegovina

2026

66

23-30

Original Scientific Article

Print ISSN: 0367-4444

Online ISSN: 2232-7266

DOI: 10.35666/2232-7266.2026.66.03

UDK: 544.272:004

Monte Carlo Simulation of a Seeded Growth Model on a Triangular Lattice: Impact of Surface Impurities on the Final Morphology

Dujak, D. [a,*], Karač, A.[b]

[a] *Faculty of Electrical Engineering, University of Sarajevo, Zmaja od Bosne bb., Kampus Univerziteta, 71 000 Sarajevo, Bosnia and Herzegovina*

[b] *Polytechnic Faculty, University of Zenica, Fakultetska 1, 72 000 Zenica, Bosnia and Herzegovina*

Article info
Received: 09/12/2025
Accepted: 05/03/2026

Keywords:
Jamming
Seeded growth
Impurities
Triangular lattice
RSA

***Corresponding author:**
Dijana Dujak
E-mail: ddujak@etf.unsa.ba
Phone: +-387 33 250 770

Abstract: This study investigates the influence of surface contamination on the final morphology generated by a seed-mediated growth model on a two-dimensional triangular lattice. Using Monte Carlo simulations, we examine the interplay between growth rules (specifically rigid k-mer extension and flexible self-avoiding random walk (SARW) chains) and the geometric properties of pre-adsorbed impurities. Contrary to the initial hypothesis of a geometric matching between the growing species and the surface impurities, our results show that the final morphology in the jamming state is remarkably insensitive to the local symmetry or compactness of the impurities. For rigid k-mers, growth arrest is primarily driven by the impurity number density, which overrides any potential advantages of linear alignment with specific defect shapes. For SARW chains, the available void space and its topological connectivity limit the length, overshadowing the advantages of impurity compactness. Our findings reveal structural robustness in surface growth processes, where intrinsic growth rules dictate length scales, but the overall impurity coverage governs the overall feature distribution. This suggests that morphological outcomes are predictable based on total contamination levels, offering a simplified framework for controlling the growth of nanostructures in realistic, inhomogeneous environments.

INTRODUCTION

Understanding particle adhesion and growth on surfaces is fundamental to processes such as heterogeneous catalysis and electrodeposition, where the final morphology dictates the efficiency and connectivity of the system (Adamczyk, 2006). In these systems, deposition often occurs irreversibly on the experimental time scale, making the Random Sequential Adsorption (RSA) model a robust framework for describing the resulting configurations (Privman, 2000; Cadilhe, 2007). RSA is a process in which objects are deposited randomly and sequentially on a substrate (Talbot, 2000). In its simplest form, the RSA model does not allow for overlapping of objects. Once deposited, the objects remain permanently fixed and affect the geometry of all subsequent depositions. During RSA, the number of deposited objects increases over time. The fraction of the substrate area covered by adsorbed objects, called the coverage fraction $\theta(t)$, describes the kinetic properties of the deposition process. The process stops when there is not enough space for another object. This state is called the jamming state, in which the coverage fraction reaches its jamming limit θ_J. It represents the final configuration of the surface covered by adsorbed objects (Perino, 2017; Ramirez-Pastor, 2019).

In the last twenty years, a variety of nanoscale building blocks of controlled size, shape, and structure have been synthesized for use in fields such as chemical engineering, medicine, and electronics. Seed growth has been shown to be effective for the production of diverse metal nanostructures suitable as substrates for further material deposition (Gole, 2004; Habas, 2007; Lohse, 2013; Xia, 2017). The model proposed in (Dujak, 2022) simulates granular growth on a triangular lattice, allowing different forms of growth without restrictions. It considers the simultaneous development of multiple finite clusters, with the initial seed concentration serving as an adjustable parameter (Roy, 2017). The jamming limit θ_J is reached

when none of the growing objects can propagate further in any required direction on the lattice.

While early models assumed spatially homogeneous substrates (Evans, 1993), real chemical surfaces are inherently inhomogeneous due to the presence of adsorbed pollutants, vacancy defects, or intentional dopants (Adamczyk, 2005; Weroński, 2005). For example, the synthesis of 2D nanomaterials and graphene nanoribbons on Au (111) or Ni (111) is strongly influenced by surface defects. Prominent examples include the growth of nitrogen (Usachov et al., 2011) and boron (Gebhardt et al., 2013) doped graphene on Ni (111), where foreign atoms on the triangular lattice change the electronic properties and network connectivity. Furthermore, the specific configuration of adsorbate, such as gold clusters, can tune the doping characteristics of the material (Wu et al., 2012). These systems demonstrate how surface inhomogeneities, whether point-like or extended, govern the morphological characteristics of the deposited phase (Vasudevan, 2019). In modelling such processes, heterogeneity is introduced by initially occupying lattice sites with objects representing localized chemical defects (Centres, 2015).

In this paper, we investigate the final surface morphology and covering structures generated by a particle-seeded growth model on a two-dimensional triangular lattice initially occupied by impurities. Instead of treating impurities as point-like obstacles, we examine how their shape (defined by internal symmetry and compactness**)** affects the final morphology in the jamming state. Our study is designed to test a central hypothesis about the morphological properties of the final lattice covering in the jamming state, with a particular focus on geometric matching and compactness. For rigid, needle-like growth (k-mers), we hypothesize that the final length distribution will be sensitive to the impurity shape; specifically, that linear impurities will align more favourably with the k-mer growth rules, leaving open pathways that allow for longer objects compared to angular or bent impurities. For flexible growth, we expect that more compact impurities with higher symmetry will lead to more interconnected coverings and longer chains by concentrating the excluded volume, thus preserving wider continuous corridors on the lattice. By analysing the resulting object length distributions, we aim to determine whether the local geometry of the surface contamination is a key design parameter. This investigation is motivated by previous findings (Dujak, 2024) that showed that, although the percolation threshold is sensitive to the shape of the impurity, the overall jamming limit remains largely invariant. Here, we aim to determine whether this invariance extends to the local morphological level or whether the intrinsic growth rules of the species play a more dominant role in shaping the final morphology**.**

EXPERIMENTAL

Definition of the model and the simulation method

The substrate for seed growth is a two-dimensional triangular lattice of size $L = 3200$. To minimize edge effects and simulate an infinite surface, periodic boundary conditions are applied to the triangular lattice (i.e. sites on an open border are connected to corresponding sites on the opposite border). This approach is standard in surface science modelling because it ensures that each lattice site experiences a statistically equivalent environment, preventing artificial nucleation at the boundaries (Binder, 2010). Furthermore, the choice of lattice size $L = 3200$ was made to mitigate finite-size effects (Evans, 1984; Lebovka, 2011). In percolation and jamming studies, the size of the system can significantly affect the observed thresholds; however, for the densities and object lengths considered here ($l = 2$), $L = 3200$ is large enough to ensure that morphological statistics (such as length distributions and jamming limits) are representative of the thermodynamic limit and are not biased by the size of the system.

The lattice was initially and randomly populated with impurities using RSA. They are created by self-avoiding random walks of length $l = k - 1$, where k represents the number of the occupied lattice sites. Three shapes of such impurities are possible, as shown in Table 1. The impurity concentrations ρ_{imp} were kept below the percolation threshold of the triangular lattice sites (given in Table 1) to ensure that the substrate remained a connected medium, allowing unhindered growth paths before the jamming state. Later, point seeds were randomly distributed on the lattice at a given concentration ρ. To ensure the physical validity of the results, the initial seed concentrations were also intentionally kept below the percolation threshold of the sites for point objects on the triangular lattice ($p_c = 0.5$). This constraint ensures that any connectivity or percolation observed in the jamming state is a direct consequence of the growth process and its interaction with the impurities, and not a by-product of the initial distribution. Seed and impurity concentrations are calculated as the fraction of lattice sites occupied by seeds/impurities.

Table I: Formation of impurities of the length $l = 2$ with corresponding order of the symmetry axis of the shape *n*, jamming coverages θ_J and percolation thresholds θ_p. The numbers in parentheses are the numerical values of the standard uncertainty of θ_J referred to the last digits of the quoted value.

Impuritiy shapes	*n*	θ_J	θ_p
(B)	2	0.836 211(4)	0.4611(9)
(C) 	1	0.834 440(4)	0.4585(11)
(D) 	3	0.796 940(5)	0.5214(9)
(B) + (C)	/	0.8525(7)	0.4587(12)
(B) + (D)	/	0.8588(6)	0.4926(12)
(C) + (D)	/	0.8625(7)	0.4910(12)

Seed growth on a lattice is modelled using self-avoiding walks, following two distinct growth rules: (i) unidirectional growth, which results in rigid, needle-like structures (k-mers), and (ii) isotropic growth, where flexible chains (SARW) are formed. During object growth, objects come into contact when there is one lattice site between them, and merged into a single cluster. If two

clusters come into contact, they merge into a single cluster. The jamming coverage θ_J is reached when growing objects can no longer grow on the lattice.

The simulation proceeds until a jamming state is reached. Physically, this corresponds to the surface saturation limit where the available free volume is fragmented into domains smaller than the minimum size of the growing species. This state provides a well-defined point for morphological analysis, representing the final stage of kinetic growth before any potential (and often much slower) thermal reorganization takes place.

Simulation method

The lattice is initially randomly occupied by impurities B, C or D or by their mixtures B+C, B+D and C+D at a given concentration ρ_{imp}, and then by point seeds randomly distributed at a given concentration ρ. Then, the deposition is turned off, and the process of random growing begins. In each Monte Carlo step, the lattice site occupied by the seed is randomly selected. After that, an unoccupied adjacent site is randomly selected according to the prescribed growth rules for the seed. In the case of needle-like growth, the selected k-mer extends in the direction of the first step in the formation of the growing object. If the corresponding adjacent site is occupied by an impurity or a previously grown object, the attempted k-mer growth is not possible and the object remains unchanged. In the case of flexible chains, the selected chain is randomly extended to one of the nearest empty neighbour sites. If all the nearest neighbour sites are occupied, the selected chain is not changed. During the process, the lattice coverage increases up to the jamming limit.

Chemical relevance and model limitations

The Monte Carlo model presented provides a theoretical framework for understanding how surface contamination affects the final lattice morphology. Although defined on a discrete triangular lattice, the model rules and parameters are specifically chosen to reflect the physical and chemical constraints of real-world surface processes.

The choice of a triangular lattice is physically justified by the (111) facet of face-centered cubic (fcc) metals (e.g., Au, Pt, Ag), which serve as the most common substrates for on-surface synthesis (Brune, 1998; Poirier, 1997; Kawasaki, 2006). In this context, the growing species serve as analogs for different classes of organic molecules. For example, rigid k-mers can represent conjugated rod-like molecules (Kondrat, 2001; Kondrat, 2002; Adamczyk, 2008), while SARW chains can model flexible polymers (oligomers) or long-chain alkanes with conformational degrees of freedom (Cornete, 2003; Pawłowska, 2012). Furthermore, the impurities of length l=2 represent the minimal extended defects, such as pre-adsorbed diatomic molecules or vacancy clusters, which introduce localized steric hindrance beyond simple point-like poisoning (Weroński, 2005).

The assumption of irreversible growth without surface diffusion is a well-established theoretical framework in the study of non-equilibrium deposition. As discussed by Privman (2000), the irreversible RSA model without detachment or diffusion leads to a fully jammed state where the coverage is limited by the exclusion of particles from gaps smaller than their size. Our model follows this established methodology to isolate the influence of geometric constraints and surface impurities on the final morphology.

The central assumption of our study is the dominance of excluded volume effects. In many chemical synthesis processes, especially under high surface coverage, steric constraints impose fundamental limits on growth and dictate the final morphology. This behavior is well-documented in self-assembled monolayers and colloidal nanocrystal assembly, where short-range steric repulsion, rather than long-range electrostatic forces, governs particle organization and packing boundaries (Boles, 2016).

Recent theoretical models of the seed-mediated growth, such as mean-field analytical studies of nanodiamond film formation as a function of seed density and initial seed size, confirm that the spatial distribution and hard-core interactions of the seeds are the primary drivers of the transition to continuous coverage (Tomellini, 2023). By focusing on these hard-core interactions, our model captures the essential physics of crowding observed in dense deposition regimes. This justifies the use of a simplified lattice model where steric repulsion and spatial accessibility are the primary controlling mechanisms for nanostructural engineering.

RESULTS AND DISCUSSION

The final morphology was tested in the jamming state for various seed concentrations $(0.1 \leq \rho \leq 0.49)$ on a triangular lattice of size $L = 3200$, and for different impurity concentrations $(0.1 \leq \rho_{imp} \leq 0.48)$ in the case of individual impurities. For impurity mixtures, the ranges were $(0.1 \leq \rho \leq 0.48)$ and $(0.1 \leq \rho_{imp} \leq 0.35)$. The data were averaged over 500 independent runs. To investigate the morphology, we consider the number of objects $N = N(l), l \geq 0$, normalized by the initial number of seeds N_0 for k-mers and SARW, and analysed for different values of ρ and ρ_{imp}.

The dependence of the ratio N/N_0 on the k-mer length for the system in the jamming state is shown in Fig. 1 and Fig. 2 for various values of the seed density ρ and all three types of impurities given in Table 1. The results for a low value of ρ_{imp} are presented in Fig. 1 while Fig. 2 shows the results for high impurity concentrations. A comparative analysis of these figures reveals a striking similarity in the morphological evolution of the growing objects, regardless of the specific internal symmetry or compactness of the impurities. It is important to note that for a fixed impurity density, the total number of impurities remains constant in all studied cases; consequently, the number density of the impurities, is identical. Our results show that at low concentrations, the final morphology is primarily determined by this number density and the resulting total excluded volume. The specific internal symmetry of the impurities (whether linear or angular) represents a second-order effect that does not significantly change the statistical distribution of the grown k-mers.

In all cases, as the seed density increases, we observe a sharp transition where the peak of the distribution shifts towards $l = 1$ (monomers). At $\rho = 0.45$, approximately

60% of the seeds do not pass a single growth step. This growth inhibition is a manifestation of the crowding effect, driven by competition for excluded volume; at high seed densities, the available lattice space is partitioned into domains smaller than the required propagation length, leading to premature jamming. There is a distinct overlap point at $l = 2$. For lengths $l > 2$, the probability of reaching longer lengths drops significantly faster for higher seed densities.

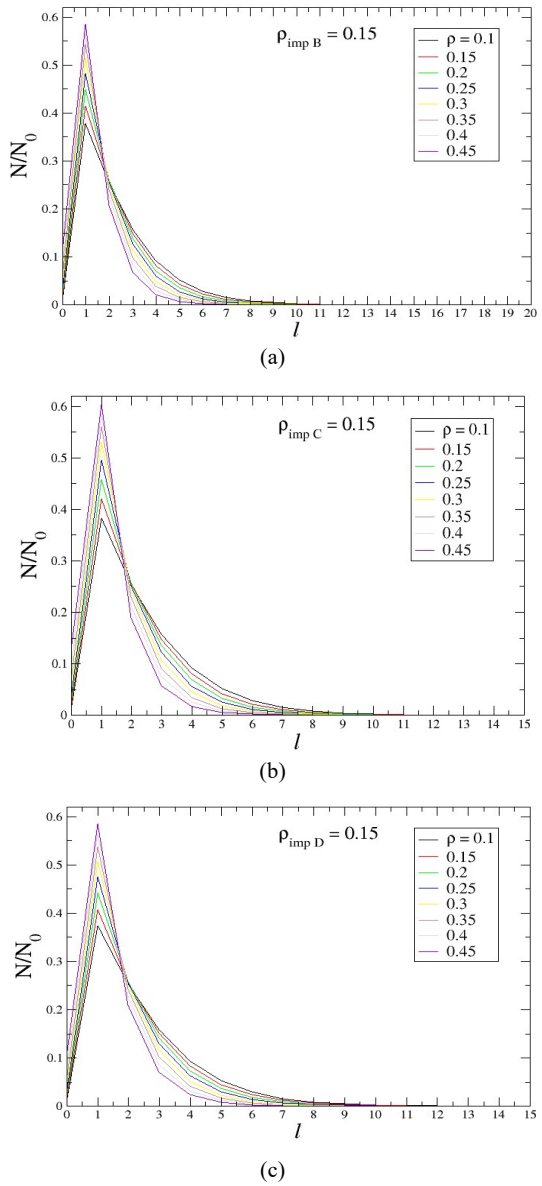

Fig 1: The dependence of the normalized number of growing k-mers on their length in the jamming state for low impurity concentration. The specific types of impurities (B, C, D), their concentrations (ρ_{imp}), and the initial seed concentrations (ρ) are indicated in the legend.

Under the conditions of extreme surface contamination, the growth process is severely hindered, as evidenced by the almost complete suppression of k-mer extension above $l = 2$. A critical observation is the collapse of the length distribution towards $l = 1$. For high seed densities ($\rho > 0.35$), the fraction of non-growing seeds exceeds 60%, representing a state of premature jamming. In this regime, the surface is so heavily fragmented by pre-adsorbed impurities that the connectivity of the triangular lattice is effectively destroyed. The fact that the distributions for shapes B, C, and D remain indistinguishable even at such high densities suggests that vacancy percolation is the fundamental phenomenon governing the morphology, rather than a specific interaction between the growth species and the impurity geometry.

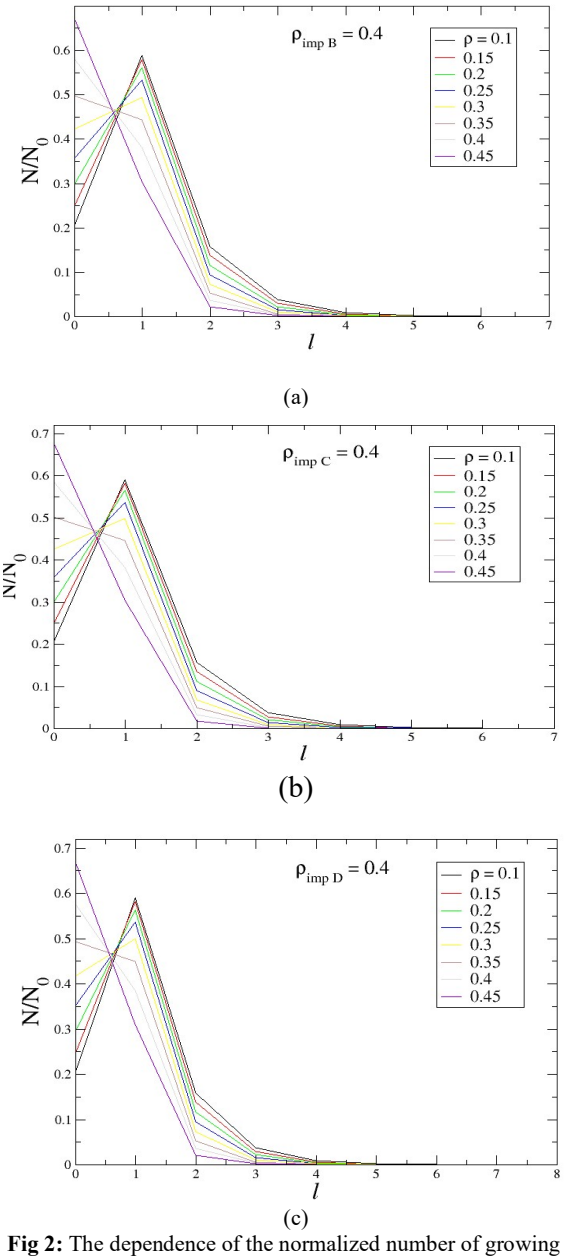

Fig 2: The dependence of the normalized number of growing k-mers on their length in the jamming state for high impurity concentration. The specific types of impurities (B, C, D), their concentrations (ρ_{imp}), and the initial seed concentrations (ρ) are indicated in the legend.

The corresponding results for random walk chains (SARW) are shown in Fig. 3 for low impurity concentrations and in Fig. 4 for high impurity concentrations. Unlike rigid k-mers, SARW chains

achieve significantly larger maximum lengths, often exceeding $l > 20$ at low ρ and ρ_{imp}. This advantage of SARW chains over k-mers highlights the role of conformational freedom in overcoming steric hindrance; while rigid k-mers are easily blocked by a single pinning site, the flexible nature of SARW allows for the exploration of a larger fraction of the available free volume.

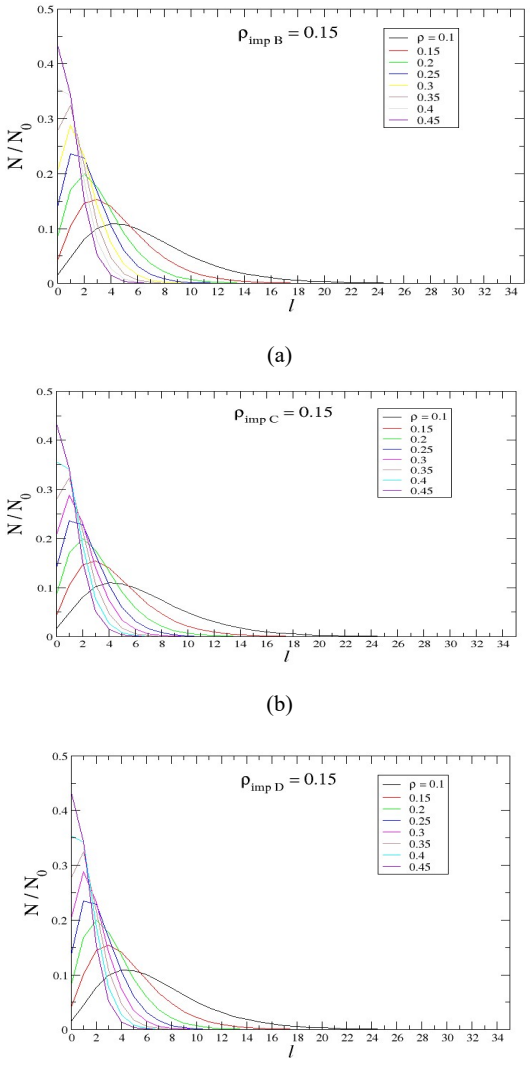

(a)

(b)

(c)

Fig 3: The dependence of the normalized number of growing SARW chains on the walk length in the jamming state for low impurity concentration. The specific types of impurities (B, C, D), their concentrations (ρ_{imp}), and the initial seed concentrations (ρ) are indicated in the legend.

At low impurity concentrations, the distribution peak shifts towards higher l values compared to k-mers, indicating that flexible growth is less sensitive to low-level surface contamination. However, as ρ and ρ_{imp} increase, this advantage decreases. The suppression of vacancy percolation at high impurity densities effectively limits the available free volume, leading to the observed growth suppression even for flexible SARW chains. At high impurity and seed densities, the system eventually converges to the behaviour observed for k-mers. This convergence occurs because the lattice fragments into geometric domains smaller than the typical persistence length of even a flexible chain, making the configurational flexibility of SARW ineffective against such severe spatial constraints.

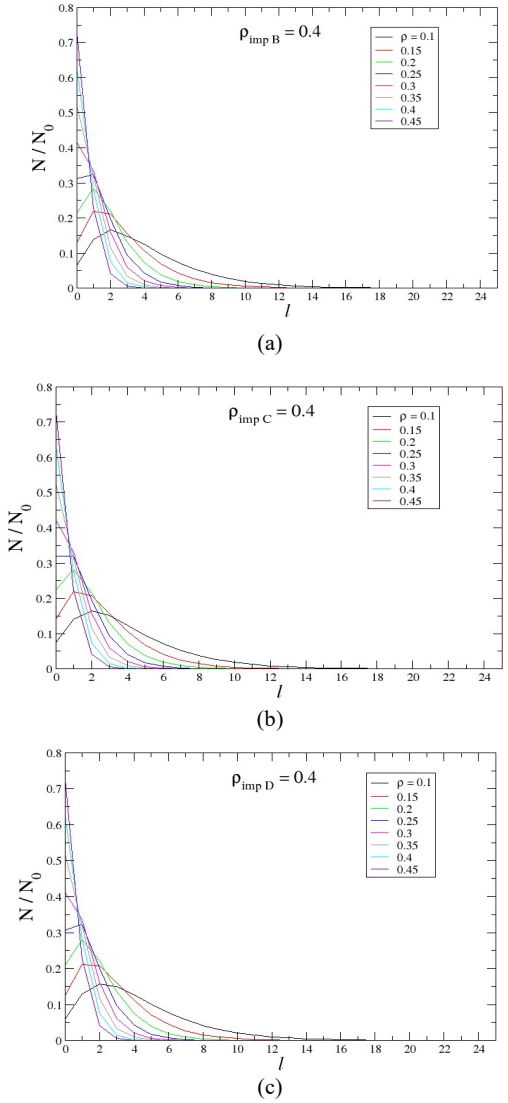

(a)

(b)

(c)

Fig 4: The dependence of the normalized number of growing SARW chains on the walk length in the jamming state for high impurity concentration. The specific types of impurities (B, C, D), their concentrations (ρ_{imp}), and the initial seed concentrations (ρ) are indicated in the legend.

Figures 5 and 6 show the normalized object length distribution for all types of impurities listed in Table 1 and their mixtures. For comparison, results for point-like impurities (k-mers with $l = 0$) and for growth without impurities are also included. Specifically, Fig. 5a presents the results for low densities of both impurities and seeds, while Fig. 5b corresponds to low impurity density and high seed density. Conversely, Figs. 6a and 6b illustrate the opposite cases. The corresponding results for SARW chains are given in Figs. 7 and 8.

The results in Figs. 5a and 5b show that, for low values of impurity and seed densities, the length distributions of the growing objects are almost identical for all impurity shapes and their mixtures.

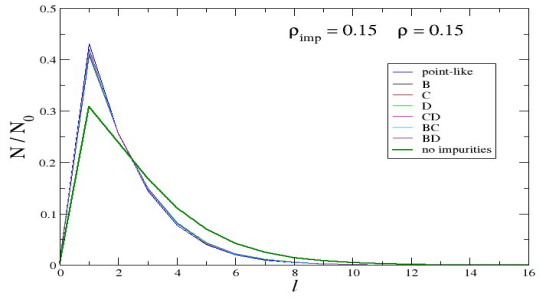

(a)

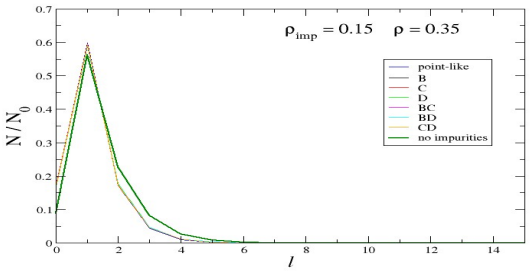

(b)

Figure 5: Comparison of object length distributions in the jamming state during k-mer growth at low impurity densities ($\rho_{imp} = 0.15$) and (a) low seed densities ($\rho = 0.15$), (b) high seed densities ($\rho = 0.35$). The type of impurities is indicated in the legend. For comparison, results for k-mer growth without impurities are also shown.

The objects attain slightly shorter lengths compared to the case without impurities, indicating a minimal but measurable steric disruption. Notably, at high seed densities and low impurity concentrations, the distributions match those observed for growing on a pure lattice. This suggests that in the high-seed regime, the inter-seed competition (the crowding effect) becomes the primary limiting factor for growth. In this scenario, the high frequency of collisions between adjacent growth fronts effectively masks the presence of rare impurities**,** as growing objects exhaust the available lattice space before they can significantly interact with the pre-adsorbed obstacles.

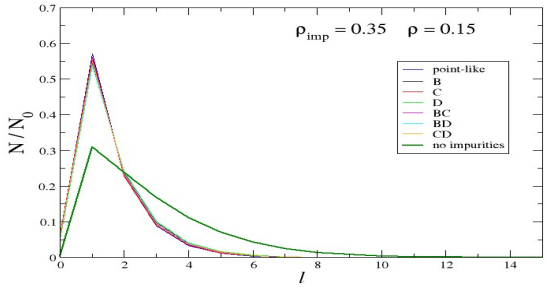

(a)

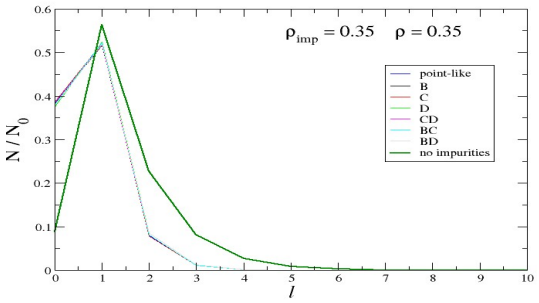

(b)

Figure 6: Comparison of object length distributions in the jamming state during k-mer growth at high impurity densities ($\rho_{imp} = 0.35$) and (a) low seed densities ($\rho = 0.15$), (b) high seed densities ($\rho = 0.35$). The type of impurities is indicated in the legend. For comparison, results for k-mer growth without impurities are also shown.

In contrast, Figs. 6a and 6b show that, at high impurity concentrations, the objects in the jamming state reach significantly shorter lengths than in the case of no-impurities. In this regime, the growth suppression is primarily caused by strong lattice fragmentation; the high density of impurities acts as a decisive barrier to chain elongation, regardless of their specific geometry.
From the growth of SARW chains shown in Figs. 7 and 8, it can be concluded that, in general, longer objects are formed compared to the growth of *k*-mers under the same conditions.

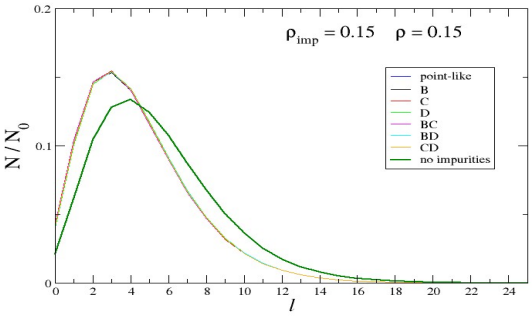

(a)

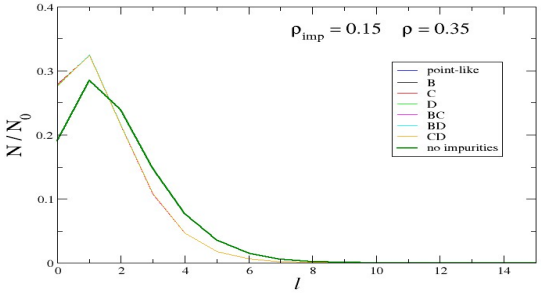

(b)

Figure 7: Comparison of object length distributions in the jamming state during SARW chains growth at low impurity densities ($\rho_{imp} = 0.15$) and (a) low seed densities ($\rho = 0.15$), (b) high seed densities ($\rho = 0.35$). The type of impurities is indicated in the legend. For comparison, results for SARW chains growth without impurities are also shown.

At low impurity densities, the length distributions remain remarkably consistent across all impurity shapes, deviating only slightly from the impurity-free case.

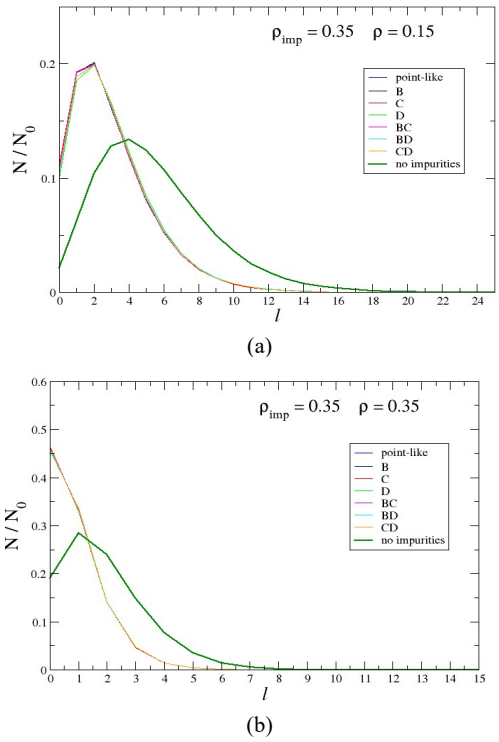

Fig 8: Comparison of object length distributions in the jamming state during SARW chains growth at high impurity densities ($\rho_{imp} = 0.35$) and (a) low seed densities ($\rho = 0.15$), (b) high seed densities ($\rho = 0.35$). The type of impurities is indicated in the legend. For comparison, results for SARW chains growth without impurities are also shown.

However, this difference becomes more pronounced at higher impurity and seed densities. In these crowded environments, growth on a clean lattice yields significantly longer chains and a lower fraction of non-growing seeds. This behaviour highlights a critical transition: while the conformational freedom of SARW chains allows them to bypass isolated obstacles, the cumulative effect of high impurity concentrations eventually leads to extreme spatial confinement. In such regimes, the impurities act as pinning sites that fragment the available growth paths into finite, isolated domains. This limits the achievable length of the flexible chains, as the probability of a random walk becoming trapped within a small empty pocket increases, ultimately reducing the morphological advantage of flexible species over rigid k-mers.

CONCLUSIONS

This study systematically assessed the influence of impurity geometry on the seeded growth of rigid k-mers and flexible SARW chains. Our findings provide a clear solution to the central hypothesis proposed in the introduction: contrary to our initial assumption, the final morphology in the jamming state is remarkably insensitive to the local geometric matching between the impurities and the growing species.

For rigid k-mers, we assumed that linear impurities would align with growth paths to allow for longer objects; however, our results reveal that the number density of impurities is the primary driver of growth arrest. The expected advantage of linear alignment is effectively negated by the stochastic nature of seed placement, which fragments the lattice regardless of the specific impurity symmetry. Similarly, for flexible SARW chains, the expected benefit of compact impurities with higher symmetry order preserving wider corridors was not observed. Instead, we found that at the concentrations studied, the percolation of void space (the global connectivity of empty sites) acts as the fundamental limiting factor, overshadowing any local advantages provided by impurity compactness. This work has demonstrated a geometric universality in surface growth, where the intrinsic growth rules (rigidity vs. flexibility) dictate the absolute length scales, but the total impurity coverage – rather than their specific shape – governs the statistical distribution of the grown objects.

These insights are particularly relevant for experimental nano-deposition on substrates like Au (111). They suggest that the morphological outcome of surface coatings is a robust property that can be predicted based on the overall level of contamination, without the need for detailed characterization of defect symmetries. This robustness simplifies the design parameters for controlling surface growth in non-ideal, realistic environments.

REFERENCES

Adamczyk Z., Jaszczt K., Michna A., Siwek B., Szyk-Warszyska L., Zembala M. (2005). Irreversible adsorption of particles on heterogeneous surfaces, *Adv. Colloid Interface Sci. 118*, 25–42.

Adamczyk Z. (2006). Particles at Interfaces: Interactions, Deposition, Structure, Interface Science and *Technology 9*, 1-743.

Adamczyk P., Romiszowski P. Sikorski A. (2008). A simple model of stiff and flexible polymer chain adsorption: The influence of the internal chain architecture, *J. Chem. Phys. 128*, 154911.

Binder K., Heermann D.W. (2010). Monte Carlo simulations in Statistical physics, 5th edition, Springer.

Boles M. A., Engel M., Talapin D. V. (2016). Self-Assembly of Colloidal Nanocrystals: From Intricate Structures to Functional Materials, *Chemical Reviews 116*, 11220–11289.

Brune H. (1998). Microscopic view of epitaxial metal growth: nucleation and aggregation, *Surface Sci. Rep. 31*, 125-229.

Cadilhe A., Araujo N. A., Privman V. (2007). Random sequential adsorption: from continuum to lattice and pre-patterned substrates, *J Phys.: Condens. Matter 19,* 065124.

Centres P. M., Ramirez-Pastor A. J. (2015). Percolation and jamming in random sequential adsorption of linear k-mers on square lattices with the presence of impurities, *J. Stat. Mech. 2015*, 10011.

Cornette V., Ramirez-Pastor A. J., Nieto F. (2003). Dependence of the percolation threshold on the size of the percolating species, *Physica A 327*, 71.

Dujak D. et al. (2022). Percolation and jamming properties in particle shape-controlled seeded growth model, *Eur. Phys. J. B 95*, 143.

Dujak D. et al. (2024). Percolation and jamming properties in an object growth model on a triangular lattice with finite-size impurities, *J. Stat. Mech. 2024,* 1742–5468.

Evans J. W., Burgess D. R., Hoffman D. K. (1984). Irreversible random and cooperative processes on lattices: spatial correlations, *J. Math. Phys. 25*, 3051–63.

Evans J. W. (1993). Random and cooperative sequential adsorption, *Rev. Mod. Phys. 65*, 1281.

Gebhardt J. et al. (2013). Growth and electronic structure of boron-doped graphene*, Phys. Rev. B* 87, pp. 155437.

Gole A., Murphy C. J. (2004). Seed-Mediated Synthesis of Gold Nanorods: Role of the Size and Nature of the Seed, *Chem. Mater. 16*, 3633–3640.

Habas S. E. et al. (2007). Shaping binary metal nanocrystals through epitaxial seeded growth, *Nature Materials 6,* 692–697.

Kawasaki M., Masaki I. (2006). Self-Assembly of Alkanethiol Monolayers on Ag−Au (111) Alloy Surfaces, *The Journal of Physical Chemistry B 110*, 21124–21130.

Kondrat G., Pekalski A. (2001). Percolation and jamming in random bond deposition, *Phys. Rev. E 64*, 056118.

Kondrat C. (2002). Influence of temperature on percolation in a simple model of flexible chains adsorption, *J. Chem. Phys.* 117, pp. 6662–6666.

Lebovka N. I., Karmazina N. N., Tarasevic Y. Y., Laptev V. V. (2011). Random sequential adsorption of partially oriented linear k-mers on a square lattice, *Phys. Rev. E 84*, 061603.

Lohse S.E., Murphy C. J. (2013). The quest for shape control: a history of gold nanorod synthesis, *Chem. Mater. 25*, 1250−61.

Pawłowska M., Żerko S., Sikorski, A. (2012). Percolation in two-dimensional flexible chains systems, *The Journal of Chemical Physics 136*, 046101.

Perino E. J., Matoz-Fernandez D. A., Pasinetti P. M., Ramirez-Pastor A. J. (2017). Jamming and percolation in random sequential adsorption of straight rigid rods on a two-dimensional triangular lattice. *J. Stat. Mech. 2017,* 073206.

Poirier G. E. (1997). Characterisation of Organosulfur Molecular Monolayers on Au (111) using Scanning Tunnelling Microscopy. *Chem. Rev.* 97, 1117-1128.

Privman V. (2000). Dynamics of Nonequilibrium Deposition, *Colloids Surf. A 165,* 231.

Ramirez-Pastor A. J., Centres P. M., Vogel E. E., Valdés J. F. (2019). Jamming and percolation for deposition of k^2-mers on square lattices: A Monte Carlo simulation study, *Phys. Rev. E 99*, 042131.

Roy B., Santra S. B. (2017). First-order transition in a percolation model with nucleation and preferential growth, *Phys. Rev. E 95*, 010101.

Talbot J., Tarjus G., Van Tassel P. R., Viot P. (2000). From car parking to protein adsorption: an overview of sequential adsorption processes, *Colloids Surf. A 165*, 287–324.

Tomellini M., Polini R. (2023). Impact of seed density on continuous ultrathin nanodiamond film formation, *Diamond and Related Materials 133*, 109700.

Usachov D. et al. (2011). Nitrogen-Doped Graphene: Efficient Growth, Structure, and Electronic Properties, *Nano Letters 11*, 5401–5407.

Vasudevan A., Shvalya V., Zidanšek A., Cvelbar U. (2019). Tailoring electrical conductivity of two-dimensional nanomaterials using plasma for edge electronics: A mini review, *Front. Chem. Sci. Eng. 13*, 427–443.

Weroński P. (2005). Application of the extended RSA models in studies of particle deposition at partially covered surfaces, *Adv. Colloid Interface Sci. 118*, 1–24.

Wu Y. et al. (2012). Tuning the Doping Type and Level of Graphene with Different Gold Configurations*, Small 8,* 3129–3132.

Xia Y., Gilroy K. D., Peng H. C., Xia X. (2017). Seed-Mediated Growth of Colloidal Metal Nanocrystals, *Angewandte Chemie Int. Ed*. 56, 60–95.

AKNOWNLEDGEMENT

This paper emerged from the project number PtF_EM_IR_04/2024.

Summary/Sažetak

U ovom radu se istražuje uticaj površinske kontaminacije dvodimenzionalne triangularne rešetke na konačnu morfologiju površine rešetke formirane modelom rasta (seed-mediated growth). Koristeći Monte Carlo simulacije, ispitivan je uticaj pravila rasta (kruti k-meri i fleksibilni SARW lanci) i geometrijskih svojstava prethodno adsorbovanih nečistoća. Suprotno početnoj hipotezi o geometrijskom podudaranju nečistoća i objekata formiranih narastanjem, rezultati pokazuju da je konačna morfologija u stanju zagušenja (*jamming state*) izuzetno neosjetljiva na lokalnu simetriju ili kompaktnost nečistoća. Kod krutih k-mera, zaustavljanje rasta prvenstveno je uzrokovano brojčanom gustinom nečistoća, što nadjačava bilo kakve potencijalne prednosti linearnog poravnanja sa specifičnim oblicima defekata. Kod SARW lanaca, raspoloživi prazan prostor i njegova topološka povezanost ograničavaju dostižnu dužinu, zasjenjujući prednosti kompaktnosti nečistoća. Uočena je strukturna robusnost u procesima površinskog rasta, gdje unutrašnja pravila rasta diktiraju skale dužine, dok ukupna prekrivenost nečistoćama upravlja cjelokupnom distribucijom objekata. Ovo sugeriše da su morfološki ishodi predvidljivi na osnovu ukupnog nivoa kontaminacije, što nudi pojednostavljen okvir za kontrolu nanostrukturnog rasta u realnim, nehomogenim okruženjima.

Glasnik hemičara i tehnologa Bosne i Hercegovine

Bulletin of the Chemists and Technologists of Bosnia and Herzegovina

2026

66

31-40

Print ISSN: 0367-4444
Online ISSN: 2232-7266

Original Scientific Article
DOI: 10.35666/2232-7266.2026.66.04
UDK: 543.31:541.1

Bentonite as an adsorbent for the removal of Cr(III) ions from galvanic wastewater: equilibrium, kinetics and thermodynamics in batch and column systems

Ahmetović, M.*, Šestan, I., Odobašić, A., Papraćanin, E., Keran, H., Junuzović, H.

Faculty of Technology, University of Tuzla, Urfeta Vejzagića 8, 75000 Tuzla, Bosnia and Herzegovina

Article info
Received: 21/11/2025
Accepted: 04/02/2026

Keywords:
Bentonite
Chromium
Galvanic wastewater
Adsorption
Batch system
Column

***Corresponding author:**
Melisa Ahmetović
E-mail: melisa.ahmetovic@untz.ba
Phone: +-387 35 320 768

Abstract: The presence of heavy metals such as chromium in waterways can lead to various health problems in humans and animals. Due to its negative effects, chromium-rich wastewater needs to be treated before being discharged into waterways. In this study, the possibility of using bentonite as an adsorbent for the removal of Cr (III) from galvanic wastewater was investigated. First, the physicochemical characterization of the used bentonite was performed, followed by the examination of process parameters such as pH value, concentration, mass, and time. Based on the obtained data, adsorption isotherms, kinetic models, and thermodynamic parameters were determined. All experiments were carried out in both batch and column systems. The results showed that bentonite can be used as a low-cost adsorbent for the efficient removal of chromium ions from galvanic industry wastewater, achieving the highest removal efficiency (99.97%) at pH 5 and a mass of 1 g. The Langmuir and Temkin adsorption isotherm models showed good agreement with the experimental data ($R^2 > 0.9$), while the best fit for the kinetic study was observed with the pseudo-first-order model.

INTRODUCTION

Industrial wastewater often contains heavy metals such as copper, zinc, chromium, lead, nickel, cadmium, and others, which pose a serious problem for the entire ecosystem (Ahmetović *et al.,*2024). For the successful implementation of the galvanization process, as one of the industrial processes, the electrolyte must contain metal ions as direct components of the galvanic bath. Therefore, during the galvanization process, galvanic wastewater becomes contaminated with heavy metals, which represent a direct threat to human health. Chromium, as one of the common components of galvanic baths, although considered an essential element necessary for the proper functioning of living organisms, can cause respiratory irritation, liver and kidney damage, and even cancer when present in concentrations exceeding the permissible limits (Gaoqian *et al.*,2024).Chromium exists in two valence states, as trivalent and hexavalent chromium ions (Dengbing *et al.,*2025). The trivalent ion appears in water in the form of Cr(III) complexes and hydrogen–oxygen complexes, whereas the hexavalent chromium ion exists in the form of ionic oxides (Wael *et al.*,2023). In order to minimize their concentrations, various methods for the removal and treatment of heavy metals have been developed in recent years (Kejin *et al.,*2025). The selection of an appropriate method for removing heavy metals from galvanic wastewater primarily depends on the type of contaminant. Among numerous methods, adsorption has attracted considerable attention due to its high availability, simplicity, selectivity, and efficiency (Joyel *et al*.,2024). In addition, adsorption can remove different types of pollutants, which makes it increasingly used in wastewater treatment processes (Ahmetović *et al.,*2024). In recent years, clays, zeolites, activated carbon, and similar materials have been increasingly used as adsorbents for the removal of heavy metal ions (Sher *et al.,*2021). A large specific surface area, high ion-exchange capacity, flexibility, and unique physical properties are some of the main advantages of clay materials (Gholamifard *et al*.,2023). Bentonite clays belong to the montmorillonite group and are characterized by very high chemical and mechanical stability, as well as diverse surface and structural properties, making them inexpensive and

environmentally friendly adsorbents for the removal of heavy metals (Tadesse,2022). Therefore, the aim of this study was to investigate the possibility of using bentonite clay for the removal of chromium ions from galvanic wastewater using both batch and column systems, in order to optimize the use of bentonite clay for Cr(III) ion removal from galvanic wastewater and to assess its potential for large-scale application.

EXPERIMENTAL

Bentonite from the Šipovo locality (Bosnia and Herzegovina) with a particle size of 75 μm was used in this study. The physicochemical characterization included the determination of the cation exchange capacity, specific surface area, point of zero charge, and the performance of SEM-EDS and FTIR analyses. The cation exchange capacity was determined using the standard 1 mol/L NH_4Cl method, while the point of zero charge (pH_{pzc}) was determined using 0.1 mol/L $NaNO_3$ as the electrolyte (Daković,2001). The specific surface area was measured by nitrogen adsorption at 77 K using a Micromeritics Tristar II Plus Analyzer, Malvern Panalytical and the surface area value of the sample was calculated using the standard Brunauer–Emmett–Teller (BET) method. The surface topography and chemical composition of the bentonite were analyzed using a JSM–6460LV, JEOL scanning electron microscope equipped with energy-dispersive X-ray spectroscopy (SEM-EDS) at an accelerating voltage of 20 kV, while functional groups were identified using an ABB Bomem MB-100 Fourier Transform Infrared Laboratory Analyzer, Bomem Inc. in the spectral range of 4000–400 cm^{-1} with a resolution of 2 cm^{-1}.

Biosorption experiments were performed using a synthetic solution and a real sample taken from the galvanic industry after metallization/chromium plating. All experiments were performed in triplicate. Synthetic solutions of different concentrations were prepared by dissolving $CrCl_3 \cdot 6H_2O$, Carlo Erba, in distilled water. This salt is pure analytical grade (p.a.>99%). The pH was adjusted by adding 0.1 mol/L and 0.01 mol/L HNO_3 and NaOH solutions. To determine the optimal adsorption conditions, the adsorbent mass of 0.5 g to 2.5 g was used, as well as contact time of 5 min to 60 min, solution initial pH of 2 to 6, temperature of 25ºC to 45°C, and initial metal ion concentration of 10 mg/L to 10000 mg/L. Adsorption was tested in the batch system by mixing 1 g of bentonite with 50 mL of the test solution on a magnetic stirrer at 300 rpm for a specified contact time. After adsorption, the solutions were filtered, and the residual concentration of chromium ions in the filtrate was determined using atomic absorption spectrometry with a Perkin Elmer AAnalyst 200 spectrophotometer (Wu,2019). The adsorption capacity q_e (mg/g) and the metal ion removal efficiency E (%) were calculated using the following equations (Saghir *et al*.,2025):

$$q_e\left(\frac{mg}{g}\right) = \frac{(c_0 - c_e)\cdot v}{m} \quad (1)$$

$$E\ (\%) = \frac{(c_0 - c_e)}{c_0}\cdot 100 \quad (2)$$

where: C_0(mg/L) – initial metal concentration, C_e(mg/L) – equilibrium metal concentration, V– volume of the solution (L), m– mass of the used adsorbent.

To obtain the breakthrough curve, the experiments were carried out in a plexiglass column with a diameter of 30 mm and a height of 230 mm. Before introducing the metal ion solution, the adsorbent was washed with a certain amount of distilled water to remove dissolved compounds. After washing and draining the column, the experiment was continued using both synthetic and real metal ion solutions. The column adsorption experiments were performed in a single-pass mode, and the effluent was collected in portions of 100 mL, after which the metal concentration in each effluent sample was determined.

RESULTS AND DISCUSSION

The point of zero charge (pH_{pzc}) was determined using the salt addition method, with $NaNO_3$ used as the electrolyte. The determined point of zero charge value for the bentonite was 9, indicating that the surface of the adsorbent is positively charged at pH values below this point, thereby attracting anions, while at pH values above this point, the surface becomes negatively charged and attracts cations (Noreen *et al*.,2021; Dhaouadi *et al.,*2021). The total exchange of all cations (CEC), determined by the standard method using 1 mol/L NH_4Cl, was 0.6147 mmol/g, which represents a slightly lower value compared to the CEC of smectites (0.80–1.50 mmol/g). This is due to the presence of non-clay materials in the bentonite structure alongside montmorillonite (Vhahangwele, 2014). Based on the obtained results, it can be concluded that Na^+ ions are dominant compared to other metals, indicating that Na^+ ions from bentonite are likely to be exchanged with Cr(III) ions through an ion-exchange mechanism. According to the results presented in Table 1, it can be concluded that after Na^+ ion, the following order of ion exchange is expected $Ca^{2+} < Mg^{2+} < K^+$.

Table 1: Cation exchange capacity (CEC) value of bentonite

Exchangeable cations	Value (mmol/g)
Ca^{2+}	0.180
Mg^{2+}	0.043
K^+	0.011
Na^+	0.380

The specific surface area of bentonite was 80.9976 m^2g^{-1}, with a pore volume of 0.064904 cm^3g^{-1} and an average pore diameter of 32.052 Å (Table 2). Similar values of specific surface area for bentonite used as an adsorbent were obtained by Kovo (2015), who used Nigerian bentonite for the removal of Ni(II) and Mn(II) ions (69.34 m^2g^{-1}), and by Petrović *et al.* (2019), who used natural bentonite for the removal of Cr(VI) ions (88.80 m^2g^{-1}).

Table 2: Values of the specific surface area of bentonite

Characteristics	Value
BET specific surface	80.9976 m^2g^{-1}
Pore volume (p/p°=0.95)	0.0649 cm^3g^{-1}
Average pore width	65.922 Å
Average pore diameter	32.052 Å

SEM-EDS micrographs are shown in Figure 1 and Figure 2, illustrating the changes in the surface structure of the adsorbent before and after adsorption of Cr(III) ions.

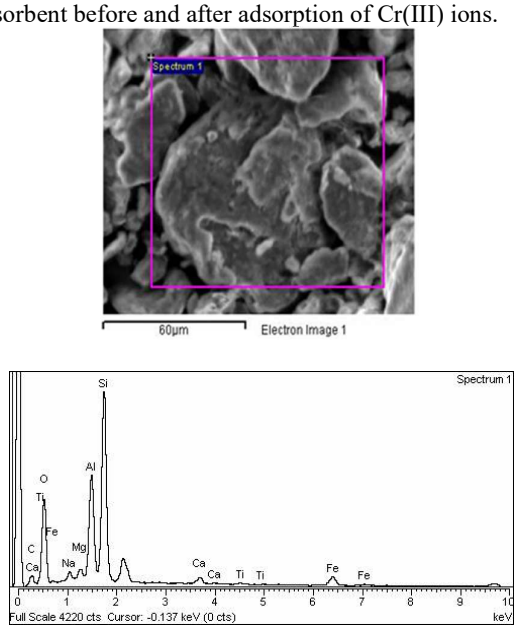

Fig 1. SEM-EDS image of native bentonite

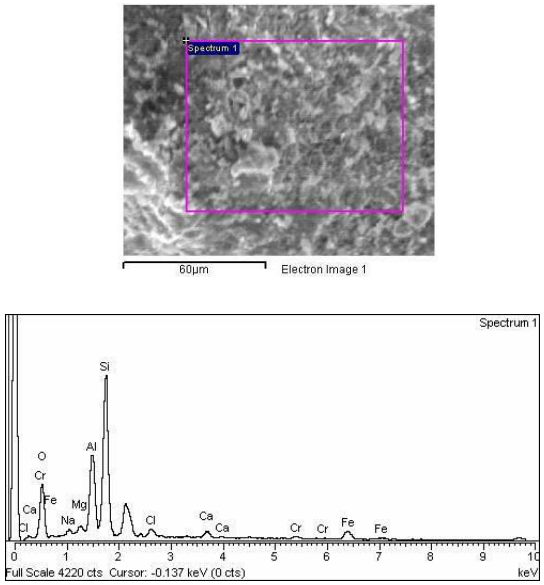

Fig 2. SEM-EDS image of bentonite after adsorption of Cr(III) ions

The morphology of the native sample showed a surface with clearly visible large cavities and macropores of randomly irregular orientation. Such a material structure is an essential prerequisite for the adsorption of heavy metals. Figure 2. shows that, after adsorption with Cr(III) ions, structural changes occurred in the bentonite, indicating that adsorption is associated with chemical alterations, which was further confirmed by FTIR analysis. The results of the SEM-EDS analysis of the native sample showed a significant mass percentage of C, O, Al, and Si, while the SEM-EDS analysis of the bentonite sample after Cr(III) ion adsorption indicated the incorporation of w(Cr)=0.97%, w(O)=47.50%, w(Si)=27.57%, w(Al)=12.59% , w(Na)= 1.67%, w(Ca)= 1.50 % and the absence of C ions. IR spectra were recorded in the range of 4000 to 400 cm^{-1}, and Figure 3. (a and b) shows the spectra of the bentonite samples before and after the adsorption process.

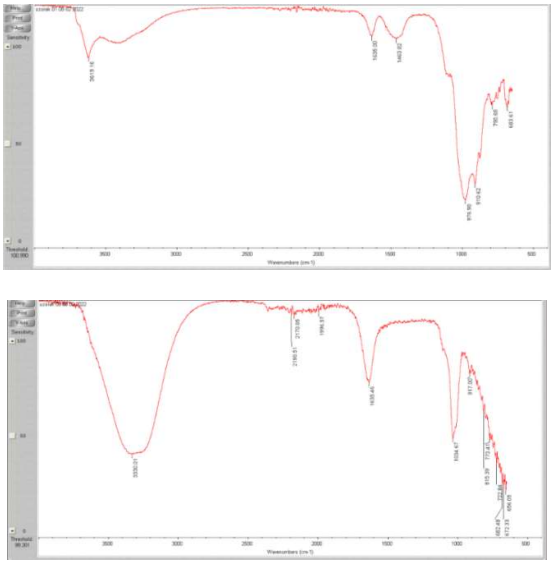

Fig 3. a) FTIR analysis of the native bentonite sample, b) FTIR analysis of the bentonite sample after adsorption of Cr(III) ions

The analysis of the native bentonite sample showed that the first peak appears at 3619.16 cm^{-1}, corresponding to the stretching vibrations of –OH groups that are part of the octahedra where Al^{3+} ions are coordinated with 6 –OH groups, which is typical for dioctahedral smectites. The peak observed at 1635 cm^{-1} is attributed to the bending vibrations of the H–O–H group, corresponding to water molecules located between the layers of the silicate matrix. The peak at 1463.82 cm^{-1} corresponds to the vibrations of the –OH group, while the peaks appearing in the range of 1400–800 cm^{-1} indicate the stretching vibrations of the Al–OH and Si–OH groups, suggesting that the bentonite composition likely contains quartz as an additive (Fonseca *et al*.,2006). Similar FTIR values were obtained by Maged *et al.* (2020) and Gandhi *et al.* (2022), who used bentonite for the removal of heavy metal ions. The FTIR analysis after adsorption of Cr (III) ions showed changes in the intensity of peaks in the region of 917.00–674.33 cm^{-1}, which can be attributed to the presence of quartz as an impurity in the bentonite, as well as the contribution of OH groups.

Results of adsorption experiments

Investigation of the effect of pH value

Figure 4 shows the effect of pH value on the adsorption capacity and removal efficiency of Cr(III) ions from the synthetic aqueous solution. As shown in Figure 4., the pH value has a significant influence on the metal ion adsorption process. At a pH value of 2, the lowest adsorption capacity of 417.627 mg/g for Cr(III) ions was recorded, while the highest adsorption capacity and metal removal efficiency were observed at pH 5, amounting to 498.966 mg/g and 99.793%, respectively. The lower adsorption capacity is probably caused by the increased

concentration of H^+ ions, whereas the higher efficiency of heavy metal removal at higher pH values can be explained by the fact that, as the pH increases, the concentration of H^+ ions decreases and the active sites of the clay undergo deprotonation, thus attracting positively charged ions through electrostatic interactions (Noyan,2007).

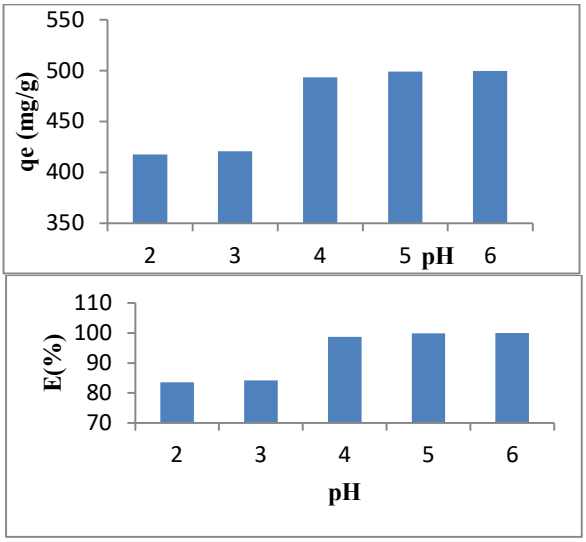

Fig 4. Effect of pH value
a) on the adsorption capacity b) removal efficiency

The obtained results are consistent with previously reported studies on the influence of pH on the adsorption of heavy metal ions on various clays (Jiang *et al*.,2010). Considering these results and the effect of pH on ion adsorption, further experiments were conducted at pH 5 to avoid precipitation in the form of hydroxides (Zhirong,2011).

Effect of initial concentration

Figure 5. shows the effect of the initial concentration on the adsorption capacity and removal efficiency of Cr(III) ions from the synthetic aqueous solution.

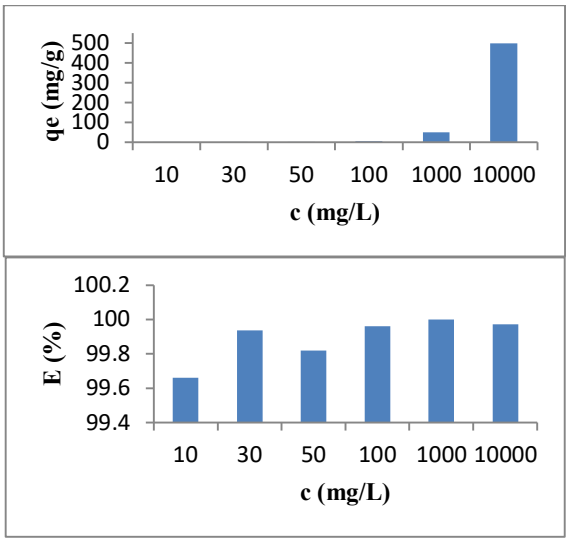

Fig 5. Effect of concentration a) on the adsorption capacity b) removal efficiency

The results show that with an increase in the initial metal concentration, the adsorption capacity also increases, reaching a maximum of 499.862 mg/g at a concentration of 10000 mg/L, which corresponds to an adsorption efficiency of 99.97%.

Effect of contact time

Figure 6 shows the effect of contact time on the adsorption capacity and removal efficiency of Cr(III) ions from synthetic and real aqueous solutions.

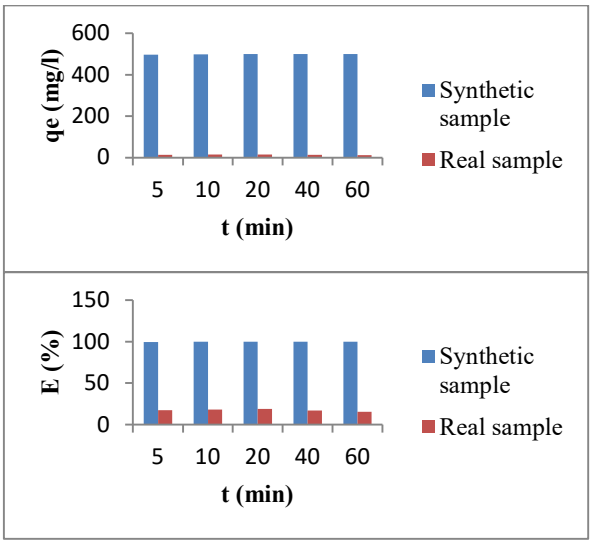

Fig 6. Effect of contact time a) on the adsorption capacity b) removal efficiency

The adsorption process occurred rapidly during the first few minutes, after which equilibrium was established, and the adsorption rate remained constant with further increases in contact time. The maximum removal efficiency of Cr(III) ions was 99.972% for the synthetic sample and 14.4% for the real sample at 60 min. The rapid removal rate can be explained by the fact that, at the beginning of the adsorption process, many active sites are available, which become occupied after a certain period once equilibrium is reached (Han,2006).

Effect of adsorbent mass

Figure 7. shows the effect of adsorbent mass on adsorption capacity and removal efficiency of Cr(III) ions from synthetic and real aqueous solutions. As can be seen from Figure 7a)., increasing the mass of the adsorbent increases the adsorption capacity of the synthetic sample, while increasing the mass of the adsorbent in the real sample decreases the adsorption capacity, which can be explained by the fact that during the adsorption process, the binding sites remain unsaturated. The presented results from Figure 7b). indicate that increasing the mass of the adsorbent leads to a significant increase in the removal efficiency of the examined ions, with a maximum efficiency for Cr(III) ions achieved at an adsorbent mass of 1 g for both synthetic and real sample. It is expected that increasing the adsorbent mass provides more binding sites on the adsorbent surface available for interaction

with metal ions, resulting in higher efficiency of metal ion removal from aqueous solutions (Bohli *et al*.,2013).

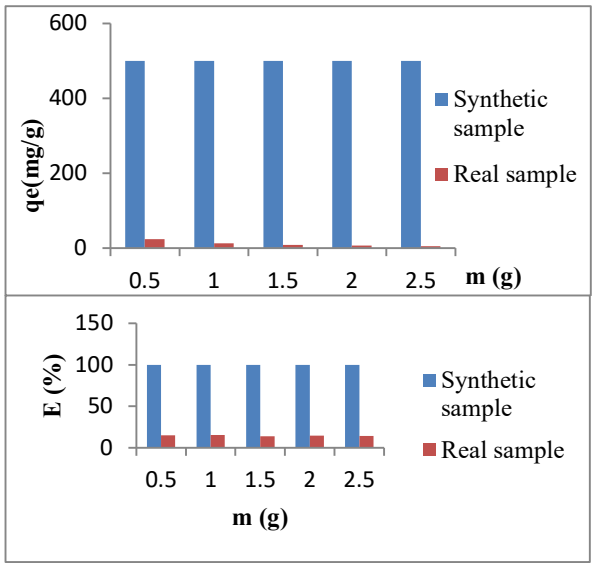

Fig 7. Effect of adsorbent mass a) on the adsorption capacity b) removal efficiency

Effect of temperature

Figure 8. shows the effect of temperature on the adsorption capacity and removal efficiency of Cr(III) ions from synthetic and real aqueous solutions.

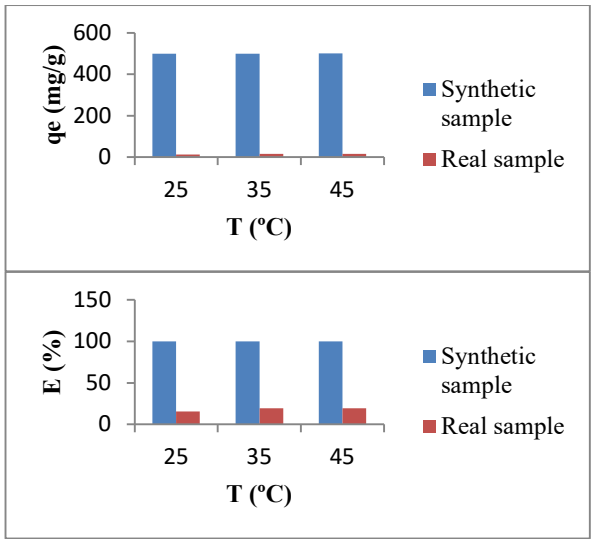

Fig 8. Effect of temperature a) on the adsorption capacity b) removal efficiency

As can be seen in Figure 8, the highest efficiency was achieved at a temperature of 45°C, with a maximum removal efficiency of Cr(III) of 99.992% for the synthetic sample and 18.870% for the real sample. Based on these results, it can be concluded that the adsorption.

The process for Cr(III) ions is endothermic (Afroze,2018).

Adsorption isotherm and models

Adsorption isotherms are very important for evaluating the maximum adsorption capacity of an adsorbent and for describing the interaction between the adsorbate and the adsorbent (Igwe, 2007). To assess the adsorption capacity of bentonite, the adsorption results of the investigated Cr(III) ions at different initial metal concentrations in synthetic aqueous solutions ranging from 10 to 10000 mg/L, and in a real solution with a concentration of 1643.57 mg/L, were analyzed using the Langmuir, Freundlich, and Temkin adsorption isotherm models. By applying the linear forms to the experimental equilibrium adsorption data, the required parameters were calculated using equations (3),(3.1.),(4), and (5), and the obtained results for the synthetic and real samples are presented in Table 3.

Langmuir adsorption isotherm

$$\frac{c_e}{q_e} = \frac{1}{K_L} + \frac{\alpha_L}{K_L} \cdot C_e \quad (3)$$

$$R_L = \frac{1}{1 + K_L \cdot C_o} \quad (3.1)$$

where: q_e (mg/g) – the amount of adsorbate adsorbed on the adsorbent at equilibrium conditions; C_e (mg/dm³) – equilibrium concentration of the adsorbate in the solution; q_{max} (mg/g) – the maximum amount of adsorbate adsorbed per unit mass of adsorbent, i.e., the maximum monolayer adsorption capacity, α_L (dm³/g) and K_L (dm³/mg) – Langmuir constants indicating the adsorption affinity of the adsorbent toward the investigated adsorbate.

Freundlich adsorption isotherm

$$log q_e = \log K_f + \frac{1}{n} \cdot \log C_e \quad (4)$$

where: q_e (mg/g) – the amount of adsorbate adsorbed on the adsorbent at equilibrium conditions; C_e (mg/dm³) – equilibrium concentration of the adsorbate in the solution; K_f ((mg/g)(dm³/mg)$^{1/n}$) – Freundlich adsorption constant; and n (dimensionless) – Freundlich constant indicating the intensity of the adsorption process and reflecting the surface heterogeneity.

Temkin adsorption isotherm

$$q_e = \frac{RT}{b} \ln K_t \; C_e \quad (5)$$

where: q_e(mg/g) – amount of adsorbate adsorbed onto the adsorbent at equilibrium conditions, C_e(mg/dm³) – equilibrium concentration of the adsorbate in the solution, R(8.314 J/mol·K) – universal gas constant, T(K)–absolute temperature, K_t(dm³/g) and b(J/mol) – Temkin constants corresponding to the adsorbate–adsorbent interaction and the heat of adsorption, respectively.

The best fit of the isotherm models with the experimental data was determined based on the correlation coefficient R^2. According to the data presented in Table 3., it can be observed that the experimental results for the removal of Cr(III) ions from the synthetic aqueous solution fit well with the Langmuir isotherm model, where the correlation coefficient R^2=1 for the investigated concentration range. The Temkin isotherm model also showed a good fit with the experimental data, with the highest correlation coefficient R^2 obtained at a concentration of 10 mg/L. The Freundlich isotherm model, which describes adsorption on a heterogeneous surface, gave the poorest results, with correlation coefficient values lower than those of the Langmuir and Temkin models (Gadd,2009). A good

agreement with the experimental results for the real sample was obtained using the Temkin and Freundlich adsorption models, where the correlation coefficient was R^2=1 for the Temkin model and R^2=0.998 for the Freundlich model.

Table 3: Values of adsorption isotherms for synthetic and real samples

Conc. (mg/L)	Isotherm model- **Freundlich model**			
	1/n	K_f (mg/g)	R^2	
10	-0.006	2.047	0.9656	
30	-0.0028	1.483	0.8576	
50	-0.0031	2.476	0.9847	
100	-0.0011	4.980	0.9265	
1000	$-2.00\cdot10^{-5}$	4.886	0.8767	
10,000	-0.0014	500.841	0.9329	
Conc. (mg/L)	Isotherm model- Langmuir model			
	Q_m (mg/g)	K (dm^3/mg)	R_L	R^2
10	0.4931	0.0003945	1.00394	1
30	1.4861	0.0004458	1.0133	1
50	2.4820	0.000496	1.0248	1
100	4.9850	$1.50\cdot10^{-4}$	1.0100	1
1000	5	$3.5\cdot10^{-6}$	1.0003	1
10,000	500	$2.0\cdot10^{-2}$	$2.01\cdot10^{2}$	1
Conc. (mg/L)	Isotherm model- **Temkin model**			
	B (J/mol)	A (l/mg)	R^2	
10	0.4883	0.993	0.9661	
30	1.4833	0.9971	0.8584	
50	2.4766	0.9968	0.9848	
100	4.9811	0.9988	0.9267	
1000	4.9990	0.9990	0.8760	
10,000	500.830	0.9985	0.9330	
Real sample				
Conc. (mg/L)	Isotherm model- **Freundlich model**			
	1/n	Kf (mg/g)	R^2	
1643.57	-4.835	2.013	0.998	
Conc. (mg/L)	Isotherm model- **Langmuir model**			
	Q_m (mg/g)	K (dm^3/mg)	R_L	R^2
1643.57	2.398	-1130.095	-1857828.1	0.996
Conc. (mg/L)	Isotherm model- **Temkin model**			
	B (J/mol)	A (l/mg)	R^2	
1643.57	504.03	0.873	1	

The values of the 1/n parameter of the Freundlich adsorption isotherm were negative for each concentration of both the synthetic and real samples at the initial concentrations of the analyzed metals, indicating that the adsorbent has a high degree of heterogeneity.

Kinetic models

To examine the kinetics of the adsorption process of Cr(III) ions on bentonite, three models were used: the pseudo-first-order model, the pseudo-second-order model and the intraparticle model. All models were calculated using equations (7),(8),(9) and (10), and the results obtained by nonlinear regression for the parameters of the kinetic models, using the Polymath program for different initial concentrations of Cr(III) ions as well as the actual concentration of the real sample, are presented in Table 4.

Pseudo-first-order model

$$\frac{dq_t}{d_t} = k_1(q_e - q_t) \quad (7)$$

where: q_t represents the amount of adsorbate bound at time t (mg/g); t – time (min); q_e – amount of adsorbate bound at equilibrium conditions.

Pseudo-second-order model

$$\frac{dq_t}{dt} = k_2(q_e - q_t)^2 \quad (8)$$

where: q_e and q_t have the same meaning as in the pseudo-first-order model, and k_2 (g/mg·min) is the rate constant of the pseudo-second-order model.

Intraparticle diffusion model

$$q_t = k_d t^{1/2} + I \quad (9)$$

where the intercept I refers to the thickness of the boundary layer on the adsorbent surface, and k_d is the rate constant of the intraparticle diffusion model.

n^{th} order model

$$\frac{dq_t}{dt} = k(q_e - q_t)^n \quad (10)$$

where: q_t represents the amount of adsorbate bound at time t (mg/g); t – time (min); q_e – amount of adsorbate bound at equilibrium conditions,k–n^{th}order rate constant (g/mg·min), n-order of adsorption kinetics.

Based on the obtained results, it can be concluded that there is a good agreement with interparticle diffusion model (R^2>0.7) and the pseudo-first-order model (R^2>0.5) at all concentrations of the synthetic sample, which implies that the rate of occupation of active sites is proportional to the number of unoccupied sites, with the adsorbate binding to a single active site. Based on the results for the real sample, it can also be concluded that the adsorption process follows the interparticle diffusion model, since the correlation coefficient (R^2) was the highest for this model, with a value of R^2=0.796. Additionally, a high correlation coefficient was obtained for the n^{th} order reaction model for the real sample, where the correlation coefficient was also R^2=0.796.

Table 4. Values of kinetic models

Conc. (mg/L)	Pseudo-first-order model		
	k_1 (l/min)	qe (mg/g)	R^2
10	0.236	0.492	0.584
30	0.236	1.484	0.583
50	0.235	2.469	0.581
100	0.236	4.950	0.580
1000	0.235	49.568	0.579
10,000	0.235	495.228	0.581
Conc. (mg/L)	**Pseudo-second-order model**		
	k_2 (g/mg·min)	qe (mg/g)	R^2
10	0.417	0.526	0.579
30	0.139	1.578	0.579
50	0.087	2.572	0.578
100	0.044	5.102	0.579
1000	0.0040	50.033	0.578
10,000	0.0004	516.023	0.579
Conc. (mg/L)	**Intraparticle diffusion model**		
	K_d (mg/g·min$^{(1/2)}$)	I (mg/g)	R^2
10	-0.0196	0.096	0.777
30	-0.059	0.291	0.777
50	-0.098	0.486	0.776
100	-0.198	0.976	0.777
1000	-1.985	9.786	0.776
10,000	-19.787	97.612	0.777
	Real sample		
Conc. (mg/L)	**Pseudo-first order model**		
	K_1 (l/min)	q_e (mg/g)	R^2
1643.57	0.204	14.085	0.766
Conc. (mg/L)	**Pseudo-second-order model**		
	k_2 (g/mg·min)	qe (mg/g)	R^2
1643.57	0.0078	18.714	0.691
Conc. (mg/L)	**Intraparticle diffusion model**		
	K_d (mg/g·min$^{(1/2)}$)	I (mg/g)	R^2
1643.57	-5.21	14.516	0.796
Conc. (mg/L)	**n order model**		
	K (g/mg·min)	q_e (mg/g)	R^2
1643.57	0.521	14.514	0.796

Table 5. presents the values of the thermodynamic parameters of the adsorption process for Cr(III) ions at three different temperatures, for both the synthetic and real samples.

Table 5. Values of thermodynamic parameters for the synthetic and real samples

Temperature (ºC)	**Termodynamic parameters syntetic sample**		
	ΔG^0 (kJ/mol)	ΔS^0 (J/mol·K)	ΔH^0 (J/mol)
25	-20.346		
35	-21.009	66.304	-587.567
45	-21.679		
Temperature (ºC)	**Termodynamic parameters real sample**		
	ΔG^0 (kJ/mol)	ΔS^0 (J/mol·K)	ΔH^0 (J/mol)
25	10.003		
35	10.342	-33.987	-122.534
45	10.682		

Based on the values given in the table, it can be concluded that the enthalpy (ΔH^o) values for both the synthetic and real samples are negative, indicating that the process is exothermic and that bentonite has a high affinity for these metal ions. The negative Gibbs energy (ΔG^o) values for the synthetic sample indicate that the process is spontaneous and that the heavy metal ions have a strong affinity toward the adsorbent (Dim,2020). Positive Gibbs energy values were recorded for the real sample, suggesting that the process is not spontaneous in this case. The increase in Gibbs energy with rising temperature for both samples indicates that the adsorption process is feasible even at higher temperatures. The positive entropy change (ΔS^o) for the synthetic sample suggests increased randomness and a rise in the degrees of freedom at the solid–liquid interface during metal ion binding, while the negative value indicates a decrease in randomness (Akar *et al.*,2013). Arshadi *et al.* (2014) explained the positive entropy value as a result of energy redistribution between the adsorbate and the adsorbent.

Column adsorption

The experiments on the adsorption of Cr(III) ions from their solutions were carried out in a fixed-bed column with an adsorbent layer height of 5 cm and a solution layer height of 22 cm. Figure 9. shows the breakthrough curve for Cr(III) ions at a time and volume of 1 dm³, pH 5, with a concentration of 10000 mg/L for the synthetic solution and 1643.57 mg/L for the real sample.

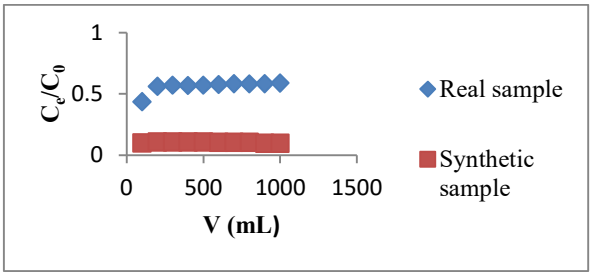

Fig 9. Breakthrough curve for the adsorption of Cr(III) ions

As can be seen from the graph, the breakthrough point for Cr(III) ions occurred at the first 100 mL of the solution and approximately 1 min for the synthetic sample, with further passage of the ion solution, the plateau of the breakthrough curve increased significantly until 800 mL of solution had passed, when the value of 0.103 was reached, after which a slight decrease was observed. The adsorption process of the real sample occurred rapidly at a flow rate of 40 mL/min, with the breakthrough point appearing immediately after passing 100 mL of the solution. With further passage of the solution, the plateau of the formed curve increased and reached a value of 0.587, indicating that the adsorption process took place rapidly but did not reach a relative equilibrium value, which suggests that the process was not yet completely finished and continued at a negligible rate. This can be explained by the Faten *et al*.,(2022), who showed that breakthrough curves at lower flow rates lead to slower equilibrium establishment but higher removal efficiency due to the longer contact time available.

CONCLUSIONS

In this study, bentonite was used as an inexpensive and easily available adsorbent for the adsorption of Cr(III) ions, proving to be highly effective in removing Cr(III) ions from galvanic wastewater. The bentonite sample was characterized using FTIR, SEM-EDS, and BET analyses, and the results showed a large specific surface area and an irregular structure with large pores, which is essential for the adsorption process. The adsorption of Cr(III) ions was evaluated by examining several parameters, including pH value, initial concentration, adsorbent mass, and contact time. The results indicated that the adsorption process occurs rapidly and that increasing the concentration leads to higher adsorption capacity and removal efficiency for both tested metal samples (E > 90%). The Langmuir and Temkin models showed the best fit with the experimental values within the studied concentration range, while the best agreement with kinetic models was achieved using the pseudo-first-order model for both samples, as well as the n order for the real sample. The column experiment results showed that the adsorption process proceeds at a high rate, with the breakthrough point occurring after the first 100 mL of the passed solution.

REFERENCES

Afroze, S., Sen, T. K. (2018). A Review on Heavy Metal Ions and Dye Adsorption from Water by Agricultural Solid Waste Adsorbents. *Water, Air, & Soil Pollution, 229(7), 225. DOI: 10.1007/s11270-018-3869-z.*

Ahmetović, M., Šestan, I., Odobašić A., Papraćanin, E. (2024). Bentonite as a Potential Adsorbent for the Removal of Copper Ions from the Galvanic Industry Wastewater. *Advanced Technologies, Systems, and Applications IX, Springer*. DOI: 10.1007/978-3-031-71694-2_47.

Ahmetović, M., Šestan, I., Odobašić, A., Papraćanin, E., Keran, H., Đozić, A. and Junuzović, H., (2024). The potential of bentonite as a low-cost adsorbent for the removal of heavy metal ions from multicomponent aqueous systems of the galvanic industry. *International Research Journal of Pure and Applied Chemistry, 25(2), pp.28-39.* DOI: 10.9734/irjpac/2024/v25i2848.

Akar, S.T., Yilmazer, D., Celik, S., Balk, Y.Y., Akar T., (2013). On the utilization of a lignocellulosic waste as an excellent dye remover: Modification, characterization, and mechanism analysis, *Chemical Engineering Journal 229:257-266.* DOI: 10.1016/j.cej.2013.06.009.

Arshadi, M., Amiri, M. J., Mousavi, S. (2014). Kinetic, equilibrium and thermodynamic investigations of Ni(II), Cd(II), Cu(II), and Co(II) adsorption on barley straw ash.*Water resources and Industry (6), 1-17.* DOI: 10.1016/j.wri.2014.06.001.

Bohli, T., Villaescusa, I., Ouedern, A. (2013). Comparative Study of Bivalent Cationic Metals Adsorption Pb(II), Cd(II), Ni(II), and Cu(II) on Olive Stones Chemically Activated Carbon. *Journal of Chemical Engineering & Process Technology, (4)04.* DOI: 10.4172/2157-7048.1000158.

Daković, A., Tomašević-Čanović, M., Dondur,V., Stojšić, D., Rottinghous, G., (2001). *Zeolites and mesoporous materials at the dawn of the 21st century* in Proceedings of the 13th International Conference. Montpellier, France. DOI: 10.1016/S1387-1811(03)00365-2.

Dengbing, W., Dingsheng, W., Anfang, W., Jun G., Chengling, P, Ze, M., Quan, F. (2025). Scalable, high flux of electrospun nanofibers membrane for rapid adsorption-reduction synergistic removal of Cr(VI) ions in wastewater. *Separation and Purification Technology, Vol. 360 (2), 130747,1383-5866.* DOI: 10.1016/j.seppur.2024.130747.

Dhaouadi, F., Sellaoui, L., Chávez-González, B., Elizabeth Reynel-Ávila H., DiazMuñoz L. L.,Mendoza-Castillo D.I., Petriciolet, A.B., Lima,E.C., Picazo J.C.T., Ben Lamine, A.B., (2021).Application of a heterogeneous physical model for the adsorption of Cd^{2+}, Ni^{2+}, Zn^{2+} and Cu^{2+} ions on flamboyant pods functionalized with citric acid. *Chemical Engineering Journal,417:127975.* DOI: 10.1007/s11356-021-12832-x.

Dim, P.E, Olu, C.S, Okafor, O.J (2020) .Kinetic and thermodynamic studies of the adsorption of Cu (II) and Cr (VI) ions from an industrial effluent on a kaolinite clay, *Journal of Chemical Technology and Metallurgy 55(5)1057-1067.*

Faten B.H., Brooke K.M.B. (2022). Fixed-bed column study of phosphate adsorption using immobilized phosphate-binding protein. *Chemosphere 295, 133908*. DOI: 10.1016/j.chemosphere.2022.133908.

Fonseca, M.G., Oliveira, M.M., Arakaki, L.N.H (2006). Removal of cadmium, zinc, manganese and chromium cations from aqueous solution by a clay mineral, *Journal of Hazardous Materials 137(1), 288–292. DOI: 10.1016/j.jhazmat.2006.02.001.*

Gadd, G. M. (2009). Biosorption: critical review of scientific rationale, environmental importance and significance for pollution treatment. *Journal of Chemical Technology & Biotechnology, 84(1), 13–28.* DOI: 10.1002/jctb.1999.

Gandhi, D., Bandyopadhyay, R., Soni, B. (2022). Naturally occurring bentonite clay: Structural augmentation, characterization and application as

catalyst. *Elsevier, Materials Today:Proceedings, 57 (1), 194-201*. DOI: 10.1016/j.matpr.2022.02.346.

Gaoqian, Y., Kezhuo, L., Jingzhe, Z., Long, D., Yage, L., Guodong, Y., Liang, H., Faliang, L., Haijun, Z., Shaowei, Z. (2024). Construction of bionic sea urchin-like $ZnFe_2O4/Bi_2S_3$ heterojunction for microwave-induced catalytic reduction of Cr(VI): Performance and mechanism insights, *Chemical Engineering Journal, Vol. 488. DOI: 10.1016/j.cej.2024.150766*

Gholamifard,H., Rasul,M.G., Rahideh,H., Azari, A., Abbasi, M., Karami, R. (2023). Experimental and numerical analysis of oily wastewater treatment using low-cost mineral adsorbent in a single and multi-fixed bed column, *Chemical Engineering Journal Advances (16) Article 100551*. DOI: 10.1016/j.ceja.2023.100551.

Han, R., Zou, W., Zhang, Z., Shi, J., Yang, J. (2006).Removal of copper(II) and lead(II) from aqueous solution by manganese oxide coated sand. *Journal of Hazardous Materials, 137(1), 384–395.* DOI: 10.1016/j.jhazmat.2006.02.021.

Igwe, C.J., Abia, A.A. (2007). Equilibrium sorption isotherm studies of Cd(II), Pb(II) and Zn(II) ions detoxification from waste water using unmodified and EDTA-modified maize husk, *Electronic Journal of Biotechnology 10(4),0717-3458*. DOI: 10.2225/vol10-issue4-fulltext-15.

Jiang, M.Q., Jin, X.Y., Lu, X.Q., Chen Z.L. (2010). Adsorption of Pb(II), Cd(II), Ni(II) and Cu(II) onto Natural Kaolinite Clay. *Desalination, 252, 33-39.* DOI: 10.1016/j.desal.2009.11.005

Joyel, P., Ahsan, Q., Sandeep, S.A., Sabu, T., Alain, D. (2024) Chitosan-based aerogels: A new paradigm of advanced green materials for remediation of contaminated water. *Carbohydrate Polymers, Vol. 338, 122198, 0144-8617*. DOI: 10.1016/j.carbpol.2024.122198

Kejin, Y., Lina Y., Siyu, Z., Ning, Z. (2025). Nanocellulose-based aerogels for the adsorption and removal of heavy-metal ions from wastewater: A review, *Materials Today Communications, Vol. 43,111744, 2352-4928.* DOI: 10.1016/j.mtcomm.2025.111744.

Kovo G. A, Folasegun A.D. (2015). Potential of a low-cost bentonite for heavy metal abstraction from binary component system, *Journal of Basic and Applied Science (4) 1-13.* DOI: 10.1016/j.bjbas.2015.02.002.

Maged, A., Kharbish, S., Ismael S.I., Bhatnagar A. (2020). Characterization of activated bentonite clay mineral and the mechanisms underlying its sorption for ciprofloxacin from aqueous solution. *Environmental Science and Pollution Research, 27:32980–32997*. DOI: 10.1007/s11356-020-09267-1

Noreen S., Khalid U., Ibrahim S. M., Javed T., Ghani A., Naz S., Iqbal,M. (2020). ZnO, MgO and FeO adsorption efficiencies for direct sky Blue dye: equilibrium, kinetics and thermodynamics studies. *Journal of Material Research and Technology:9(3)5881–5893.* DOI: 10.1016/j.jmrt.2020.03.115.

Noyan H., Önal M., Sarıkaya Y. (2007). The effect of sulphuric acid activation on the crystallinity, surface area, porosity, surface acidity, and bleaching power of a bentonite. *Food Chemistry 105(1)156–163*. DOI: 10.1016/j.foodchem.2007.03.060.

Petrović,R., Gajić,D., Obrenović, Z., Bodroža, D., Popadić,N.,Davidović,D., Ćulumović, M., (2019). Kinetics of Cr(VI) adsorption from aqueous medium onto bentonite,*Glasnik hemičara, tehnologa i ekologa Republike Srpske (15) 9-16.* DOI: 10.7251/GHTE1915009P.

Sher, F., Hanif, K., Rafey,A., Khalid, U., Zafar,A., Ameen,M., Lima,E.C (2021). Removal of micropollutants from municipal wastewater using different types of activated carbons„*Journal of Environmental Management, 278 (2) 111302.* DOI: 10.1016/j.jenvman.2020.111302.

Tadesse, S.H. (2022). Application of Ethiopian bentonite for water treatment containing zinc. *Journal of Emerging Contaminants 8 (1): 113-122*. DOI: 10.1016/j.emcon.2022.02.002.

Vhahangwele, M., Mugera, W.G., Tholiso, N. (2014). Defluoridation of drinking water using Al^{3+} modified bentonite clay: optimization of fluoride adsorption conditions*, Toxicological & Environmental Chemistry, 96(9),1294-1309.* DOI: 10.1080/02772248.2014.977289.

Wael,I. M., Ali, E.N., Ahmed, M.K., Niroshika, P., Balal, Y., Ronggui, T., Shengsen, W., Yanjiang, C., Scott, X.C. (2023). Biogeochemical behaviour and toxicology of chromium in the soil-water-human nexus: A review, *Chemosphere, Vol. 331, 138804, 0045-6535*. DOI: 10.1016/j.chemosphere.2023.138804.

Wu, Y., Pang, H., Liu, Y., Wang, X., Yu, S., Fu, D., et al. (2019). Environmental remediation of heavy metal ions by novel-nanomaterials: a review. Environmental Pollution 246, 608–620. DOI: 10.1016/j.envpol.2018.12.076.

Saghir,Y., Chaoui,A., Farsad,S., Ben H.A, Amjlef,A., Benafqir,M., Alem,E.N., Ez-zahery, M. (2025). Improving the adsorption efficiency of a low-cost natural adsorbent for the removal of an organic pollutant: optimization and mechanism study. *Materials Advances, Volume 6, (4), Pg 4857-4873*. DOI: 10.1039/d5ma00253b.

Zhirong L., Azhar, U. M., Zhanxue S. (2011). FT-IR and XRD analysis of natural Na-bentonite and Cu(II)-loaded Na-bentonite. *Spectrochim Acta A Mol Biomol Spectrosc.79(5),1013-6*. DOI:10.1016/j.saa.2011.04.013.

Summary/Sažetak

Prisustvo teških metala poput hroma u vodotocima može da dovede do različitih zdravstvenih problema kod ljudi, ali i životinja. Zbog negativnog učinka prije ispuštanja u vodotoke otpadne vode obogaćene hromom potrebno je pročistiti. U ovom radu proučavana je mogućnost upotrebe bentonita kao adsorbensa za uklanjanje hroma iz otpadnih voda galvanske industrije. Najprije je urađena fizičko-hemijska karakterizacija korištenog bentonita, a zatim je ispitan uticaj procesnih parametara poput pH vrijednosti, koncentracije, mase i vremena. Na osnovu dobijenih podataka urađene su i adsorpcijske izoterme, kao i kinetički modeli i termodinamika. Svi provedeni eksperimenti su rađeni saržnim sistemom i sistemom u koloni. Rezultati su pokazali da se bentonit može koristiti kao jeftini adsorbens za efikasno uklanjanje jona hroma iz otpadne vode galvanske industrije, te da pri pH 5, masi od 1g postiže najveća efikasnost uklanjanja (99.97%). Langmuirov i Temkinov model adsorpcijskih izotermi pokazao je dobro slaganje sa eksperimentalnim vrijednostima (R^2>0.9), dok je najbolje slaganje sa kinetičkim modelom zabilježeno kod pseudo-prvog modela.

Glasnik hemičara i tehnologa Bosne i Hercegovine

Bulletin of the Chemists and Technologists of Bosnia and Herzegovina

2026

66

41-46

Print ISSN: 0367-4444
Online ISSN: 2232-7266

Original Scientific Article
DOI: 10.35666/2232-7266.2026.66.05
UDK: 54[628.19:502.17]

Stabilization of Waste Sludge from Municipal Wastewater Treatment Plant

Džambić, M.[a*], Stuhli, V.[b], Čorbić, M.[b], Kusur, A.[b], Hodžić, S.[b], Mešanović Š.[b]

[a]*Federal Administration for Inspection Affairs, Fehima ef. Čurčića 6, Sarajevo, Bosnia and Herzegovina*

[b]*Faculty of Technology, University of Tuzla, Urfeta Vejzagića 8, Tuzla, Bosnia and Herzegovina*

Article info
Received: 05/12/2025
Accepted: 17/02/2026

Keywords:
Wastewater treatment
Waste sludge
Sludge treatment
Stabilization
Pyrophyllite schist

***Corresponding author:**
Mirsad Džambić
E-mail: mirsad.dzambic@fuzip.gov.ba
Phone: +38761148602

Abstract: Municipal wastewater treatment generates significant amounts of waste sludge that needs to be stabilized before disposal or reuse due to environmental and health risks. This study evaluated the effectiveness of microbiological, biological, and physical sludge treatment methods using physicochemical, microbiological, and ecotoxicological analyses. Microbiological treatment with a mixed microbial culture resulted in odor reduction and partial changes in organic matter content. Biological treatment with *Eisenia fetida* led to gradual structural transformation of the sludge and a reduction in pathogenic indicators, although a longer treatment time was required. Physical stabilization using pyrophyllite schist significantly increased total solids (from 17.75% to 48.32%), reduced volatile solids (to 2.26 %) due to combined stabilization and dilution effects, immobilized selected heavy metals, and eliminated fecal bacteria and other pathogenic microorganisms. Ecotoxicological assessment showed an increase in LC_{50} values from 27% in raw sludge to 58% after physical treatment, indicating reduced toxicity. The results show that pyrophyllite schist is an effective natural material for improving the physicochemical stability and hygienic safety of wastewater sludge and highlight the potential of combining biological agents and natural mineral materials for sustainable sludge management.

INTRODUCTION

Wastewater treatment is a process aimed at reducing pollution to levels at which treated effluent can be safely discharged into receiving water bodies without adverse effects on human health and the environment (Pešević, 2022). An inevitable by-product of municipal wastewater treatment is waste sludge, the amount and composition of which depend on both the characteristics of the influent wastewater and the applied treatment technology. Higher treatment efficiency generally results in increased sludge production and a more complex sludge composition (Vouk et al., 2016). Waste sludge typically represents approximately 1–2% of the total volume of treated wastewater, and retains up to 50–80% of the originally present pollutants. At the same time, sludge is a valuable source of organic matter and nutrients, containing on average about 40% organic carbon, nearly 10% nitrogen, and approximately 3% phosphorus. Due to these characteristics, waste sludge has the potential for beneficial use, particularly in agriculture. However, its application is limited by the presence of heavy metals, pathogenic microorganisms, and various organic contaminants such as polycyclic aromatic hydrocarbons, polychlorinated biphenyls (PCBs), pharmaceuticals, pesticides, and microplastics (Nguyen et al., 2022). Improper treatment or disposal of waste sludge can result in environmental pollution and loss of valuable resources. The importance of effective sludge management has therefore increased significantly, driven by the expansion of sewerage systems, the construction of new wastewater treatment plants, and the modernization of existing infrastructure (Shaddel et al., 2019). In order to reduce environmental risks, sludge stabilization is required to prevent further biodegradation, reduce odors, and improve hygienic safety.

Conventional sludge stabilization methods include biological, physicochemical, and thermal processes (Tezel et al., 2011; Zhen et al., 2017; Zhang et al., 2021). Although these methods can be effective, they are often associated with high operational costs, increased energy consumption, incomplete stabilization, or secondary environmental impacts such as excessive alkalinity or nutrient loss. In addition, many stabilization approaches

rely on aggressive chemical agents, which can limit the sustainable reuse of treated sludge. These limitations highlight the need for alternative or complementary stabilization strategies that are environmentally compatible, cost-effective, and based on locally available materials. Natural mineral materials have recently attracted attention for their potential to improve sludge stability through adsorption, immobilization of contaminants, and moisture reduction. In this study, pyrophyllite schist was selected as a physical stabilization agent due to its mineral composition, layered aluminosilicate structure, adsorption capacity, local availability, and low environmental impact. These properties suggest that pyrophyllite schist can contribute to both physicochemical stabilization and hygienic improvement of waste sludge. In addition to physical stabilization, biological approaches play an important role in sludge treatment. In this context, microbiological treatment refers to the application of selected microbial consortia to improve biochemical transformation processes, while biological treatment involves higher organisms, such as earthworms (*Eisenia fetida*), which facilitate organic matter degradation through vermicomposting mechanisms. Although both approaches are biologically based, they differ in their mechanisms, time requirements, and effects on sludge properties.

Therefore, the aim of this study was to comparatively evaluate microbiological, biological, and physical stabilization methods for municipal waste sludge, with a particular emphasis on the application of pyrophyllite schist as a natural stabilization material. The effectiveness of each treatment was assessed using physicochemical, microbiological and ecotoxicological parameters to determine their potential contribution to sustainable sludge management.

EXPERIMENTAL

Materials

Sludge from the municipal wastewater treatment plant of the city of Živinice was used as the basis for this research. Microbiological treatment of the sludge was carried out using microorganisms from the eMB starter culture (including lactic acid bacteria, photosynthetic bacteria, and PDM 7 group of microorganisms) from the company EM Plus, Doboj, Bosnia and Herzegovina. Biological treatment was carried out using earthworms (*Eisenia fetida*), while physical treatment included the use of pyrophyllite schist purchased from Parsovići-Konjic, Bosnia and Herzegovina, and delivered by AD Harbi d.o.o. Sarajevo. Pyrophyllite schist is a natural aluminosilicate mineral characterized by a layered structure and adsorption capacity, which makes it suitable for binding moisture and inorganic pollutants. Recent mineral science studies have documented its characterization and beneficiation (Bhukte et al., 2024).

Methods

A series of analytical tests were carried out to assess the physicochemical and biological parameters of the sludge. Standard and modified standard methods for wastewater analysis were applied, according to BAS EN ISO, EN ISO, and APHA methodologies. The modifications primarily concerned sample preparation and dilution steps, as standard wastewater treatment methods were adapted to the high solid content and heterogeneous nature of sludge samples.

Physicochemical Analysis

The characterization of the raw material (waste sludge) and the mixtures obtained after treatment was performed by measuring the pH value and determining the total solids (TS) and volatile solids (VS) contents, together with the concentrations of total Kjeldahl nitrogen (TKN) and total phosphorus (TP), expressed on a dry matter basis. The pH value was measured using a pH meter (Mettler Toledo FE20/EL20) with direct electrode immersion into the samples. The total solids (TS) and volatile solids (VS) contents were determined according to Standard Methods 2540 B and 2540 E, respectively (American Public Health Association, 2005). The TKN concentration was determined using Method 4500 (American Public Health Association, American Water Works Association, Water Environment Federation, 2023), while the total phosphorus concentration was analyzed according to the standard BAS EN ISO 6878:2006. Heavy metals were determined by atomic absorption spectrometry in accordance with EN 16174:2012 (European Committee for Standardization, 2012). The concentration of polychlorinated biphenyls (PCBs) was analyzed using the US EPA SW-846 Test Method 3546 (United States Environmental Protection Agency).

Microbiological Analysis

For the purpose of microbiological characterization of the sludge, several key microbiological parameters were analyzed using standard microbiological techniques:

Total aerobic mesophilic bacteria at 22°C and 37°C: Serial dilutions were prepared up to 10^{-6} using a vortex mixer. From each dilution, 1 mL was pipetted into sterile Petri dishes and overlaid with 15 mL of Nutrient Agar. The plates were incubated at 22°C and 37 °C for 72 hours. After incubation, colony-forming units (CFUs) were counted, and results were expressed as CFU/mL.

Total coliform bacteria (MPN method): The most probable number (MPN) method was used to estimate the number of total coliforms in 100 mL of sample. The method, based on colorimetry, involves inoculation into lactose-based broth (e.g., MacConkey broth) containing Durham tubes. After 48 hours of incubation at 37°C, the presence of acid and gas was used as a positive indicator. The results were calculated using MPN tables and expressed as MPN/1 L.

Yeast/molds: Serial dilutions of the sample were prepared under aseptic conditions. Aliquots from each dilution were transferred to sterile Petri dishes and mixed with Rose Bengal Chloramphenicol Agar (RBCA). After solidification, the plates were incubated at 28°C for 5 days, which is the standard incubation period for the enumeration of yeasts and molds on this medium. After incubation, colonies exhibiting morphology typical of yeasts and molds were counted, and the results were reported as CFU/mL, adjusted for the appropriate dilution factors.

Fecal streptococci (Enterococci): Membrane filtration was used to determine the number of fecal streptococci (enterococci). Salturius nitrocellulose membrane filters

with a pore size of 0.45 µm were used. The filters were placed on Slanetz-Bartley agar and incubated at 36°C for 48 hours. Colonies with a red appearance were subcultured onto Bile Esculin agar and incubated for 2 hours at 44.5°C. Colonies that turned dark or formed a dark zone were counted. Results were expressed as CFU/100 mL.

Fecal coliforms: The Eijkman test was used to determine the presence of fecal coliforms. Sample aliquots were inoculated into a lactose-based selective medium and incubated at 44–45°C for 48 hours, the temperature range used to detect thermotolerant coliforms. Tubes showing gas formation were considered presumptively positive.

Proteus species: Serial dilutions were prepared using sterile distilled water. Samples were inoculated into MacConkey broth and incubated for 48 hours at 37°C, followed by streaking on MacConkey agar and incubation for 24 hours at 37°C. Characteristic large, spreading (swarming) colonies indicated the presence of *Proteus* spp.

Sulfite-reducing clostridia (membrane filtration method): After dilution, the samples were filtered through Salturius nitrocellulose membrane filters with a pore size of 0.22 µm, and the membrane filter was carefully placed on the bottom of a sterile Petri dish. Approximately 18 mL of molten complete medium (cooled to about 50°C) was poured over the filter. The plates were incubated under anaerobic conditions at 37±1°C for 20±4 and 44±4 hours. Black colonies were counted and recorded as sulfite-reducing clostridia.

Pseudomonas aeruginosa (MPN method): Five test tubes, each containing 10 mL of Asparagine broth, were inoculated with 10 mL of the diluted sample. After shaking, the tubes were incubated for 48 hours at 35°C. Tubes showing fluorescence or turbidity were considered positive.

Experimental procedure

To complete the sludge treatment process, the following experimental procedures were conducted: microbiological treatment of sludge, biological treatment of sludge and stabilization of sludge with natural material. Raw waste sludge (T0), stored under the same environmental conditions without any treatment, was used as a control sample for comparison with the treated samples.

Microbiological treatment of sludge was carried out using eMB starter cultures containing lactic acid bacteria, photosynthetic bacteria, and PDM (a consortium of seven groups of beneficial microorganisms). In this procedure, the sludge was mixed with a liquid microbial solution by layering. First, a portion of the microbial culture (primarily lactic acid bacteria of dairy origin) was sprayed onto the cleaned concrete surface. Then, a 10 cm layer of sludge was applied, followed by another layer of the microbial solution. This layering process (microorganisms–sludge–microorganisms) was repeated until a pile approximately 80 cm in height was formed. The pile was left to stand for 7 days. A total of 5 liters of microbial solution per 1 m³ of sludge was used. The mixture was aerated by turning the pile every 7 to 10 days. After 45 days, a sample was taken for further analysis.

In the biological treatment experiment, 1 m^3 of dehydrated sludge was mixed with 50 kg of a mixture containing California earthworms and compost. The compost included both mature earthworms and newly established colonies of smaller earthworms, mixed with organic residues such as fruit and vegetable scraps, paper, and leaves. The mixture was thoroughly homogenized and left to settle. It was manually stirred every 7 days. After 180 days, a sample was collected and analyzed. In the experimental treatment of sludge with a natural material, dehydrated sludge was mixed with pyrophyllite schist. The ratio used was 1 kg of pyrophyllite schist to 10 kg dehydrated sludge, and the mixture was stored in a dry and dark place. The mixture was stirred every 7 days. By the end of the experiment, the characteristic unpleasant odor of the dehydrated sludge had completely disappeared. After 30 days, the sample was collected and analyzed.

Fig 1. Microbiological treatment of sludge

Fig 2. Biological treatment of sludge

Fig 3. Stabilization of sludge with natural materials

RESULTS AND DISCUSSION

Based on the physicochemical analyses of sludge treated by different methods, the results are presented in Table 1. The addition of pyrophyllite schist to the waste sludge (T3) resulted in a significant increase in total solids (TS) and a change in the ratio of volatile solids (VS), total Kjeldahl nitrogen (TKN), and total phosphorus (TP) in the raw sludge. This effect can be attributed to the high mineral content and adsorption properties of pyrophyllite, which not only increases the solid fraction but also immobilizes certain organic and nutrient components, thereby reducing the volatiles content and changing the availability of nitrogen and phosphorus.

In addition, the physical structure of the schist can improve sludge drainage and compaction, which contributes to the observed changes in the composition of solids and

nutrients. The content of metal elements in the treated sludge was lower compared to the untreated sludge, which directly improves the suitability of the material for application. It is particularly important to note that the concentrations of almost all analyzed metals (except Ni) were significantly below the maximum permissible values prescribed by the Regulation on the Determination of Permissible Quantities of Harmful and Hazardous Substances in Soil and Methods of Their Testing (Official Gazette of FBiH, No. 96/22) and the Regulation on Sludge Management from Municipal Wastewater Treatment Plants (Official Gazette of FBiH, No. 28/24).

Table 1: Physicochemical parameters in the analyzed samples.

Parameter	Unit	T_0	T_1	T_2	T_3
pH	-	8.08	7.45	6.82	7.10
TS	%	17.75	22.19	16.17	48.32
VS	%	9.82	12.56	12.89	2.26
TP	g/kg	186.78	156.48	69.5	41.619
TKN	g/kg	9.67	11.07	2.04	11.7
Fe	mg/kg	0.2024	0.217	6.92	0
Mn	mg/kg	0.068	0.08	0.206	0
Cu	mg/kg	118	77.7	141	37.8
Cr	mg/kg	41.7	56.1	88.1	1.14
Pb	mg/kg	27.9	52.7	32.2	18.8
Ni	mg/kg	123	146	96.6	79.8
Ca	g/kg	22.2	26.7	32.3	30.8
PCB	mg/kg	0.01	0.01	0.01	0.01

T_0-raw waste sludge from the Živinice municipal wastewater treatment plant; T_1-microbiologically treated sludge; T_2-biologically processed sludge; T_3-physically stabilized sludge using natural material.

The pH value decreased from 8.08 in the raw sludge to 6.82 in the biologically treated sample (T2), indicating the formation of acidic compounds during the decomposition of organic matter. The slight increase in pH to 7.10 in sample T3 suggests partial buffering and stabilization of the medium after the addition of pyrophyllite schist. The total proportion of solids (TS) increased from 17.75% in the raw sludge to 48.32% in the sample (T3), primarily due to the reduction of moisture and the addition of mineral material. In contrast, samples T1 and T2, showed an increase in volatile solids (VS) content compared to raw sludge, which can be attributed to microbial activity combined with reduced water content, leading to a relative concentration of organic matter in the dry fraction (Arnaiz et al., 2006). A significant drop in VS (to 2.26%) was observed in sample T3, reflecting an increased proportion of inert mineral material and improved stability, thereby reducing the potential for further biological degradation. The total phosphorus content decreased in all treatments, from 186.78 g/kg in the raw sludge to 41.62 g/kg in the sample with the addition of pyrophyllite schist. This decrease indicates the loss of phosphorus compounds during biological processes, where part of the phosphorus is transferred to the liquid phase or consumed in microbial growth. The addition of pyrophyllite schist further reduces the phosphorus content due to the adsorption of phosphate ions on the mineral surface.

The TKN values varied across all treatments. The slight increase in T1 (11.07 g/kg) compared to the raw sludge (9.67 g/kg) can be attributed to the concentration of organic matter and microbial activity. In T2, there was a significant decrease (2.04 g/kg) due to the degradation and loss of nitrogen compounds in the form of ammonia or other soluble forms, while the physically treated sample T3 showed a higher TKN value (11.7 g/kg), which is a result of stabilization and the addition of mineral material, which reduced TKN losses. Regarding heavy metals, the concentrations of all metals were variable. The reported concentrations of iron (Fe) and manganese (Mn), which in certain samples were equal to 0 mg/kg, indicate values below the analytical detection limits of the applied method rather than the complete absence of these elements, resulting in apparently inconsistent trends. In contrast, copper (Cu), lead (Pb), and nickel (Ni) generally decreased only in the sample treated with pyrophyllite schist, suggesting possible immobilization effects due to the addition of the stabilizing material. In the same sample (T3), chromium (Cr) exhibited a significant reduction from 56.1 mg/kg to 1.14 mg/kg, which may indicate its precipitation or adsorption on the mineral surface. The unchanged concentration of polychlorinated biphenyls (PCBs) in all treatments (0.01 mg/kg) indicates the pronounced persistence of these compounds and the limited effectiveness of the applied biological and physical stabilization methods, which is in accordance with literature reports on the long-term persistence of PCBs in the environment (Othman et al., 2022). The results obtained indicate an effective stabilization of organic matter and a partial reduction of potentially hazardous elements. The observed variations in nutrient and metal content reflect the complex biochemical and physicochemical interactions that occur during the biological treatment and stabilization processes. Both biological and physical treatments significantly improved the physicochemical characteristics of the sludge, reducing the organic load and improving its quality. Together with metal concentrations well below the legally permissible limits, these findings confirm that the treated sludge possesses favorable properties for controlled use, provided that continuous monitoring of persistent organic pollutants is ensured. The results of biological parameters after sludge treatment by different methods are presented in Table 2. LC50 values (Lethal Concentration causing 50% mortality after 48 hours) increased after treatment, particularly in sample T3, indicating a reduced acute toxicity of the stabilized sludge. Although a qualitative notation was applied due to methodological constraints, the results suggest improved ecotoxicological safety following physical stabilization. The presence of harmful bacteria, which is considered a key limitation in the application of waste sludge, was significantly reduced after treatment with pyrophyllite schist from the “Parsovići” deposit (AD Harbi, Konjic, Bosnia and Herzegovina). In particular, the use of pyrophyllite schist greatly reduced the presence of pathogenic bacteria. In fact, no bacteria were detected after this treatment.

Table 2: Biological parameters in the analyzed samples.

Parameter	Unit	T_0	T_1	T_2	T_3
LC_{50} (48 h)	%	27	7	20	58
AMB 22°C	CFU/mL	7.2×10^6	5.1×10^6	2.5×10^4	390
AMB 37°C	CFU/mL	2.4×10^7	2.2×10^7	1.8×10^4	17
TCB	MPN/L	2.4×10^6	1.9×10^6	>3800	9
Yeasts/molds 28°C	CFU/mL	6.7×10^5	5.5×10^5	1.0×10^3	-
Fecal streptococci	/	+	+	+	-
Fecal coliforms (Eijkman test)	/	+	+	+	-
Proteus spp.	/	+	+	-	-
P.aeruginosa	/	+	+	-	-
SR clostridia (10 mL)	/	+	+	-	-

LC_{50}-Lethal Concentration 50 % after 48 hours; AMB-Aerobic Mesophilic Bacteria; TCB-Total Coliform Bacteria; SR clostridia- Sulfite-reducing clostridia; The "+" sign indicates presence, while the "–" sign indicates absence.

During the biological treatment of the sludge (T1–T3), the decrease in odor intensity and changes in sludge appearance qualitatively supported the microbiological and ecotoxicological results. A significant decrease in aerobic mesophilic bacteria (AMB) and fecal indicators (total coliform bacteria and sulfite-reducing clostridia) was observed, indicating effective pathogen reduction. After six months of treatment, the unpleasant odor was no longer present, and the sludge showed a heterogeneous coloration, which is consistent with partially biologically stabilized fractions. LC_{50} values increased after treatment, particularly in sample T3, suggesting reduced acute toxicity and improved ecotoxicological safety. Taken together, these observations demonstrate the effectiveness of the applied treatments in improving sludge stability and reducing biological hazards.

CONCLUSION

Waste sludge can be stabilized by microbiological, biological, or physical treatment methods, primarily by altering its microbiological and physicochemical characteristics. The use of a mixed culture of microorganisms significantly reduced unpleasant odors and contributed to the reduction of sludge volume, while at the same time stimulating the development of new microbial communities. Biological treatment using earthworms (*Eisenia fetida*) in combination with compost material is a relatively long process, resulting in gradual structural changes in the sludge and a noticeable reduction in odor intensity, consistent with partial biological stabilization. The use of a natural clay material, pyrophyllite schist, provided several additional advantages. In addition to odor reduction, this treatment resulted in a final product with a significantly lower moisture content and the complete removal of harmful microorganisms, particularly fecal bacteria. Compared to the commonly used alkaline stabilizing agent $Ca(OH)_2$, which is quite aggressive and strongly alkaline, pyrophyllite schist proved to be a milder but effective alternative for sludge stabilization. These results indicate that combining biological agents and natural materials in waste sludge treatment can produce more stable and environmentally acceptable by-products with reduced odor emissions, highlighting the potential of this approach to improve the sustainability of sludge management practices.

AKNOWNLEDGEMENT

The authors would like to sincerely thank AD Harbi d.o.o. Konjic for kindly providing the pyrophyllite schist used in this research. Their support played an important role in making this study possible.

REFERENCES

American Public Health Association (2025) Standard Methods for the Examination of Water and Wastewater (21st ed.) Washington, DC, APHA

American Public Health Association. (2005). *Standard Methods for the Examination of Water and Wastewater* (21st ed.). Washington, DC: APHA.

American Public Health Association, American Water Works Association, Water Environment Federation. (2023). *Standard Methods for the Examination of Water and Wastewater* (24th edition ed.). (W. Lipps WC, E. Braun-Howland, & T. Baxter, Eds.) Washington, DC: APHA Press.

Arnaiz, C., Gutierrez, J., and Lebrato, J. (2006). Biomass stabilization in the anaerobic digestion of wastewater sludges. *Bioresource Technology, 97*(10), 1179-1184. doi:doi.org/10.1016/j.biortech.2005.05.010

Bhukte, P., Daware, G., Chaddha, M., Bhosale, T., and Agnihotri, A. (2024). Characterization and Beneficiation of Pyrophyllite. In K. Randive, A. Nandi, P. Jain, & S. Jawadand (Eds.), *Current Trends in Mineral-Based Products and Utilization of Wastes: Recent Studies from India* (pp. 159-167). Springer Nature Switzerland. doi:10.1007/978-3-031-50262-0_12

European Committee for Standardization. (2012). *EN 16174:2012: Sludge, treated biowaste and soil – Digestion of aqua regia soluble fractions of elements.* Brussels: CEN.

Nguyen, M., Hadi, M., Lin, C., Nguyen, H.-L., Thai, V.-B., Hoang, H.-G., H.-G., N Vo, D-V., Tran, H.-T. (2022). Microplastics in sewage sludge: Distribution, toxicity, identification methods, and engineered technologies. *Chemosphere, 308*(3). doi:10.1016/j.chemosphere.2022.136455

Official Gazette of FBiH, No. 28/24. (2024). *Regulation on the Management of Sludge from Wastewater Treatment Plants When the Sludge Is Used in Agriculture.* Official Gazette of the Federation of Bosnia and Herzegovina.

Official Gazette of FBiH, No. 96/22. (2022). *Regulation on Determination of Permitted Quantities of Harmful and Dangerous Substances in Soil and Methods of Their Testing.* Official Gazette of the Federation of Bosnia and Herzegovina.

Othman, N., Ismail, Z., Selamat, M., Sheikh Abdul Kadir, S., and Shibraumalisi, N. (2022). A Review of Polychlorinated Biphenyls (PCBs) Pollution in the Air: Where and How Much Are We Exposed to? *International Journal of Environmental Research and Public Health, 19*. doi:10.3390/ijerph192113923

Pešević, D. (2022). *Upravljanje otpadom.* Banja Luka: Univerzitet u Banjoj Luci, Prirodno-matematički fakultet.

Shaddel, S., Bakhtiary-Davijany, H., Kabbe, C., Dadgar, F., and W. Østerhus, S. (2019). Sustainable Sewage Sludge Management: From Current Practices to Emerging Nutrient Recovery Technologies. *Sustainability*. doi:doi.org/10.3390/su11123435

Tezel, U., Tandukar, M., and Pavlostathis, S. (2011). Anaerobic biotreatment of municipal sewage sludge. In *Comprehensive Biotechnology* (Second Edition ed.). Academic Press. doi:10.1016/B978-0-08-088504-9.00329-9

United States Environmental Protection Agency. Retrieved 05 08, 2023, from SW-846 Test Method 3546: Microwave Extraction: https://www.epa.gov/sites/default/files/2015-12/documents/3546.pdf

Vouk, D., Serdar, M., Nakić, D., and Anić-Vučinić, A. (2016). Korištenje mulja s UPOV-a u proizvodnji cementnog morta i betona. *Građevinar, 68*(3), 199-210. doi:10.14256/JCE.1374.2015

Zhang, S., Wang, F., Mei, Z., Lv, L., and Chi, Y. (2021). Status and Development of Sludge Incineration in China. *Waste and Biomass Valorization, 12*(7). doi:10.1007/s12649-020-01217-9

Zhen, G., Lu, X., Kato, H., Zhao, Y., and Li, Y.-Y. (2017). Overview of pretreatment strategies for enhancing sewage sludge disintegration and subsequent anaerobic digestion: Current advances, full-scale application and future perspectives. *Renewable and Sustainable Energy Reviews, 69*, 559-577. doi:10.1016/j.rser.2016.11.187

Summary/Sažetak

Tretman komunalnih otpadnih voda proizvodi značajne količine kanalizacionog mulja koji zahtijeva stabilizaciju prije odlaganja ili ponovne upotrebe zbog potencijalnih rizika po okolinu i zdravlje ljudi. U ovom radu procijenjena je efikasnost mikrobioloških, bioloških i fizičkih metoda tretmana mulja primjenom fizičko-hemijskih, mikrobioloških i ekotoksikoloških analiza. Mikrobiološki tretman mješovitom kulturom mikroorganizama doveo je do smanjenja neugodnih mirisa i djelimičnih promjena sadržaja organske materije. Biološki tretman primjenom vrste *Eisenia fetida* rezultirao je postepenom strukturnom transformacijom mulja i smanjenjem patogenih indikatora, ali je zahtijevao produženo vrijeme tretmana. Fizička stabilizacija primjenom pirofilitnog škriljca značajno je povećala ukupni sadržaj suhe materije (sa 17,75% na 48,32%), smanjila sadržaj isparljivih materija (na 2,26%) usljed kombinovanih efekata stabilizacije i razrjeđenja, imobilizirala odabrane teške metale te dovela do eliminacije fekalnih bakterija i drugih patogenih mikroorganizama. Ekotoksikološka procjena pokazala je povećanje vrijednosti LC_{50} sa 27% u sirovom mulju na 58% nakon fizičkog tretmana, što ukazuje na smanjenu toksičnost. Dobijeni rezultati potvrđuju da pirofilitni škriljac predstavlja efikasan prirodni materijal za unapređenje fizičko-hemijske stabilnosti i higijenske sigurnosti kanalizacionog mulja te ukazuju na potencijal kombinovanja bioloških agenasa i prirodnih mineralnih materijala kao održivog pristupa upravljanju muljem.

Glasnik hemičara i tehnologa Bosne i Hercegovine

Bulletin of the Chemists and Technologists of Bosnia and Herzegovina

2026

66

47-56

Print ISSN: 0367-4444
Online ISSN: 2232-7266

Original Scientific Article
DOI: 10.35666/2232-7266.2026.66.06
UDK: 577.1:591.133.1.2-442

Characterization of zein-based core-shell microcapsules and matrix nanocapsules with encapsulated carvacrol

Spasojević, Lj.[a], Rajić, D.[a,b,*], Tošković, D.[b], Gojković Cvjetković, V.[b], Bučko, S.[a], Škrbić, J.[a], Fraj, J.[a], Milinković Budinčić, J.[a], Petrović, L.[a], Katona, J.[a]

[a] *Faculty of Technology, University in Novi Sad, Boulevard Cara Lazara 1, 21102 Novi Sad, Serbia*

[b] *Faculty of Technology Zvornik, University of East Sarajevo, Karakaj 34a, 75400 Zvornik, Bosnia and Herzegovina*

Article info
Received: 04/10/2025
Accepted: 16/12/2026

Keywords:
Nanoparticles
Natural proteins
Essential oil
Bioactive compound delivery

***Corresponding author:**
Danijela Rajić
E-mail: danijelarajic@tfzv.ues.rs.ba
Phone: +387 65 864 519

Abstract: Composite micro- and nanocapsules made from natural proteins are increasingly used for various bioactive compound delivery applications due to their versatile nature and ability to carry a wide variety of therapeutic drug molecules. Capsules, both, core-shell and matrix types, have gained prominence in diverse sectors, from pharmaceuticals to food technology. Their widespread use is due to their encapsulation efficiency and controlled release properties. This study provides a physical-morphological characterization and a presentation of the preparation of particles derived from the corn protein-zein, with emphasis on core-shell and matrix configurations. Due to its strong antimicrobial effect against many different strains of bacteria and fungi, carvacrol was considered in this work. It was found that Pickering emulsions prepared as 10% O/W emulsion with 15% GA with the ratio Z:O=1:1.5 and the ratio Z:OSA starch=1:1 and 20 % of carvacrol on dry matter were the most suitable for the preparation of dry capsules. Analysis of matrix-type nanocapsules with 10% encapsulated carvacrol showed that the particles were spherical in shape with a smooth surface and could be successfully dried and prepared in this formulation.

INTRODUCTION

Nanoparticle synthesis is a complex process, and hence there is a wide range of techniques available to produce different types of nanoparticles. The encapsulation process forms a protective barrier (a matrix or polymer coating), preventing chemical interactions and shielding it from environmental factors (such as temperature, pH, enzymes, and oxygen). The primary goals of encapsulation are to enhance the stability of bioactive compounds against unfavorable environmental factors, facilitate their incorporation into food matrices, thus imparting functional properties to the products, and ensure their controlled release at targeted sites (Corrêa-Filho et al., 2019; De Jong and Borm, 2008). One of the main challenges is the increased production costs associated with advanced techniques (Misra et al., 2021; Tarone et al., 2020). Therefore, it is very important to examine different types of particles and their preparation methods in order to obtain clear formulations with minimal economic investment. Depending on the physicochemical characteristics of the bioactive compound, it is now possible to choose the best preparation method and the best polymer to achieve an efficient entrapment of the bioactive compound (Pinto Reis et al., 2006). Core-shell particles consist of a core coated with an outer shell layer, which reduces the reactivity of the core and increases the dispersibility of the modified particle. These classes of particles are known as “smart particles” and have a wide range of applications in various fields, such as drug delivery, biosensors, chemical separation, biomaterials, catalysis and similar suitable materials for semiconductors (Tiwari et al., 2021; Yadav et al., 2023; Kumar et al., 2013). In core-shell capsules, there are clearly defined internal phase boundaries that represent the container system (Baghaban-Eslaminejad et al., 2017). Matrix-type capsules are solid colloidal particles in which encapsulated substances are dissolved, entrapped, chemically bound, or uniformly adsorbed within a homogeneous polymer matrix component. In addition to providing mechanical strength and ensuring protection for their encapsulated guest molecules, nanospheres offer a relatively simple way to adjust the degree of porosity, allowing for fine-tuning of the cargo release profile (Muttaquien et al. 2023; Brannon-Peppas, 1995; Gummustas et al. 2017; Soppimath et al., 2001). The carrier plays an important role in the formulation of

colloidal particles, so there is an increasing trend to use natural biodegradable materials that are readily available. Compared to carbohydrates or metals, protein-based particles are considered ideal for medical, nutritional, and cosmetic applications. Proteins offer the possibility of surface modifications and binding of drugs and other biomolecules through covalent, ionic, hydrogen, and other bonding (Reddy, 2021; Weber, 2000; Rahimnejad, 2009). As a natural protein, zein has good mechanical properties that allow it to be mixed with other substances, as well as modified to obtain the desired product. However, biodegradability and biocompatibility are key parameters enabling new uses of zein and zein-based materials in biotechnological fields (Corradini et al., 2014). The tertiary structure of globular-type zein provides the possibility of creating nanoparticles. Side chains of polar amino acids are located on the surface of the zein molecule, interact with polar solvents (water, ethanol) and allow the protein to remain in solution (Guo et al., 2005).

Essential oils as active substances obtained from different parts of plant species are notable for their excellent activity against bacteria, viruses, fungi, parasites and insects. As a monoterpenoid phenol, carvacrol is a component of many essential oils and is usually found in plants together with its isomer, thymol. Carvacrol, either alone or in combination with other compounds, has a strong antimicrobial effect on many different strains of bacteria and fungi that are dangerous to humans, which is why it was taken into consideration in this paper. Carvacrol also exerts strong anti-inflammatory properties by preventing the peroxidation of polyunsaturated fatty acids (Aprotosoaie, 2019; Mączka et al., 2023). The aim of this work is to present the two preparation methods for obtaining core-shell type and matrix type capsules shown side by side, where in both cases zein was used as a carrier and carvacrol as an active component. The emphasis was placed on finding the best formulation with the given ingredients in order to obtain a stable product with a sufficient amount of encapsulated active substance. This work also aims to perform separated physical and morphological characterization of both type particles obtained with natural polymers.

EXPERIMENTAL

Materials

Zein (Zein purified, CAS 9010-66-6) was purchased from Acros Organics (USA), and carvacrol (Carvacrol 5-isopropyl-2-methylphenol, 98% CAS 499-75-2) was purchased from Sigma Aldrich (Germany). Ethanol (96%) was purchased from Reahem (Serbia). Gum Arabic (GA) was purchased from Sigma Aldrich (Germany). OSA starch (OS) was purchased from National Starch & Chemical (UK) and sunflower oil was purchased from Dijamant (Serbia). All chemicals were of analytical grade unless stated otherwise.

Preparation of zein nanoparticles

2% wt. zein stock solutions were prepared in 100 mL sealed flasks by dissolving zein powder in 90% v/v aqueous ethanol by constant stirring using a magnetic stirrer for 1 hour. The solutions were left overnight in a sealed container at room temperature to ensure complete dissolution of zein. The solutions were subsequently filtered through quantitative filter paper to remove any undissolved particles. 20 mL of 2% wt. zein stock solution was added in a continuous stream to 80 mL of water, in a flask with the ground joint, with constant stirring on a magnetic stirrer to prepare zein nanoparticles. The stirring was continued for 30 min after all of the stock solution was added to water to ensure complete precipitation of zein. In this way, 0.4% wt. nanoparticle suspensions were prepared. Rotary evaporation was used to prepare concentrated zein suspensions. 500 mL of 0.4% wt. suspension was evaporated to 200 mL of 1% wt. zein suspension. Two batches of 1% wt. suspensions were combined and evaporated to 100 mL of 4% wt. zein suspension. Furthermore, an 8% wt. zein suspension was obtained by evaporating 200 mL of 4% wt. zein suspension to 100 mL

Preparation of O/W stock emulsions without and with carvacrol

20 g emulsion of sunflower oil in water of 5%, 10%, 20% and 50% wt. (S1-S4 respectively, Table 1) was prepared by dispersing sunflower oil in the continuous phase using Ultra Turrax IKA T25 (IKA, Germany) homogenizer at 15000 rpm for 15 min at 25^{o}C. The continuous phase emulsions were 3%, 5%, 10% and 15% wt. gumarabic (GA) solution in water, based on mass of sunflower oil for each emulsion (S11-S14; S21-S24; S31-S34; S41-S44, Table 1). GA solutions were prepared by dissolving GA powder in water at T=80^{o}C. In this way, sunflower oil droplets in emulsions were stabilized with GA molecules adsorbed at the O/W interface. Some of the GA molecules were not adsorbed, but remained dissolved in the continuous phase of the emulsions. To remove unadsorbed GA molecules, the emulsion was centrifuged for 10 minutes at 4000 rpm, resulting in an upper, creamy layer rich in oil and a lower aqueous phase depleted of oil droplets. The creamy layer was carefully collected, while the lower aqueous phase was discarded. The cream was then diluted with demineralized water to obtain the initial emulsion mass. The centrifugation–dilution cycle was repeated three times to ensure that all GA not adsorbed on the surface of the oil droplets was removed from the continuous phase of the emulsions. In this way, GA stabilized stock emulsions were obtained. Different stock emulsion compositions were prepared to obtain the most stable one for further research as shown in Table 1.

The droplet size distribution of the 10% O/W stock emulsion with 15% gum arabic was determined by analyzing microphotographs of the emulsions obtained with a Biooptica BEL-3000 microscope (BEL-photonics, Germany) using Belview software. After the most stable formulation was determined, the preparation of emulsions with the addition of carvacrol began. Similarly, 10% stock emulsions were prepared with 8.33%, 25%, and 50% of carvacrol in the oil phase (S5, S6, S7, Table 1), where appropriate mixtures of sunflower oil and carvacrol were used as the oil phase. The continuous phase of these emulsions was a 15% wt. solution of gum arabic (GA) in water, based on the weight of sunflower oil.

Table 1: Specification of prepared stock O/W emulsions without and with carvacrol

Sample ID	Sunflower Oil (g)	Carvacrol (g)					
				S11	S12	S13	S14
S1-5% O/W	1.00	0.0	Gum Arabic (g)	0.03	0.05	0.10	0.15
			Water (g)	18.97	18.95	18.90	18.85
			Stability	U	U	U	U
				S21	S22	S23	**S24**
S2-10% O/W	2.00	0.0	Gum Arabic (g)	0.06	0.10	0.20	**0.30**
			Water (g)	17.94	17.90	17.80	**17.70**
			Stability	U	U	U	**S**
				S31	S32	S33	S34
S3-20% O/W	4.00	0.0	Gum Arabic (g)	0.12	0.20	0.40	0.60
			Water (g)	15.88	15.80	15.60	15.40
			Stability	U	U	U	U
				S41	S42	S43	S44
S4-50% O/W	10.00	0.0	Gum Arabic (g)	0.30	0.50	1.00	1.50
			Water (g)	9.70	9.50	9.00	8.50
			Stability	U	U	U	U
			Gum Arabic (g)		Water (g)		
S5-10% O/W	1.84	0.16	0.28		17.72		
S6-10% O/W	1.50	0.50	0.23		17.77		
S7 10% O/W	1.00	1.00	0.15		17.85		

*U- Unstable after 24h; *S-Stable after 24h

Preparation of Pickering emulsions with and without carvacrol

Pickering emulsions were prepared by mixing the selected stock emulsion with a previously prepared suspension of zein nanoparticles. First, a 10% stock emulsion was added to a 0.4% suspension of zein nanoparticle to obtain 30 g of Pickering emulsion with a zein:oil (Z:O) ratio of 1:1, where three different homogenization methods i.e. Ultra Turrax T25 (3000 rpm), magnetic stirring, and propeller mixer (both 600 rpm, for 5 min), were applied in order to determine the optimal homogenization method (PE1, PE2, PE3, Table 2). The 0.4% zein nanoparticle suspension was used only in a preliminary screening step to identify a technically feasible homogenization device (Ultra-Turax, magnetic stirrer, or propeller mixer) under conditions that avoid excessive viscosity and clogging. Once the propeller mixer was selected, all Pickering emulsions discussed in this paper were prepared with a 1.0% zein nanoparticle suspension and targeted Z:O ratios. 10% stock emulsion was added to a 1% suspension of zein nanoparticles to facilitate Pickering emulsions 1:2, 1:1.5, 1:1, 1.5:1, 2:1 and 4:1 (PE4-PE9,, Table 2), with Z:O ratios using propeller stirring at 600 rpm for 5 min. These emulsions were then analyzed by light microscopy. In addition, immediately after the emulsion preparation, the emulsions were transferred into sealed 10 mL graduated glass cylinders and left for 24 hours at room temperature to visually observe their colloidal stability. Furthermore, the flocculation of Pickering emulsions during mild stirring was investigated. Pickering emulsions with Z:O ratios of 1:2, 1:1.5, 1:1, 1.5:1, 2:1 and 4:1 were allowed to stir on a magnetic stirrer for 30 min and their stability towards flocculation was visually observed.

Table 2: Specification of prepared stock O/W emulsions without and with carvacrol

Sample ID	Zein Conc. (%)	Z:O Ratio	Homogenization Method	Carvacrol in Oil Phase	Stability Test	Flocculation Test
Choosing the appropriate method of homogenization						
PE1	0.4	1:1	Ultra Turrax (3000 rpm)	No	Yes	No
PE2	0.4	1:1	Magnetic stirrer (600 rpm)	No	Yes	No
PE3	**0.4**	**1:1**	**Propeller stirrer (600 rpm)**	**No**	**Yes**	**No**
Choosing the most stable Z:O ratio						
PE4	1.0	1:2	Propeller stirrer (600 rpm)	No	Yes	Yes
PE5	**1.0**	**1:1.5**	**Propeller stirrer (600 rpm)**	**No**	**Yes**	**Yes**
PE6	1.0	1:1	Propeller stirrer (600 rpm)	No	Yes	Yes
PE7	1.0	1.5:1	Propeller stirrer (600 rpm)	No	Yes	Yes
PE8	1.0	2:1	Propeller stirrer (600 rpm)	No	Yes	Yes
PE9	1.0	4:1	Propeller stirrer (600 rpm)	No	Yes	Yes

Preparation of Pickering emulsions with OSA starch

OSA starch solutions of 6%, 8%, 12%, and 21% wt. were added to the zein suspension of 8% wt., to obtain a 4% wt. zein suspension, with mass ratios of zein to OSA starch of 1:0.75, 1:1, 1:1.5, and 1:3.5, (PE-OS1, PE-OS2, PE-OS3, PE-OS4, Table 3). Furthermore, 40 g of a 10% O/W stock emulsion was added to 100 g of a suspension mixture of zein and OSA starch to obtain a Z:O mass ratio of 1:1.5, and homogenized using a propeller mixer at 600 rpm, for 5 min. Pickering emulsions containing 3.35%, 10%, and 20% carvacrol were prepared by dispersing 40 g of stock O/W emulsions with 8.33%, 25%, and 50% of carvacrol, in 100 g of a zein and OSA starch suspension mixture, with the most preferred mass ratio of zein and OSA starch being1:1. The emulsion was homogenized using a propeller mixer at 600 rpm, for 5 min.

Drying of Pickering emulsions

Prepared Pickering emulsions with ratio Z:O=1:1.5 and added OSA starch (zein:OSA starch ratio=1:0.75; 1:1; 1:1.5) were spray-dried using Mini Spray Drier (Buchi 190, Switzerland). Two different inlet temperatures were applied, 105ºC and 130ºC, and the outlet temperature was around 60ºC. The sample flow rate varied between 3.2–6.0 mL/min, and the air flow rate was maintained at 0.6 m^3/min. In each batch, 140–240 g of emulsion was dried with or without OSA starch. OSA starch was used to prevent agglomeration and improve drying efficiency. The number mean diameter (d_{10}) and Sauter mean diameter (d_{32}) of dry powder particles, with a ratio of Z:OS=1:1, dried at 105°C and 130°C, were determined.

Table 3: Summary table of data on Pickering emulsions with OSA starch

Sample ID	Zein suspension conc. (wt. %)	OSA starch concentration (wt. %)	Zein:OSA starch ratio	Carvacrol conc. (%)	Z:O ratio	Drying applied	Drying temp. (°C)
PE-OS1	4.00	6.00	1:0.75	-	1:1.5	Yes	105, 130
PE-OS2	**4.00**	**8.00**	**1:1**	**-**	**1:1.5**	**Yes**	**105, 130**
PE-OS3	4.00	12.00	1:1.5	-	1:1.5	Yes	105, 130
PE-OS4	4.00	21.00	1:3.5	-	1:1.5	Yes	105, 130
PE-OS-C1	4.00	8.00	1:1	3.35	1:1.5	Yes	130
PE-OS-C2	4.00	8.00	1:1	10	1:1.5	Yes	130
PE-OS-C3	4.00	8.00	1:1	20	1:1.5	Yes	130

HPLC determination of carvacrol

The amount of encapsulated carvacrol from dried samples of Pickering emulsions with 3.35%, 10%, and 20% carvacrol, on a dry matter basis, with a mass ratio of Z:O 1:1.5 and zein:OSA starch ratio of 1:1, was analyzed by HPLC using a method adapted from Rajić et al. (2021). 10 mg of dry carvacrol nanocapsule was dispersed in 2 ml plastic vials and vortexed (Eppendorf Mix Mate, USA) for 5 minutes. After that, the vials were transferred to a centrifuge (Rotina 380 R, Hettichzentrifugen, Germany), and centrifuged at 13000 rpm for 20 minutes. The supernatant was collected, filtered through 0.45 µm PVDF syringe filters, and transferred to 2 ml vials for HPLC analysis. The sample was analyzed using a HPLC 1260 Series device (Agilent Technologies, Germany) equipped with an Agilent ZORBAX Eclipse Plus C18 column (4.5 µm, 100×3.5 mm, Agilent, USA). Chromatograms were recorded and integrated by the 1260 LC Chromatography Data System. A binary mixture of methanol and water was used as the mobile phase, and the flow rate was 5 µL/min at 25°C. The chromatograms were recorded at 275 nm, and each sample was analyzed in triplicate. Encapsulation efficiency was calculated using HPLC data and oil concentration as input parameters.

Preparation of matrix type nanocapsule

Matrix-type nanocapsule were prepared according to the method given in a previous study of Rajić et al. (2021). Carvacrol was added to the previously prepared 2% zein solutions at a concentration of 10% wt. based on the mass of zein. 20 ml of the stock solution of zein with carvacrol was injected using a syringe into 80 ml of water to obtain a 0.4% wt. suspension, which was further stirred for 30 min on a magnetic stirrer. The resulting suspension was lyophilized and zein nanoparticles with encapsulated carvacrol were obtained. The prepared nanoparticles were stored in sealed containers at 4°C and used for further experiments.

Characterization of matrix-type nanocapsule

The zeta potential and particle size of carvacrol-encapsulated zein nanocapsule were determined in suspension by electrokinetic measurements and dynamic light scattering (DLS) respectively, using a Zetasizer Nano ZS (Malvern Instruments, UK), at pH 3–10. Samples were diluted to 0.1 wt% with demineralized water, and the pH of the samples was adjusted using 0.1 M HCl and 0.1 M NaOH. All samples were equilibrated for 60 s at 25°C inside the instrument before analysis. Size measurement data were collected over 12 consecutive readings for 10s. Each sample was analyzed in triplicate, and the results were collected as the cumulative mean intensity diameter. Zeta potential measurements for all nanoparticle samples were performed in triplicate, and average values were reported.

FESEM analysis of matrix type nanocapsule

A suspension of nanocapsules of 0.4% wt. with 10% wt. encapsulated carvacrol was pipetted onto glass and after drying, imaged with a scanning electron microscope. FESEM of the obtained samples was performed on a Tescan Mira 3XMU (Tescan, Czech Republic) for morphological characterization. Before analysis, the samples were coated with a layer of gold using a Polaron SC502 sputter coater.

RESULTS AND DISCUSSION

Properties of sunflower O/W emulsions

Oil-in-water emulsions in concentrations 5%, 10%, 20% and 50% were prepared by emulsifying sunflower oil in an aqueous solution of gum arabic. Gum arabic as a stabilizer was added to each emulsion in amounts of 3%, 5%, 10% and 15% based on the oil mass. After 1 hour of observation, it was found that only the 10% O/W emulsion (S24, Table 1) with the addition of 15% gum arabic to the mass of oil remained stable. All other emulsions were unstable, and the oil phase separated on the surface within 30 min after the preparation of the emulsions. The selected 10% O/W emulsion with 15% gum arabic also remained stable for 24h after preparation, as shown at Table 1. These results imply that emulsion S24 can be used for further experiments as the most stable.

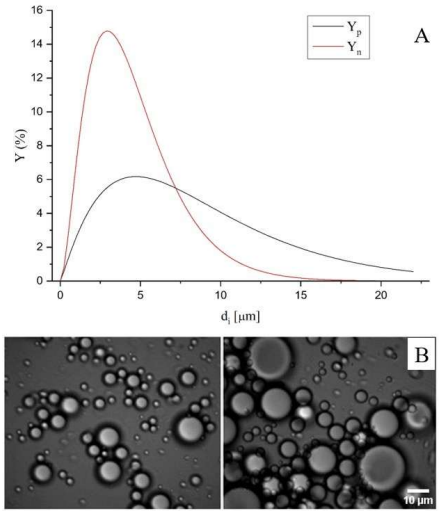

Fig 1: Emulsion with 10% sunflower oil and 15% gumarabic (S24): A- Droplet size distribution by number (Yn) and by surface area of droplets (Yp); B- Microphotographs of emulsion (40x)

Figure 1A shows the droplet size distribution by number (Yn) and by surface area of droplets (Yp) for an emulsion with 10% wt. sunflower oil and 15% wt. gum arabic (S24), without carvacrol. The obtained particle size distributions are monomodal where Yp is quite broad compared to Yn, indicating that a small number of droplets with large diameter have a large contribution to the total surface area of droplets in the O/W emulsion. The average number diameter (d_{10}) of this emulsion was 3.64 μm, and the Sauter ,diameter (d_{32}) was 13.54 μm. Figure 1B shows microphotographs of the previously described emulsion. Microscopic analysis showed spherical oil droplets, with no coalescence observed, which confirmed the good stability of the selected emulsion and its suitability for further analyses.

Preparation of Pickering emulsions

Three different homogenization procedures of zein NP suspension and O/W emulsion were investigated in order to prepare a stable Pickering emulsion, based on the interaction of positively charged zein NP and negatively charged GA molecules on the surface of oil droplets in the stock O/W emulsion. During the procedure involving ultraturax homogenization, the turbine became clogged due to the formation of agglomerates of zein nanoparticles, so this procedure was discarded. Furthermore, the procedure using a magnetic stirrer did not provide sufficient mixing, so the nanoparticle suspension and the stock emulsion eventually separated, leading to the abandonment of this procedure. Finally, stable Pickering emulsions with the following zein to oil ratio (Z:O) 1:2; 1:1.5; 1:1; 1.5:1; 2:1 and 4:1 were formed using a propeller stirrer for 5 minutes at 600 rpm and room temperature. Therefore, this method of homogenization was used in further experiments.

Subsequently, the stability of prepared Pickering emulsions was investigated under the mild stirring conditions for 24 h at room temperature. During the stability testing, in PE4, Z:O=1:2 and PE6, Z:O=1:1 emulsion, aggregates formation and phase separation occurred after 5-10 minutes. Pickering emulsions PE7, PE8 and PE9 with the ratio Z:O=1.5:1; Z:O=2:1 and Z:O=4:1 were stable for 4 hours, after which aggregates formed. Pickering emulsion PE5 with a Z:O=1:1.5 ratio proved to be the most stable during 24 hours of observation and was used for further analyses.

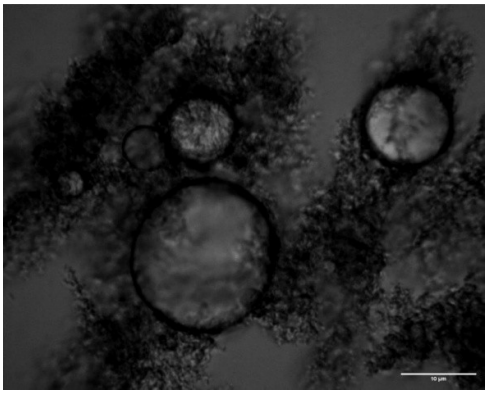

Fig 2: Microphotograph of Pickering emulsion PE5 with Z:O=1:1.5 ratio (40x)

Figure 2 shows a microphotograph of the most stable Pickering emulsion with a zein:oil ratio Z:O=1:1.5 at 40x magnification. The picture shows oil drops from the stock O/W emulsion. The droplets kept their spherical shape, while at the same time they were surrounded by aggregates of zein nanoparticles. Zein nanoparticles were bound to the surface of the oil droplets due to the electrostatic interaction of negatively charged gum arabic molecules adsorbed on the drop's surface and positively charged zein nanoparticles (Spasojević et al., 2020).

Spray-drying of Pickering emulsions

Pickering emulsions with 2.36% wt. and 6.81% wt. dry matter (zein + sunflower oil), without OSA starch, were dried at 105°C and a sample flow rate 6 mL/min. It was observed that under these drying conditions the efficiency of the drying process was very low. Most of the particles were not fully dried and remained stuck to the drying chamber walls. The dry particle yield was very low. This was, most probably, due to the low temperature and high sample flow rate.

Pickering emulsion, with 6.81% wt. dry matter (zein + sunflower oil) was dried at 130ºC and a sample flow rate 3.2 mL/min. The higher inlet temperature and lower flow rate improved the drying efficiency. Dry powder of particles was obtained after drying 240 g of the Pickering emulsion and the yield of drying process was 18.36%. OSA starch was added to Pickering emulsions to improve the efficiency of the drying process. OSA starch was added in four different zein:OSA starch mass ratios (1:0.75, 1:1, 1:1.5, and 1:3.5). Four Pickering emulsions (PE-OS1, PE-OS2, PE-OS3, PE-OS4) were spray–dried as shown in Table 3. The effect of increased temperature on the mean particle diameter is shown in Table 4A. It can be seen that the increased temperature had a slight influence on both d_{10} and d_{32}.

Table 4. A-Influence of drying temperature on the number mean diameter (d_{10}) and Sauter mean diameter (d_{32}) of the particles obtained by Pickering emulsion spray drying; B-Influence of zein:OSA starch ratio on particle size of obtained nanocapsules shown as (number mean diameter (d_{10}) and Sauter mean diameter (d_{32}); C-Influence of carvacrol concentration on the number mean diameter (d_{10}) and Sauter mean diameter (d_{32}) of redispersed powder of spray-dried Pickering emulsions with encapsulated carvacrol

A				
T (°C) drying temperature	**Number mean diameter (d_{10}) (μm)**	**Y err (d_{10})**	**Sauter mean diameter (d_{32}) (μm)**	**Y err (d_{32})**
105	16.05	0.372	22.97	0.940
130	11.84	0.392	27.02	0.155
B				
zein:OSA starch ratio	**Number mean diameter (d_{10}) (μm)**	**Y err (d_{10})**	**Sauter mean diameter (d_{32}) (μm)**	**Y err (d_{32})**
1:0	11.84	0.086	27.02	0.093
1:0.75	10.54	0.586	25.91	0.271
1:1	13.39	0.056	16.61	0.370
1:1.5	9.17	0.100	21.4	0.377
C				
C carvacrol (%)	**Number mean diameter (d_{10}) (μm)**	**Y err (d_{10})**	**Sauter mean diameter(d_{32}) (μm)**	**Y err (d_{32})**
3.35%	6.37	0.293	8.56	0.266
10%	11.69	0.240	16.8	0.472
20%	11.58	0.355	13.83	0.091

Table 4B shows the effect of the mass ratio of zein to OSA starch on d_{10} and d_{32} of the redispersed spray-dried particles. It can be observed that increasing the OSA starch ratio leads to a decrease in both d_{10} and d_{32}. The decrease is much more pronounced for d_{32}, compared to d_{10}, indicating that fewer aggregates are formed when the OSA starch ratio is higher. However, as more OSA starch is added, the total oil concentration in the dried particles decreases, and the optimal (minimal) zein:OSA starch mass ratio needs to be determined. Spray drying of emulsions with 1:0 and 1:0.75 zein:OSA starch mass ratios was difficult, and the spray–drier nozzle clogged several times, so the drying process was stopped. On the contrary, at 1:1.5 zein:OSA starch mass ratio there was no nozzle cloggage and drying was easily performed, but at this ratio the theoretical total oil concentration is only 2.5% wt. based on the dry matter of the emulsion, which was too low for application. The drying efficiency at 1:1 and 1:1.5 zein:OSA starch mass ratios was comparable. Given that the proportion of OSA starch should be as low as possible, 1:1 zein:OSA starch mass ratio was determined to be optimal and help balance the spray drying formulation for encapsulation of carvacrol.

Encapsulation of carvacrol in Pickering emulsions

Three different Pickering emulsions with 3.35%, 10%, and 20% carvacrol were prepared and dried, on a dry matter basis, with a Z:O mass ratio 1:1.5 and zein:OSA starch 1:1 ratio. Table 4C shows the effect of carvacrol concentration on the d_{10} and d_{32} of spray-dried particles encapsulating carvacrol, after redispersion in water. It can be seen that the largest particles were obtained at a carvacrol concentration of 10%. With the addition of 3.35% carvacrol, the d_{10} was 6.37 μm and d_{32} was 8.56 μm. With the addition of 10% carvacrol, the d_{10} was 11.69 μm and d_{32} was 16.8 μm. The particles obtained as the final product with the addition of 20% carvacrol by dry matter mass had a d_{10}, 11.58 μm and a d_{32} 13.83 μm. Figure 3 shows microphotographs of dry powder of particles encapsulating 3.35% (A), 10% (B) and 20% (C) of carvacrol, redispersed in water. Non-spherical, irregular shape of the redispersed particles indicate that the solid shell of the capsules remained intact after particle dispersion in water.

Determination of carvacrol encapsulation efficiency

Table 5 shows the effect of carvacrol concentration on encapsulation efficiency. It can be seen that for all three carvacrol concentrations studied, the encapsulation efficiency was higher than 85%. Particles with encapsulated 3.35% carvacrol by weight of dry matter had an average encapsulation efficiency 94.39%. With 10% encapsulated carvacrol, the efficiency was 88.18%, and with 20% encapsulated carvacrol, the encapsulation efficiency was 90.14%.

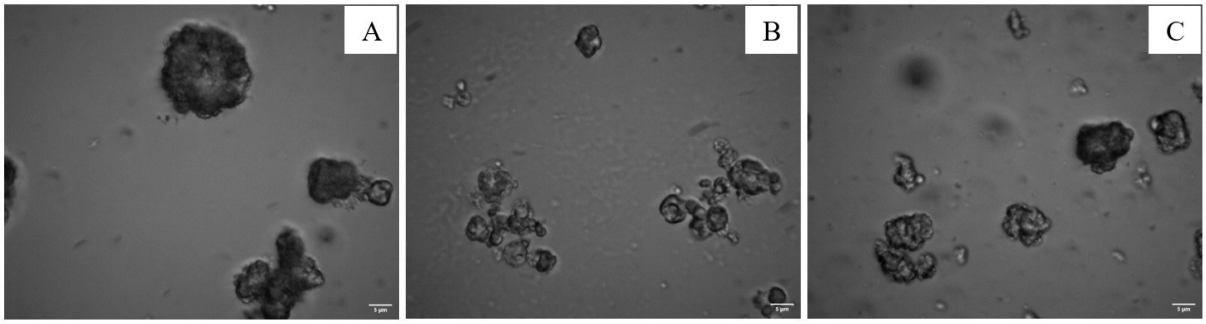

Fig 3: Microphotographs of dry powder of particles encapsulating carvacrol, redispersed in water in following concentrations: (A) 3.35%; (B) 10%; (C) 20%

Table 5. Influence of carvacrol concentration on encapsulation efficiency (EF)

C carvacrol (%)	EF (%)	Yerr EF
3.35	94.396	0.099
10	88.180	0.375
20	90.148	0.762

Development and characterization of matrix-type nanocapsules

The zeta potential of fresh dispersions with 10% carvacrol was determined by electrokinetic measurements at pH 3–9, Figure 4A. Figure 4A shows that the particles were positively charged at pH 3-5 and negatively charged at pH 6–9. The most negative value was -42.83 mV at pH=8, while the highest positive value was measured at pH=5, i.e. 31.27 mV. At pH=4, which is the value of freshly prepared samples, the zeta potential was 29.37 mV. With increasing pH, the zeta potential decreases and an isoelectric point is reached, which is at pH=5.42. The obtained values are in accordance with previously published results (Patel and Velikov, 2014). With a further increase in pH, the nanocapsules become negatively charged.

Figure 4B shows the effect of pH on the mean intensity diameter of particles with 10% encapsulated carvacrol. It can be observed that the zein nanoparticles were smallest at pH 3–4, while the largest diameters were at pH=6, which is consistent with the results of zeta potential measurements. Namely, the largest particles were obtained at pI (isoelectric point), where the nanospheres were effectively uncharged, were the least electrostatically stable and therefore prone to particle aggregation. A decrease in particle size, Figure 4B, was observed as the pH moved away from pI

Figure 5 shows FESEM micrographs of prepared samples with 10% encapsulated carvacrol. FESEM analysis was consistent with the determination of particle size by the method of dynamic light scattering. The largest particles recorded have a diameter of 150-200 nm when individual particles are involved, but range up to 1.5-15µm when aggregates of nanospheres are formed. At a magnification of 10,000x (Figure 5A), agglomerates of the resulting particles are presented, while at a magnification of 100,000 times (Figure 5B), individual particles are shown.

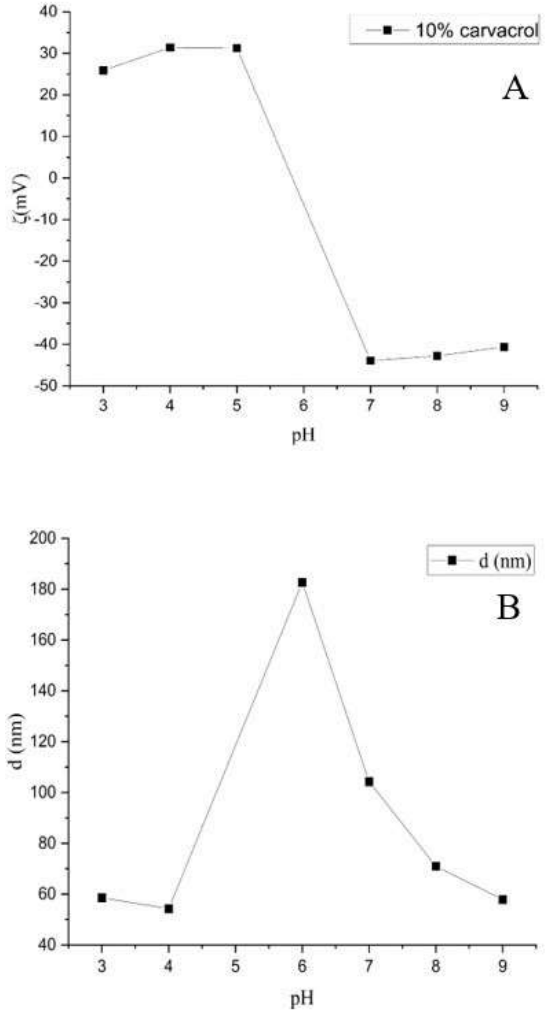

Fig 4: Nanocapsules with 10% carvacrol: A- Effect of pH on the zeta potential; B-Effect of pH on the size of nanocapsules

.

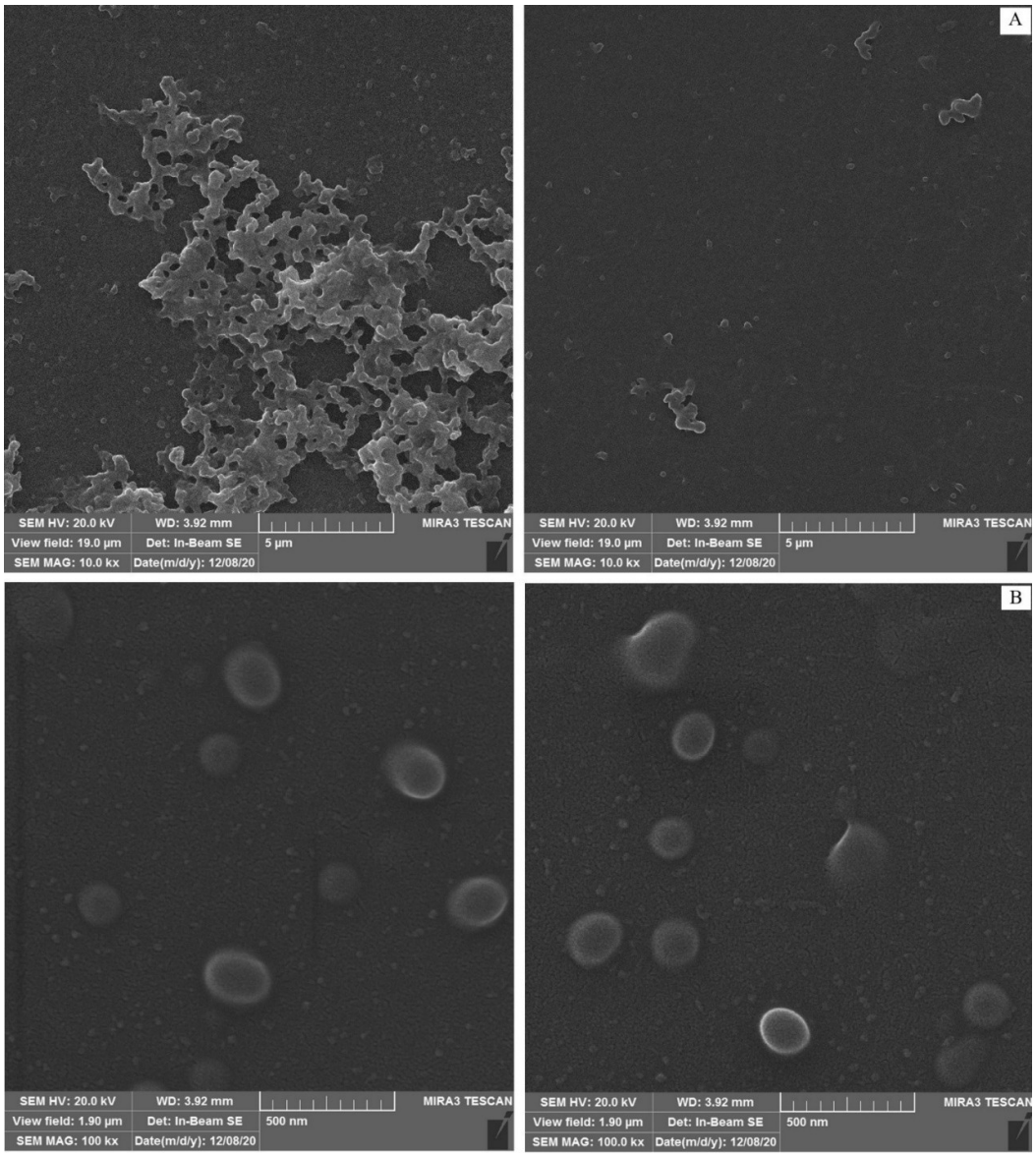

Fig 5: FESEM microphotographs of zein nanoparticle samples with 10% encapsulated carvacrol (magnification 10kx-A, 100kx-B)

CONCLUSION

This work has shown that zein can be successfully used to prepare , core-shell microcapsules, where zein nanoparticles are used to stabilize Pickering O/W emulsions with the active component i.e. carvacrol, and matrix nanocapsules, where zein nanoparticles are used as a matrix carrier for carvacrol. In both cases, carvacrol was used as the encapsulated bioactive compound. The size of the nanocapsules was strongly influenced by the pH of the suspension, where the largest size was obtained at pI. The encapsulation efficiency of the core-shell microcapsules was influenced by the carvacrol content in the formulation, where the encapsulation efficiency of capsules with 3.35% carvacrol by weight of dry matter was 94.39%, with 10% carvacrol was 88.18% and with 20% carvacrol encapsulation efficiency was 90.14%. The ratio of components used to prepare Pickering emulsions significantly affected the spray drying process and the preparation of dried capsules. It was found that Pickering emulsions prepared as 10% O/W emulsion with 15% GA with the ratio Z:O=1:1.5 and the ratio Z:OSA starch=1:1 and 20% carvacrol on dry matter were the most suitable for the preparation of dried capsules. Different Z:O ratios were taken to test a wider range of proportions of both components and to find the one that is the most stable over the longest period of time and is homogeneous enough to be dried in a spray drier, while at the same time having the largest possible amount of emulsion, i.e. oil, to be later determined by HPLC. FESEM analysis of matrix-type nanocapsules with 10% encapsulated carvacrol showed that the particles were spherical in shape with a smooth surface and could be successfully dried and prepared in this formulation. Finally, it was shown that the preparation procedure and formulation significantly affect the properties of core-shell microcapsules and matrix nanocapsules in terms of particle size, encapsulation efficiency, charge and stability.

REFERENCES

Aprotosoaie, A. C., Vlad Luca, S., Trifan, A., Miron, A. (2019). Antigenotoxic Potential of Some Dietary Non-phenolic Phytochemicals. *Studies in Natural product Chemistry*, 60, 223-297. https://doi.org/10.1016/B978-0-444-64181-6.00007-3

Baghaban-Eslaminejad, M., Oryan, A., Kamali, A., Moshiri, A. (2017). *Chapter 25 - The role of nanomedicine, nanotechnology, and nanostructures on oral bone healing, modeling, and remodeling*, In Micro and Nano Technologies, Nanostructures for Oral Medicine, Elsevier, 777-832, ISBN 9780323477208, https://doi.org/10.1016/B978-0-323-47720-8.00026-22

Brannon-Peppas, L. (1995). Recent advances on the use of biodegradable microparticles and nanoparticles in controlled drug delivery. *Int. J. Pharm.*, *116*, 1–9. https://doi.org/10.1016/0378-5173(94)00324-X

Corrêa-Filho, L. C., Moldão-Martins, M., Alves, V. D. (2019). Advances in the application of microcapsules as carriers of functional compounds for food products. *Applied Sciences, 9*, 571. https://doi.org/10.3390/app9030571

Corradini, E., Curti, P. S., Meniqueti, A. B., Martins, A. F., Rubira, A. F., Muniz, E. C. (2014). Recent advances in food-packing, pharmaceutical and biomedical applications of zein and zein-based materials. *International journal of molecular sciences*, *15*(12), 22438–22470. https://doi.org/10.3390/ijms151222438

De Jong, W. H. and Borm, P. J. (2008). Drug delivery and nanoparticles: applications and hazards. *International journal of nanomedicine*, *3*(2), 133–149. https://doi.org/10.2147/ijn.s596

Gumustas, M., Sengel-Turk, C.T., Gumustas, A., Ozkan, S.A., Uslu, B. (2017). Effect of polymer-based nanoparticles on the assay of antimicrobial drug delivery systems. In *Multifunctional Systems for Combined Delivery, Biosensing and Diagnostics*; Elsevier: Amsterdam, 67–108. https://doi.org/10.1016/B978-0-323-52725-5.00005-8

Guo, Y., Liu, Z., An, H., Li, M., and Hu, J .(2005). Nano-structure and properties of maize zein studied by atomic force microscopy. *Journal of Cereal Science*, 41(3), 277-281. https://doi.org/doi:10.1016/j.jcs.2004.12.005

Kumar, K., S., Kumar, B., V., Paik, P. (2013). Recent Advancement in Functional Core-Shell Nanoparticles of Polymers: Synthesis, Physical Properties, and Applications in Medical Biotechnology, *Journal of Nanoparticles* ,http://dx.doi.org/10.1155/2013/672059

Mączka, W., Twardawska, M., Grabarczyk, M., Wińska, K. (2023). Carvacrol-A Natural Phenolic Compound with Antimicrobial Properties. *Antibiotics (Basel, Switzerland)*, *12*(5), 824. https://doi.org/10.3390/antibiotics12050824

Misra, S., Pandey, P., Mishra, H. N. (2021). Novel approaches for co-encapsulation of probiotic bacteria with bioactive compounds, their health benefits and functional food product development: A review. *Trends in Food Science & Technology, 109*,340–351. https://doi.org/10.1016/j.tifs.2021.01.039

Muttaqien, S.E., Khoris, I.M., Pambudi, S., Park, E.Y. (2023). Nanosphere Structures Using Various Materials: A Strategy for Signal Amplification for Virus Sensing. *Sensors*, *23*, 160. https://doi.org/10.3390/s23010160

Patel, A. Velikov, K. (2014). Zein as a source of functional colloidal nano- and microstructures. *Current Opinion in Colloid & Interface Science*, 19, 450-458. https://doi.org/10.1016/j.cocis.2014.08.001

Pinto Reis C., Neufeld, R. J., Ribiero, A. J., Veiga, F. (2006). Nanomedicine Nanoencapsulation I. Methods for preparation of drug-loaded polymeric nanoparticles, Nanomedicine: Nanotechnology, Biology and Medicine, 2 (1), 8–21. https://doi.org/10.1016/j.nano.2005.12.003

Rahimnejad, M., Mokhtarian, N., and Ghasemi, M. (2009). Production of protein nanoparticles for food and drug delivery system. *African Journal of Biotechnology*, 8 (19), 4738-4743

Rajić, D., Spasojević, L., Gojković Cvjetković, V., Bučko, S., Fraj, J., Milinković Budinčić, J., Petrović, L., Pilić, B., Sharipova, A., Babayev, A., Aidarova, S., Katona, J. (2021). Zein–resin composite nanoparticles with coencapsulated carvacrol. *Journal of Food Processing and Preservation*, 00, e15741. https://doi.org/10.1111/jfpp.15741

Reddy, N. and Rapisarda, M. (2021). Properties and Applications of Nanoparticles from Plant Proteins. *Materials*,*14*, 3607. https://doi.org/10.3390/ma14133607

Soppimath, K.S., Aminabhavi, T.M., Kulkarni, A.R., and Rudzinski, W.E. (2001). Biodegradable polymeric nanoparticles as drug delivery devices. *J. Control. Release*, *70*, 1–20. https://doi.org/10.1016/S0168-3659(00)00339-4

Spasojević, Lj., Bučko, S., Kovačević, D., Bohinc, K., Jukić, J., Abram, A., Požar, J., and Katona, J. (2020). Interactions of zein and zein/rosin nanoparticles with natural polyanion gum arabic, *Colloids and Surfaces B: Biointerfaces*, 196, https://doi.org/10.1016/j.colsurfb.2020.111289

Tarone, A. G., Cazarin, C. B. B., & Junior, M. R. M. (2020). Anthocyanins: New techniques and challenges in microencapsulation. *Food Research International, 133*, 109092. https://doi.org/10.1016/j.foodres.2020.109092

Tiwari A., Tripathi A.K., and Khare P. (2021). A comprehensive study of synthesis and applications of core/shell nanoparticles. I*nternational Journal of Engineering, Science and Technology, 13(1),* 153-157. https://doi.org/10.4314/ijest.v13i1.23S

Weber, C., Coester, C., Kreuter, J., and Langer, K. (2000). Desolvation process and surface characterisation of protein nanoparticles. *International journal of pharmaceutics*, *194*(1), 91–102. https://doi.org/10.1016/s0378-5173(99)00370-1

Yadav, A. S., Tran, D. T., Teo, A. J. T., Dai, Y., Galogahi, F. M., Ooi, C. H., Nguyen, N.T. (2023). Core–Shell Particles: From Fabrication Methods to Diverse Manipulation Techniques. *Micromachines*, *14*(3), 497. https://doi.org/10.3390/mi14030497

Summary/Sažetak

Kompozitne mikro- i nanokapsule napravljene od prirodnih proteina se sve više koriste za razne primjene isporuke bioaktivnih jedinjenja zbog svoje svestrane prirode i sposobnosti da nose širok spektar molekula. Kapsule jezgro-ljuska i matričnog tipa imaju značaj u različitim sektorima, od farmaceutske do prehrambene tehnologije. Široka upotreba je posljedica njihove efikasnosti inkapsulacije i svojstava kontrolisanog oslobađanja. Ovaj rad pruža fizičko-morfološku karakterizaciju i prezentaciju pripreme čestica dobijenih od kukuruznog proteina-zeina kao nosača, sa akcentom na stabilnost dobijenog proizvoda. Karvakrol je uzet kao bioaktivno jedinjenje u ovom radu zbog svog snažnog antimikrobnog dejstva na mnoge različite sojeve bakterija i gljivica. Utvrđeno je da su Pikering emulzije pripremljene kao 10% U/V emulzija sa 15% GA sa odnosom Z:O=1:1,5 i odnosom Z:OSA skroba=1:1 i 20% karvakrola na suvu materiju bile najpogodnije za pripremu suvih kapsula. Analiza nanokapsula matričnog tipa sa 10% enkapsuliranog karvakrola pokazala je da su čestice sfernog oblika sa glatkom površinom i da se mogu uspešno osušiti i pripremiti u toj formulaciji.

Glasnik hemičara i tehnologa Bosne i Hercegovine

Bulletin of the Chemists and Technologists of Bosnia and Herzegovina

2026

66

Print ISSN: 0367-4444
Online ISSN: 2232-7266

Original Scientific Article
DOI: 10.35666/2232-7266.2025.66.07
UDK: 547.913:541.1

57-66

Antioxidant and Antibacterial Activity of Essential Oil of *Syzygium aromaticum* (L.) Merr. & L. M. Perry and its Application as Eco-Friendly Copper Corrosion Inhibitor

Horozić, E.[a], Marčetić, M.[b], Zdravković, M.[c], Tasić, G.[b], Grekulović, V.[c], Mekić, L.[d], Huseinović, E.[e], Dedić, J.[e], Cipurković, S.[e], Šehić, M.[e]

[a]*Faculty of Technology, University of Tuzla, Urfeta Vejzagića 8, Tuzla 75000, Bosnia and Herzegovina*

[b]*Faculty of Pharmacy, University of Belgrade, Vojvode Stepe 450, Belgrade 11221, Serbia*

[c]*Technical Faculty in Bor, University of Belgrade, Vojske Jugoslavije 12, Bor 19210, Serbia*

[d]*Faculty of Pharmacy, University of Tuzla, Urfeta Vejzagića 8, Tuzla 75000, Bosnia and Herzegovina*

[e]*Faculty of Sciences, University of Tuzla, Urfeta Vejzagića 4, Tuzla 75000, Bosnia and Herzegovina*

Article info
Received: 03/11/2025
Accepted: 12/03/2026

Keywords:
clove,
hydrodistillation,
GC-FID/MS analysis,
natural antioxidants,
ecoinhibitor

Emir Horozić
E-mail: emir.horozic@untz.ba
Phone: +387 61 026 160

Abstract: In this study, the essential oil of commercial clove (*Syzygium aromaticum* L. Merr. & L. M. Perry) was isolated. The chemical composition of the clove essential oil (CEO) was analyzed by GC-FID/MS. The reducing ability was analyzed by Ferric Reducing Antioxidant Power (FRAP) assay, while the free radical neutralization efficiency was tested by DPPH Radical Scavenging Assay. Antibacterial screening was analyzed on reference bacterial strains by diffusion test. The potential impact of CEO as a copper corrosion inhibitor was investigated by electrochemical frequency modulation (EFM), taking into account that compounds that have antibacterial and antioxidant effects also affect metal corrosion. GC-FID/MS analysis confirmed the high presence of eugenol (74.41%), (*Z*)-isoeugenol acetate (13.18%) and (*E*)-β-caryophyllene (10.60%) in CEO. The content of polyphenols is extremely high and correlates with the results of antioxidant activity. The essential oil was found to be highly effective in inhibiting the growth of the tested bacterial strains, at test concentrations of 40 and 80 mg/mL The inhibition zones of CEO were generally larger than those of the control antibiotics. The EFM results show that CEO acts as an effective inhibitor of copper corrosion in NaCl solution with a concentration of 0.5 mol/L, where it is adsorbed on the surface by physisorption according to the Langmuir adsorption isotherm.

INTRODUCTION

Aromatic plants have been an integral part of traditional medicine and culinary practices for centuries, largely due to their abundance of biologically active compounds. These plants exhibit a wide range of therapeutic properties, including antimicrobial, antioxidant, antiparasitic, antiprotozoal, antifungal, and anti-inflammatory activities (Christaki et al., 2012). Even today, a significant proportion of the global population relies on traditional herbal medicines for primary healthcare care. According to the World Health Organization, approximately 80% of people, predominantly in developing countries, use plant-derived medicines, and nearly 25% of modern pharmaceutical drugs are based on compounds originally obtained from plants or their synthetic analogs (Gurib-Fakim, 2006). The therapeutic efficacy of plants can be attributed to their ability to produce a wide variety of substances, collectively known as secondary metabolites. Historical records show that the use of medicinal plants dates back to around 2600 BC, and Mesopotamian texts document over 1000 plant-based remedies. Among the various applications of plant-derived compounds, aromatherapy has emerged as a popular complementary therapy. It uses essential oils, i.e. volatile

aromatic compounds extracted by various extraction techniques from different parts of plants such as flowers, bark, stems, leaves, roots and fruits. (Ghorbanpour et al., 2017). One such plant with extensive ethnomedicinal and commercial applications is *Syzygium aromaticum* (L.) Merr. & L.M. Perry, commonly known as clove. As a member of the Myrtaceae family, clove is used in food, medicine, nutraceuticals, and agriculture (Singletary, 2014). Traditionally, clove has been valued for its pungent, astringent flavor and health benefits, including enhanced circulation, improved digestion, and relief from gastrointestinal disorders (Dey & Mukherjee, 2021). Clove essential oil is rich in bioactive components, primarily eugenol, its most abundant constituent, along with chavibetol, β-caryophyllene, eugenyl acetate, and α-humulene (Otunola, 2022). Other notable phytochemicals include flavonoids such as kaempferol and quercetin and their derivatives, as well as phenolic acids such as caffeic, ferulic, ellagic, and salicylic acids. Minor constituents such as methyl salicylate, crategolic acid, and benzaldehyde contribute to the distinct aroma and therapeutic effects of cloves (Hussain et al., 2017).

In dentistry,clove is very popular for its analgesic properties, which is why it is used in many medicinal preparations (Daniel et al., 2009; Sachan et al., 2018). Essential oils and extracts of cloves show very high antioxidant activity *in vitro*, as well as dose dependent antimicrobial activity (Otunola, 2022). Cloves also possess significant antitumor activity, as reported in *in vitro* studies where they successfully inhibited tumor incidence in rats with mammary carcinoma (Kubatka et al., 2017). Gas Chromatography-mass Spectrometry (GC-MS) is a key analytical technique for the identification and quantification of essential oil components, especially for the assessment of their medicinal quality and bioactivity (Van Asten, 2002).

Previous studies investigating cloves as corrosion inhibitors have shown that clove flower extract (*Syzygium aromaticum*) acts as a corrosion inhibitor in neem biodiesel with an inhibition efficiency of 97.96% (Iyyappan et al., 2024). Aqueous extract of cloves acts as a corrosion inhibitor on carbon steel in the presence of four strains of corrosion-causing bacteria with an inhibition efficiency of about 87% (Parthipan et al., 2021). Clove essential oil also has a corrosion inhibitory effect on mild steel X70 in 1 mol/L hydrochloric acid with an inhibition efficiency of 99.33% at an inhibitor concentration of 1 g/L, for 2 hours of immersion (Adjal et al., 2023). Cu-DUP copper, which is high-purity copper (>=99.9% Cu) deoxidized with phosphorus, is often used for pipeline construction. Thus, this pipeline comes into contact with chloride ions due to the addition of chlorine to the water and due to contact with seawater, therefore its protection by applying corrosion inhibitors is very important (Zdravković et al., 2023). Based on the literature and the compounds present in clove essential oil, it can be assumed that this oil can act as an environmental inhibitor of copper corrosion under chloride conditions.

The aim of this study is to analyze the chemical composition of *Syzygium aromaticum* essential oil (CEO) by GC-MS and evaluate its antioxidant and antibacterial activities, as well as the potential use of CEO as an inhibitor of copper corrosion in chloride conditions using the electrochemical frequency modulation (EFM) method. The findings will contribute to a deeper understanding of the therapeutic potential of clove oil and support its application in the development of natural health products. Also, the results will enable the possibility of using CEO as an environmental inhibitor of copper corrosion in a 0.5 mol/L NaCl solution.

MATERIAL AND METHODS

The clove sample was purchased from a local market. Before hydrodistillation, the sample was crushed in an electric mill and immediately used for the isolation of the essential oil. Methanol, ethanol, glacial acetic acid, hydrochloric acid and sodium carbonate were purchased from Semikem (Bosnia and Herzegovina). Dimethyl sulfoxide (DMSO), 2,2-diphenyl-1-picrylhydrazyl (DPPH) and 2,4,6-tris(2-pyridyl)-s-triazine (TPTZ), were purchased from Sigma Chemical Co. (St. Louis, Missouri, USA). Folin-Ciocalteu reagent, iron (III) chloride hexahydrate and ascorbic acid were purchased from Merck (Darmstadt, Germany). Sodium chloride for electrochemical testing was purchased from Zorka Pharma (Šabac, Serbia). All chemicals used were of p.a. purity and were used as received, without any further purification.
All working solutions were prepared using demineralized water. An Agilent 6890 N GC system was used to determine the chemical composition of SEAO. Spectrophotometric measurements were performed on a Perkin Elmer Lambda 25 spectrophotometer. In the case of all spectrophotometric analyses, measurements were performed in triplicate, and the results were expressed as the mean value.

CEO preparation

Clove essential oil was isolated using a Clevenger apparatus. The crushed clove material (50 grams) was mixed with 1 liter of distilled water and heated for 5 hours. The obtained essential oil was separated, dried on anhydrous sodium sulfate and stored at -20°C until analysis. Yield: 2.94%

GC-FID/MS analysis

The volatile profile was determined by gas chromatography coupled to flame ionization detection and mass spectrometric analysis (GC-FID/MS). Measurements were performed on an Agilent 6890 N GC system with a 5975 mass selective detector and an FID, employing an HP-5 MS capillary column (30 m × 0.25 mm; 0.25 μm film thickness). Samples were introduced in an injection volume of 0.002 mL, with the injector maintained at 200°C and operating in split mode (10:1). Helium served as the carrier gas at a constant flow rate of 1.0 mL/min. Separation was achieved by a programmed oven temperature starting at 60°C and increasing to 280°C at 3°C/min, followed by a 5-minute isothermal period at the final temperature. The transfer line was maintained at 250°C, while the FID detector was operated at 300°C. Electron ionization mass spectra were recorded at 70 eV within the m/z interval of 35to 550. Experimental retention indices were calculated in relation to a homologous series of n-alkanes (C8–C40) analysed under the same chromatographic conditions. Component identification was based on matching retention index values and mass spectrum data with those of reference compounds, as well as with entries from the NIST AMDIS system, Wiley spectral libraries, the Adams database, and relevant literature sources. Quantitative composition was expressed as relative percentages derived from GC peak area normalization.

Analysis of total polyphenols content (TPC)

Total polyphenolic content of the CEO was quantified spectrophotometrically using the Folin–Ciocalteu assay,

following the procedure described by Singleton et al. (1999). For this purpose, an aliquot of CEO (0.2 mL) was mixed with 2.54 mL of 10% Folin–Ciocalteu reagent. After an incubation period of 5 min, 0.42 mL of 10% sodium carbonate was added. After 60 minutes incubation, 0.910 mL of distilled water was added. The absorbance of the resulting blue-colored solution was measured at 765 nm. The content of total polyphenols was expressed as gallic acid equivalent (GAE) in milligrams per gram of essential oil.

Analysis of antioxidant activity

Ferric Reducing Antioxidant Power (FRAP) Assay

The test of the reducing ability of the CEO was tested using the FRAP (ferric reducing antioxidant power) method, according to the published procedure (Benzie and Strain, 1999). The FRAP reagent (3 mL) was mixed with 0.1 mL of CEO, and the absorbance was recorded at 593 nm after incubation at 37°C for 30 min. The FRAP value was calculated from the calibration curve of iron (II) sulfate heptahydrate and expressed in μmol per gram of essential oil. Ascorbic acid was used as a comparator.

DPPH Radical Scavenging Assay

The DPPH radical neutralization assay was performed according to the published method (Horozić et al., 2019). CEO was mixed with absolute methanol and then mixed with a DPPH radical solution (0.5 mM). Absorbance measurements were performed at 517 nm, after which the DPPH radical inhibition was calculated according to the equation:

$$I = Ac - As / Ac \times 100\ [\%] \quad (1)$$

where As is the absorbance of the solution containing the sample at 517 nm, and Ac is the absorbance of the DPPH solution. Results are expressed as IC_{50} value. Ascorbic acid was used as a reference.

.

Analysis of antibacterial activity

Antimicrobial activity was tested on reference bacterial strains from the WDCM collection of Gram-positive and Gram-negative bacteria, as prescribed by the Clinical and Laboratory Standards Institute, 2009. Reference bacterial strains were cultivated overnight in brain heart infusion (BHI) broth at 37°C, aerobically. A 0.5 McFarland turbidity suspension (density of 10^7-10^8 CFU/mL) was prepared in a sterile physiological solution. The strains were then plated on the surface of Mueller-Hinton agar, which was poured into sterile 4 mm thick Petri dishes. 10 mm diameter wells were made in the agar and 0.1 mL of the essential oil was added to each well. After the dishes were left at room temperature for 15 minutes to allow the substance to diffuse into the agar, they were incubated at 37°C/24 hours. After incubation, the size of the inhibitory zone was measured. The concentration of CEO in this analysis was 40 and 80 mg/mL Amoxicillin/AMX (30 μg), Vancomycin/VAN (30 μg) and Imipenem/IMP (10 μg) antibiotic discs were used as controls.

Electrochemical Frequency Modulation (EFM)

The electrochemical frequency modulation (EFM) method was used to investigate the influence of CEO on the corrosion of copper - deoxidized high phosphorus (Cu-DHP) in a NaCl solution with a concentration of 0.5 mol/L. An electrochemical system with a three-electrode cell and a potentiostat (Gamry Interface 1010e potentiostat/galvanostat/ZRA, Gamry Instruments, USA) was used. The results obtained from the EFM modulation spectra were analyzed using Gamry Echem Analyst software package, Gamry Instruments, USA.

The experiments were performed at room temperature. The electrochemical cell consisted of three electrodes: a working electrode (Cu-DHP), a counter electrode (platinum), and a reference electrode (saturated calomel electrode, +0.244 V/SHE at 25°C). The working electrode was made of Cu-DHP sheet (99.97% Cu, 0.0198% P, and 0.0005% Pb), according to the procedure of Zdravković et al., 2023. NaCl solutions with a concentration of 0.5 mol/L without and with the addition of CEO (0.1-0.5 ppm) were used as electrolytes. The surface of the working electrode was polished using a polishing cloth with alumina slurry (particle size 0.3 μm), then washed with distilled water and ethanol.

The base frequency for the EFM experiments was 1 Hz, with frequencies of 2.0 and 5.0 Hz used. The number of cycles was 16. The inhibition efficiency (IE_{EFM}, %) was calculated according to the equation (Al-Mobarak et al., 2011):

$$IE_{EFM} = (1-j_{corr(inh)}/j_{corr}) \cdot 100 \quad (2)$$

where j_{corr} is the corrosion current density in the blank solution and $j_{corr(inh)}$ is the corrosion current density in the presence of CEO.

RESULTS AND DISCUSSION

Chemical composition

Table 1 shows the chemical composition of clove essential oil (CEO). Figure 1. shows the GC-FID total ion chromatogram (TIC) of the tested essential oil. The main compound in the investigated oil is phenylpropanoid eugenol (74.41%). The content of eugenol is slightly lower than the Pharmacopoeia given limit (75.0-88.0%) that defines the quality of herbal drugs and preparations such as essential oils (Ph. Eur.). The oil also contained significant amounts of (*Z*)-isoeugenol acetate (13.18%) and sesquiterpene (*E*)-β-caryophyllene (10.6%). The content of (*E*)-β-caryophyllene was within the Pharmacopoeia defined limits (5.0-14.0%). The Pharmacopoeia defines the eugenol acetate (4.0-15%) in clove oil (Ph. Eur.), and the investigated oil contained its isomer (Z)-isoeugenol acetate (13.18%). Isoeugenol acetate is usually present in low concentrations in clove oil (Jirovetz et al., 2066; Amelia et al., 2017) and is probably formed by isomerization of eugenol acetate during storage (Brock et al., 2024). Sesquiterpene α-humulene was present in low amount (1.17%) while the concentrations of other compounds were below 1%.

Table 1: The composition (%) of CEO

Component	RI	Composition (%)
3-octanol	967	0.05
6-methyl-heptan-2-ol	977	0.05
Methyl salicilate	1243	0.03
Chavicol	1306	0.12
Eugenol	1437	74.41
α-Copaene	1453	0.13
(*E*)-β-Caryophyllene	1506	10.60
α-Humulene	1544	1.17
(*E*,*E*)-α-Farnesene	1595	0.11
(*Z*)-Isoeugenol acetate	1613	13.18
Elemol acetate	1690	0.20

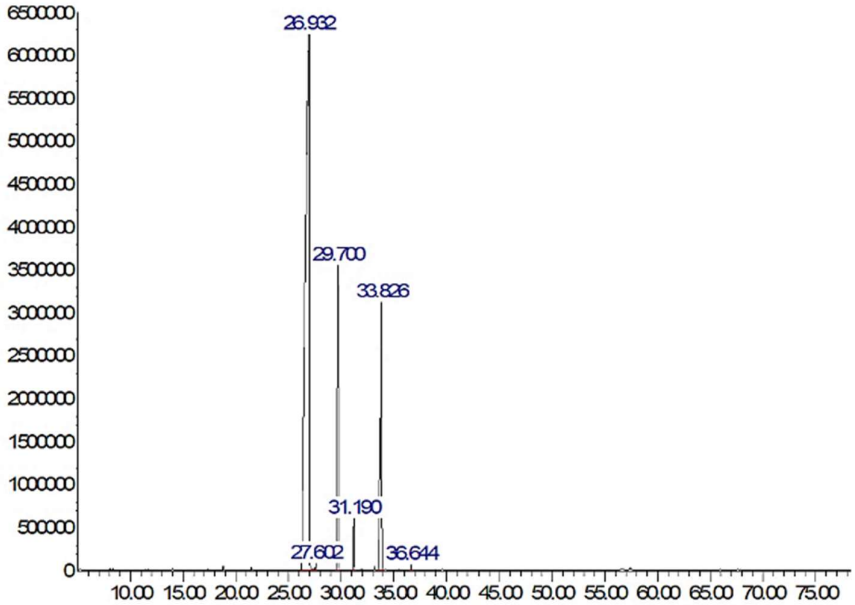

Figure 1: The GC- FID total ion chromatogram (TIC) of clove essential oil (CEO)

Total polyphenols content and antioxidant activity

The results of the total polyphenols content and antioxidant activity of the CEO are shown in Table 2. The total polyphenols content is extremely high (441.04 mg GAE/g of CEO). A review of previously published results of similar studies confirmed the high content of polyphenolic compounds in CEO (Sarrami et al., 2023; Das et al., 2024). The high reducing capacity and DPPH radical neutralization efficiency correlate with the high content of polyphenolic compounds in isolated CEO. Compared to ascorbic acid, which was used as a control, CEO showed a higher antioxidant capacity.

Table 2: Results of polyphenol content and antioxidant activity of CEO

Sample	TPC [mg GAE//g]	FRAP value [µmol/g]	DPPH IC_{50} value [mg/mL]
CEO	441.04	16220	0.005
Ascorbic acid	-	14250	0.030

Antibacterial activity

A total of six bacterial strains were tested in this study, including three Gram-positive strains (*Staphylococcus aureus*, *Listeria monocytogenes*, *Bacillus subtilis*) and three Gram-negative strains (*Salmonella enterica*, *Pseudomonas aeruginosa*, *Escherichia coli*). This classification allowed for a comparative evaluation of the antibacterial efficacy of *Syzygium aromaticum* essential oil against bacteria with distinct cell wall structures. The results showed significant growth inhibition in both groups, with certain strains showing larger inhibition zones compared to the tested control antibiotics (amoxicillin, vancomycin, and imipenem), which were used for comparison purposes. The antibacterial activity results of *S. aromaticum* essential oil are summarized in Table 3

Table 3: Results of antibacterial activity of CEO and control antibiotics

Reference strains	WDCM number	Inhibition zone [mm]				
		EO [80 mg/mL]	EO [40 mg/mL]	AMX [30 µg]	VAN [30 µg]	IPM [10 µg]
S. enterica	00030	30	26	21	n.t.	n.t.
P. aeruginosa	00025	20	18	n.t.	n.t.	20
E. coli	00012	35	31	20	n.t.	33
S. aureus	00034	27	22	33	20	n.t.
L. monocitogenes	00109	30	25	32	18	n.t.
B. subtilis	00003	30	26	14	n.t.	n.t.

*EO - essential oil; AMX - Amoxicillin; VAN - Vancomycin; IPM - Imipenem; n.t. - not tested

Both tested concentrations of the essential oil (40 mg/mL and 80 mg/mL) showed antibacterial activity against all isolates (*S. enterica, P. aeruginosa, E. coli, S. aureus, L. monocytogenes, B. subtilis*), showing moderate to high efficacy. Larger inhibition zones were observed at a higher concentration (80 mg/mL), with the largest zone recorded for the *E. coli* 00012 strain, consistent with the general principle that higher concentrations of bioactive substances usually result in enhanced effects.

As shown in Table 3, both concentrations of the essential oil demonstrated higher antibacterial activity against *S. enterica* 00030, *E. coli* 00012, and *B. subtilis* 00003 compared to amoxicillin. Imipenem, tested on *E. coli* 00012, showed a smaller inhibition zone compared to both essential oil concentrations. Moderate to high antibacterial activity was also observed against *P. aeruginosa, S. aureus,* and *L. monocytogenes*, with inhibition zones comparable to or slightly lower than those of the tested control antibiotics. *S. aureus* and *L. monocytogenes* showed larger inhibition zones in response to the essential oil compared to the control antibiotic vancomycin. According to standard criteria for evaluating the antibacterial potential of plant extracts, including essential oils, an inhibition zone of less than 10 mm indicates bacterial resistance, 10–15 mm indicates weak activity, 16–20 mm indicates moderate activity, and a zone of ≥20 mm indicates high antibacterial activity.

The main bioactive component of *S. aromaticum* essential oil is eugenol, responsible for most of its therapeutic properties, including its antibacterial effect. Numerous studies consistently confirm the antibacterial potential of this essential oil (Selles et al., 2020; Wadi et al., 2025; Valarezo et al., 2025; Maggini et al., 2024).
In a paper published by Teles et al. (2024), the antibacterial activity of clove essential oil was demonstrated against both Gram-positive and Gram-negative bacteria. It was observed that the antibacterial activity was stronger against gram-positive bacteria and that clove essential oil also had a stronger effect than eugenol alone, indicating that the biocomplex was responsible for the stronger inhibitory activity.

The authors of a review article (Maggini et al., 2024) suggested that the antimicrobial activity of EOs can be influenced by various factors: characteristics of the target microorganisms, temperature, pH, concentration of antimicrobial substances and the presence of organic matter. It was observed that the antimicrobial activity of *S. aromaticum* EO was twenty times higher at a temperature of 37°C. Since temperature affects the fluidity of the lipid layer of membrane, higher temperatures compromise membrane function and increase permeability, resulting in greater cell sensitivity to antimicrobial agents. Regarding the presence of organic material, the bactericidal activity of clove EO is preserved but reduced, which highlights its potential as an antimicrobial agent for external use, for example, in dentistry or for the treatment of skin problems.
The antibacterial mechanism of essential oils involves disruption of the cell membrane, resulting in loss of membrane stability, leakage of cell contents, and ultimately cell death. *S. aromaticum* essential oil has been shown to inhibit the growth of Gram-negative bacteria such as *Salmonella spp., Escherichia coli, Klebsiella pneumoniae, Pseudomonas aeruginosa,* and *Agrobacterium spp*., as well as Gram-positive bacteria, including *Streptococcus spp.* and *Staphylococcus aureus* (Haro-González et al., 2021), which confirms our findings.

Previous research by Hernández-Ochoa et al. (2014), Guran et al. (2015), Khaleque et al. (2016), and Teles et al. (2024) have shown that essential oils, including *S. aromaticum*, generally exhibit stronger inhibitory effects on Gram-positive bacteria compared to Gram-negative bacteria. This is explained by the structural differences in the bacterial cell wall: Gram-positive bacteria possess a thick peptidoglycan layer that is directly accessible to essential oils, while the outer membrane of Gram-negative bacteria, rich in lipopolysaccharides, restricts the passage of hydrophobic molecules, reducing their susceptibility. Our results are consistent with these observations, showing strong antibacterial activity against Gram-positive strains, as well as significant activity against Gram-negative strains.
According to a study published in 2025 (El-Wehedy et al., 2025), the essential oil of *S. aromaticum* showed significant antibacterial activity against multidrug-resistant bacterial strains, such as *P. aeruginosa*, indicating its potential as one of the possible candidates for the development of new plant-based antibacterial drugs. In our study, *S. aromaticum* essential oil showed moderate antibacterial activity against *P. aeruginosa*. Beta-lactamase-producing strains, including *P. aeruginosa* and *E. coli*, showed high inhibition zones when tested with this essential oil (Mejía-Argueta et al., 2020).

Gram-positive bacteria such as *L. monocytogenes, S. aureus,* and *B. subtilis* are common causes of food spoilage. The use of *S. aromaticum* essential oil as a natural preservative is supported by its potent antimicrobial and antifungal activity. The primary bacteria investigated in this context included *Listeria monocytogenes, Escherichia coli, Staphylococcus aureus, and Bacillus cereus* (Valarezo et al., 2025), where high inhibition zones were observed, which is consistent with the findings of our study.

Electrochemical Frequency Modulation (EFM)

The EFM method was used to determine corrosion parameters in an electrochemical system where a basic solution of 0.5 mol/L NaCl and solutions with CEO added (50 ppm - 300 ppm) , were used as electrolytes. All experiments were carried out in a Faraday cage at room temperature. The results are presented as intermodulation spectra for the electrolyte without the CEO (Figure 3), for electrolytes with the addition of 50 ppm CEO (Figure 4), 100 ppm CEO (Figure 5), 150 ppm CEO (Figure 6) and 300 ppm CEO (Figure 7).

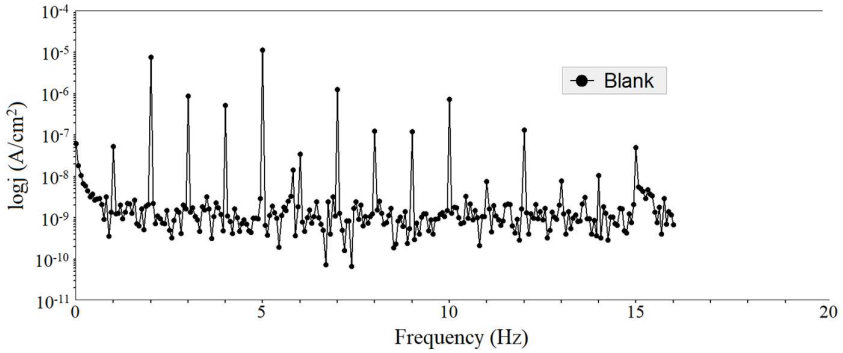

Figure 3: Intermodulation spectrum for Cu-DHP in 0.5 mol/L NaCl electrolyte (blank solution)

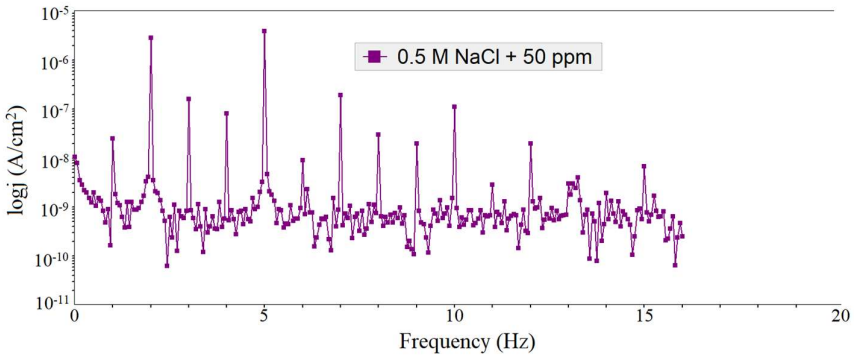

Figure 4: Intermodulation spectrum for Cu-DHP in 0.5 mol/L NaCl electrolyte with added 50 ppm CEO

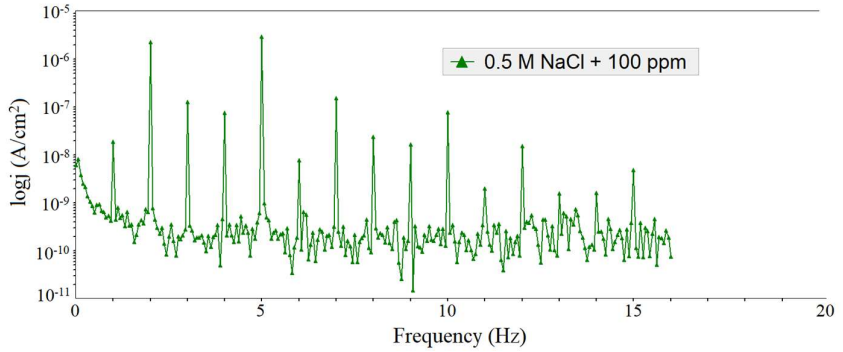

Figure 5: Intermodulation spectrum for Cu-DHP in 0.5 mol/L NaCl electrolyte with added 100 ppm CEO

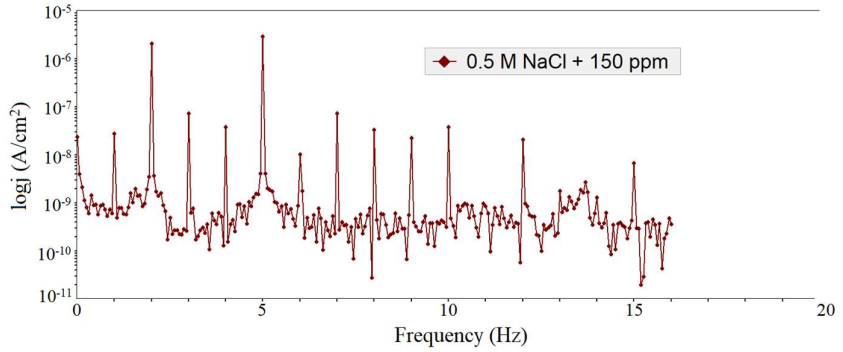

Figure 6: Intermodulation spectrum for Cu-DHP in 0.5 mol/L NaCl electrolyte with added 150 ppm CEO

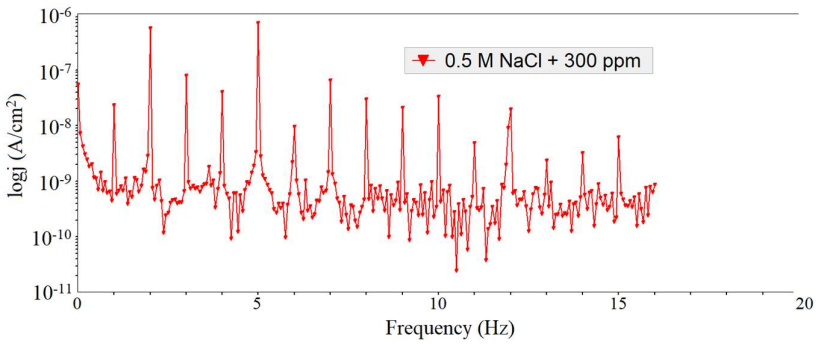

Figure 7: Intermodulation spectrum for Cu-DHP in 0.5 mol/L NaCl electro lyte with added 300 ppm CEO

Using electrochemical software, the adjusted results were used to obtain EFM electrochemical parameters (Table 4). The values of corrosion current (j_{corr}), anodic Tafel slope (β_1), cathodic Tafel slope (β_2), causal factors (CF2 and CF3), corrosion rate (CR) were obtained, while the percentage values of inhibitor efficiency (IE_{EFM}) were calculated using the equation (2). The value of the corrosion current density decreases significantly when CEO is added to the electrolyte, and this decrease is greater with increasing CEO concentration (Zdravković et. al, 2023; Fouda and Wahed, 2016). At the highest concentration, CEO acts as a mixed type of copper corrosion inhibitor in the tested electrolyte, while at lower concentrations it acts as a dominant cathodic corrosion inhibitor (El-Haddad, 2013). The values of the parameters CF2 and CF3 correspond to the theoretical values and the reviewed literature (El-Haddad, 2013; Fouda and Wahed, 2016). The corrosion rate and percent inhibition efficiency increase with increasing CEO concentration (Khaled, 2008). The highest effectiveness (97.06%) of the tested oil as an inhibitor of copper corrosion is achieved with the addition of 300 ppm CEO. Based on the comparison with the results of experiments where copper corrosion inhibitors were tested using the same method, it can be concluded that the tested clove oil has a significant effect on reducing copper corrosion in chloride conditions (El-Haddad, 2013). The effect of CEO can be explained by the compounds present in the oil. The high content of eugenol in CEO may indicate the effect of this oil as an inhibitor of copper corrosion, considering that eugenol has been shown to be an inhibitor of copper corrosion in chloride solution (Samontha and Lugsanangarm, 2019). CEO also contains (*Z*)-isoeugenol acetate, (*E*)-β-caryophyllene and α-humulene, where isoeugenol acetate was found in the *Cupressus sempervirens* L. extract, which acts as an inhibitor of copper corrosion (Dahmani et al., 2023), and α-humulene was found in the essential oil extracted from *Moroccan Salvia officinalis L.*, which acts as an aluminum corrosion inhibitor in a 3% NaCl solution (Belcadi et al., 2023). Also, it is common for substances that have an antibacterial effect to also act as metal corrosion inhibitors (Feng et al., 2020). Pipelines are often exposed to corrosion caused by the presence of bacteria, so as Cu-DHP is used for the construction of pipelines, it is important to test the antibacterial effect of the corrosion inhibitors (Javed et al., 2016). In addition, research shows that the positive effect of plants as corrosion inhibitors has an antioxidant effect, with moringa leaf extract and bitter leaf lxtract being shown to be ecological inhibitors of oil and gas pipelines, which have a high antioxidant effect (Ogboro et al., 2025). In this case, the antibacterial and antioxidant effect of CEO gives positive indications for the protection of copper pipes themselves, in addition to the aforementioned protection against chloride ions, which means that is possible to apply CEO in industries where pipelines made of copper come into contact with chloride ions, especially with seawater solutions.

Table 4: Electrochemical parameters obtained by EFM measurements for copper in sodium chloride electrolyte in the presence and absence of CEO

C_{inh} [ppm]	j_{corr} [μA/cm²]	β_1 [mV/dec]	β_2 [mV/dec]	CF-2	CF-3	CR [mpy]	IE_{EFM} [%]
0	20.93	66.71	193.6	1.72	2.85	159.8	-
50	7.720	84.33	137.1	1.83	2.95	58.95	63.12
100	5.949	83.42	163.8	1.82	2.95	45.43	71.56
150	4.391	72.66	89.19	1.91	3.10	33.53	79.02
300	0.61	36.74	58.15	1.96	2.98	12.54	97.06

Adsorption of CEO on copper surface

When determining the adsorption method of CEO molecules on the copper surface in chloride conditions, it was determined that the electrochemical results correspond best to the Langmuir adsorption isotherm (Zdravković et al., 2024). The IE_{EFM} data from Table 4 were used to form the adsorption isotherm, whereby the value of the degree of surface coverage (θ) was obtained as the ratio of $IE_{EFM}/100$ (Miralrio and V´azquez, 2020). This parameter, in combination with the inhibitor concentration, was used to plot the Langmuir adsorption isotherm graph (Figure 8) and in the formula (Zdravković et al., 2023):

$$\frac{C_{inh}}{\theta} = C + \left(\frac{1}{K_{ads}}\right)$$

where C_{inh} is inhibitor concentration and K_{ads} is the equilibrium constant.

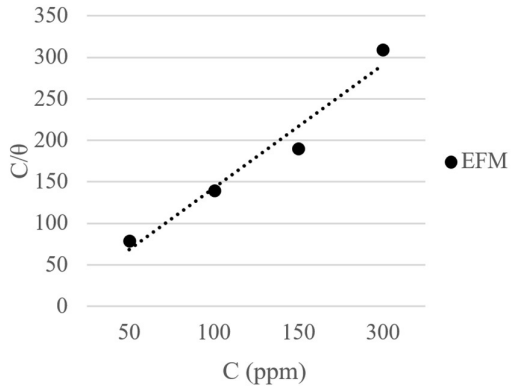

Figure 8: Langmuir adsorption isotherm for an electrochemical system with copper and electrolyte 0.5 mol/L NaCl with added CEO

The regression equation was obtained by fitting the results to the graph:

$$y = 0.8789 \cdot x + 44.66225, R^2 = 0.99057$$

The regression equation obtained by fitting with Langmuir model has a slope of 0.8789, and this deviation from 1 is the result of interactions between adsorbates or the average number of sites occupied by one adsorbed inhibitor molecule or the number of adsorbed water molecules displaced from the surface by one adsorbed inhibitor molecule (Kokalj et al., 2023).The high value of the correlation coefficient (R^2) clearly confirms that the adsorption takes place according to the Langmuir adsorption isotherm, which means that each adsorbed molecule occupies one free place on the copper surface and does not interact with other adsorbed compounds (Vaszilcsin et al., 2023). Another significant parameter that describes the CEO adsorption process on the copper surface in detail is the Gibbs free energy of adsorption (ΔG°_{ads}), which was calculated using the equation (Walczak et al., 2019; Mas'ud et al., 2020):

$$\Delta G^{\circ}_{ads} = -RTln(55.5K_{ads})$$

where R is the universal gas constant (J/mol·K), T is absolute temperature (K) and 55.5 is molar concentration of water. Based on the intercept from the regression equation, the value of K_{ads} was obtained. The obtained value for K_{ads} was 0.0224 dm^3/mol and ΔG°_{ads} was -533 J/mol. The obtained negative value of ΔG°_{ads} has a smaller value of -20 kJ/mol which indicates the spontaneous physisorption of CEO molecules on the copper surface in a NaCl solution of 0.5 mol/L, whereby a protective film is formed that protects the copper surface from the negative influence of chloride ions (Othman et al., 2025; Vaszilcsin et al., 2023; Zdravković et al., 2023; Khaled, 2008). Earlier research shows that under chloride conditions, eugenol is adsorbed by physisorption according to the Fremkin adsorption isotherm (Samontha and Lugsanangarm, 2019). Based on the large presence of eugenol in CEO and adsorption according to the Langmuir adsorption isotherm, it can be concluded that the influence of copper inhibition by the application of CEO is influenced by other substances present in the oil besides to eugenol.

CONCLUSION

Commercial clove essential oil of isolated by hydrodistillation shows high efficiency in neutralizing DPPH radicals and high reducing capacity. The results of the content of polyphenolic compounds correlate with antioxidative capacity. SEAO was also confirmed to have extremely high efficiency in inhibiting the growth of reference bacterial strains from the WDCM collection. The obtained results indicate that essential oil of cloves is a good candidate for further studies in terms of its broad biological activities. Using Electrochemical Frequency Modulation (EFM), CEO was found to act as a highly effective copper corrosion inhibitor in a solution containing 0.5 mol/L NaCl, with a maximum efficiency of 97.06% at 300 ppm CEO. Its action as a corrosion inhibitor is reflected in physical adsorption on the copper surface, where the adsorption takes place spontaneously according to the Langmuir adsorption isotherm. In this way, a barrier is created that prevents the corrosive action of chloride ions and reduces the copper corrosion process. Considering the identified composition of CEO and the reviewed literature, it is assumed that eugenol has the most dominant influence on the inhibition of copper corrosion, but that the other compounds present also have an influence. In addition to the fact that a high inhibitor efficiency value is achieved at a low inhibitor concentration, the novelty of this work is that this oil is tested for the first time as an inhibitor of Cu-DHP corrosion under chloride conditions, with the results corresponding to the antibacterial and antioxidant effects of CEO, which confirms that the higher the antioxidant and antibacterial effect, the better it acts as a corrosion inhibitor.

REFERENCES

Adams, R. P. (2007). Identification of Essential Oil Components by Gas Chromatography/Mass Spectroscopy. Allured Publishing Corp., Carol Stream.

Adjal, F., Menasra, H., Bouabdallah, IA., Chagra, K., Almi, S. (2023). Physicochemical properties, antibacterial activity, and corrosion inhibition of clove (*Syzygium aromaticum* L.) essential oil. *Journal of Survey in Fisheries Sciences*, *10(3)*, 610-617.

Al-Mobarak, N. A., Khaled, K. F., Hamed, M. N., Abdel-Azim, K. M. (2011). Employing electrochemical frequency modulation for studying corrosion and corrosion inhibition of copper in sodium chloride solutions, *Arabian Journal of Chemistry*, *4(2)*, 185-193.

Amelia, B., Saepudin, E., Cahyana, A. H., Rahayu, D. U., Sulistyoningrum, A. S., Haib. (2017). JGC-MS analysis of clove (*Syzygium aromaticum*) bud essential oil from Java and Manado. *AIP Conference Proceedings, 1862*, 030082.

Belcadi, H., Chraka, A., El Amrani, S., Raissouni, I., Moukhles, A., Zantar, S., Toukour, L., Mansour, AI. (2023). Investigation and valorization of the moroccan *Salvia officinalis* L. essential oil: Phytochemistry, potential in corrosion inhibition, antibacterial activity, and theoretical modeling. *Journal of Bio-and Tribo-Corrosion*, *9(3)*, 50.

Benzie, IFF., Strain, JJ. (1999). Ferric reducing/antioxidant power assay: direct measure of total antioxidant activity of biological fluids and modified version for simultaneous measurement of total antioxidant power and ascorbic acid concentration. *Methods in Enzymology*, *299*, 15-27.

Brock, W. J., Greene, T., Van Landingham, C., Gentry, R. (2024). A weight of evidence evaluation of the mode of action of isoeugenol. *Regulatory Toxicology and Pharmacology, 150*, 105642.

Christaki, E., Bonos, E., Giannenas, I. Florou-Paneri, P. (2012). Aromatic plants as a source of bioactive compounds. *Agriculture*, *2(3)*, 228-243.

Dahmani, K., Galai, M., Ech-Chebab, A., Al-Zaqri, N., Ouakki, M., Elgendy, A., Ez-Zriouli, R., Kim, S. C., Touhami, M. E., Cherkaoui, M. (2023). Investigating the inhibitory properties of *Cupressus sempervirens* extract against copper corrosion in 0.5 M H_2SO_4: combining quantum (density functional theory calculation–monte carlo simulation) and electrochemical-surface studies. *ACS Omega*, *8(27)*, 24218-24232.

Daniel, A. N., Sartoretto, S. M., Schmidt, G., Caparroz-Assef, S. M., BersaniAmado, C. A., Cuman, R. K. N. (2009). Anti-inflammatory and Antinociceptive Activities A of Eugenol Essential Oil in Experimental Animal Models. *Revista Brasileira de Farmacognosia*, *19*, 212-217.

Das, J. K., Chatterjee, N., Nanda, P. K., Das, A., Nath, S., Pal, S., et al. (2024). Encapsulation and Delivery of Clove Essential Oil Using Nanoemulsions: Impact on the Physicochemical, Microbial, and Sensory Properties of Chicken Meatballs. *Food Biophysics*, *19*, 701-716.

de Souza, FS., Spinelli, A. (2009). Caffeic acid as a green corrosion inhibitor for mild steel. *Corrosion Science*, *51(3)*, 642-649.

Dey, B. K., Mukherjee, S. S. (2021). Potential of Clove and its Nutritional Benefits in Physiological Perspective: A Review. *International Journal of Physiology, Nutrition and Physical Education*, *6(1),* 103-106.

El-Haddad, M.N. (2013). Chitosan as a green inhibitor for copper corrosion in acidic medium. *International Journal of Biological Macromolecules*, *55*, 142-149.

El-Wehedy, E., El-Sharkawy, H., El-Diasty, E.M., El-Wakeel, S. A., Abdelrahman, M. A., & Mahmoud, R. M. (2025). Contamination of meat and its products by *Pseudomonas* species and assessment of the antibacterial effect of clove (*Syzygium aromaticum*) essential oil on multidrug-resistant *P. aeruginosa*. *Open Veterinary Journal, 15(4)*, 412-420.

European Pharmacopoeia (10th edition). (2019). Strasbourg, France: Cauncil of Europe, 1396-1397.

Feng, L., Zhang, S., Tao, B., Tan, B., Xiang, B., Tian, W., Chen, S. (2020). Two novel drugs as bio-functional inhibitors for copper performing excellent anticorrosion and antibacterial properties. *Colloids and Surfaces B: Biointerfaces*, *190*, 110898.

Fouda, A. S., Wahed, H. A. (2016). Corrosion inhibition of copper in HNO_3 solution using thiophene and its derivatives. *Arabian Journal of Chemistry*, *9*, S91-S99.

Ghorbanpour, M., Hadian, J., Nikabadi, S., Varma, A. (2017). Importance of medicinal and aromatic plants in human life. In Ghorbanpour, M., Varma, A. (Eds), *Medicinal plants and environmental challenges.* (p.p. 1-23). Cham: Springer International Publishing.

Guran, H. S., Oksuztepe, G., Coban, O. E., & Incili, G. K. (2015). Influence of different essential oils on refrigerated fish patties produced from bonito fish (*Sarda sarda* Bloch, 1793). *Czech Journal of Food Sciences, 33*(1), 37-44.

Gurib-Fakim, A. (2006). Medicinal plants: traditions of yesterday and drugs of tomorrow. *Molecular aspects of Medicine*, *27(1)*, 1-93.

Haro-González, J. N., Castillo-Herrera, G. A., Martínez-Velázquez, M., & Espinosa-Andrews, H. (2021). Clove essential oil (*Syzygium aromaticum* L. Myrtaceae): Extraction, chemical composition, food applications, and essential bioactivity for human health. *Molecules, 26*(20), 6387.

Hernández-Ochoa, L., Aguirre-Prieto, Y. B., Nevárez-Moorillón, G. V., Gutierrez-Mendez, N., & Salas-Muñoz, E. (2014). Use of essential oils and extracts from spices in meat protection. *Journal of Food Science and Technology, 51*(5), 957-963.

Horozić, E., Zukić, A., Kolarević, L., Bjelošević, D., Ademović, Z., Šarić-Kundalić, B., Husejnagić, D., Kudumović, A., Hamzić, S. (2019) Evaluation of antibacterial and antioxidant activity of methanol needle extracts of *Larix Decidua* Mill., *Picea Abies* (L.) H. Karst. and *Pinus Nigra* J. F. Arnold. *Technics Technologies Education Management*, *14(1)*, 14-19.

Hussain, S., Rahman, R., Mushtaq, A., Zerey-Belaskri, A. E. (2017). Clove: A Review of a Precious Species with Multiple Uses. *International Journal of Chemical and Biochemical Sciences*, *11*, 129-133.

Iyyappan, S., Vinod Kumar, KP., Ponram, P., Karthik, B. (2024). Exploring copper corrosion inhibition in value added neem biodiesel: Evaluation by traditional and machine learning approaches. *Industrial Crops and Products*, *219*, 119073.

Javed M. A, Neil W., Adam G., Wade S. A. (2016). Microbiologically influenced corrosion of copper and its alloys–a review, *Corrosion & Prevention*, 84, 1-4.

Jirovetz, L., Buchbauer, G., Stoilova, I., Stoyanova, A., Krastanov, A., Schmidt, E. (2006). Chemical Composition and Antioxidant Properties of Clove Leaf Essential Oil. *Journal of Agricultural and Food Chemistry*, *54*, 6303-6307.

Kokalj A. (2023). On the use of the Langmuir and other adsorption isotherms in corrosion inhibition, *Corrosion Science*, 217, 111112.

Khaled, K. F. (2008). Guanidine derivative as a new corrosion inhibitor for copper in 3% NaCl solution. *Materials Chemistry and Physics*. *112(1)*, 104-111.

Khaleque, M. A., Keya, C. A., Hasan, K. N., Hoque, M. M., Inatsu, Y., Bari, M. L. (2016). Use of cloves and cinnamon essential oil to inactivate *Listeria monocytogenes* in ground beef at freezing and refrigeration temperatures. *LWT, 74*, 219-223.

Kubatka, P., Uramova, S., Kello, M., Kajo, K., Kruzliak, P., Mojzis, J., et al. (2017). Antineoplastic Effects of Clove Buds (*Syzygium Aromaticum* L.) in the Model of Breast Carcinoma. *Journal of Cellular and Molecular Medicine, 21(11)*, 2837-2851.

Maggini, V., Semenzato, G., Gallo, E., Nunziata, A., Fani, R., & Firenzuoli, F. (2024). Antimicrobial activity of *Syzygium aromaticum* essential oil in human health treatment. *Molecules, 29*(5), 999.

Mas'ud, Z. A., Darmawan, N., Dawolo, J., Apriliyanto, Y. B., (2020). Fatty Amidine as Copper Corrosion Inhibitor. *Journal of Chemistry*, *2020*, 1092643.

Mejía-Argueta, E. L., Santillán-Benítez, J. G., Canales-Martinez, M. M., Mendoza-Medellín, A. (2020). Antimicrobial activity of *Syzygium aromaticum* L. essential oil on extended-spectrum beta-lactamases-producing *Escherichia coli*. *Bulletin of the National Research Centre, 44*, 201.

Miralrio, A., V´azquez, A. E. (2020). Plant Extracts as Green Corrosion Inhibitors for Different Metal Surfaces and Corrosive Media: A Review. *Processes*, *8*, 942.

Ogboro, O. S., Uko S. A. (2025). Mitigating Corrosion in Oil Pipelines Using Moringa Leaf and Bitter Leaf Extracts as Eco-friendly Inhibitors. InSPE Nigeria Annual International Conference and Exhibition (p. D032S028R001). SPE.

Othman, K. A., Hamad, W. M., Omer, R. A. (2025). Theoretical and experimental exploration of organic molecules adsorption on iron surfaces for corrosion inhibition: A review. *Corrosion Reviews*, *43(3)*, 335-359.

Otunola, G. A., 2022. Culinary spices in food and medicine: an overview of *Syzygium aromaticum* (L.) Merr. and LM Perry [Myrtaceae]. *Frontiers in Pharmacology*, *12*, p.793200.

Parthipan, P., AlSalhi, MS., Devanesan, S., Rajasekar, A. (2021). Evaluation of *Syzygium aromaticum* aqueous extract as an eco-friendly inhibitor for microbiologically influenced corrosion of carbon steel in oil reservoir environment. *Bioprocess and Biosystems Engineering*, *44(7)*, 1441-1452.

Sachan, A. K., Kumar, S., Kumari, K., Singh, D. (2018). Medicinal Uses of Spices Used in Our Traditional Culture: World wide. *Journal of Medicinal Plants Studies*, *6(3)*, 116-122.

Samontha, A., Lugsanangarm, K. (2019). Corrosion inhibition and adsorption mechanism of eugenol on copper in HCl medium. *Protection of Metals and Physical Chemistry of Surfaces*, *55(1)*, 187-194.

Sarrami, S., Mohajeri, F. A., Sadeghizadeh-Yazdi, J., Jambarsang, S., Sadrabad, E. K. (2023). Chemical Composition and Antioxidant Activity of Clove Essential Oil and its Effect on Stability of Sesame Oil under Accelerated Condition. *Journal of Nutrition and Food Security*, *8(3)*, 343-352.

Selles, S. M. A., da Silva, L. R., Oliveira, F., et al. (2020). Chemical composition, *in vitro* antibacterial and antioxidant activities of clove (*Syzygium aromaticum*) essential oil. *Antioxidants, 9*(12), 1187.

Singletary, K. (2014). Clove: overview of potential health benefits. *Nutrition Today*, *49(4)*, 207-224.

Singleton, VL., Orthofer, R., Lamuela-Raventós, RM. (1999). Analysis of total phenols and other oxidation substrates and antioxidants by means of folin-ciocalteu reagent. *Methods in Enzymology*, *299*, 152-178.

Teles, A. M., Silva-Silva, J. V., Fernandes, J. M. P., Abreu-Silva, A. L., Calabrese, K. D. S., Mendes Filho, N. E., Mouchrek, A. N., & Almeida-Souza, F. (2021). GC-MS Characterization of Antibacterial, Antioxidant, and Antitrypanosomal Activity of *Syzygium aromaticum* Essential Oil and Eugenol. *Evidence-based complementary and alternative medicine*, 2021, 6663255.

Valarezo, E., Ledesma-Monteros, G., Jaramillo-Fierro, X., Radice, M., Meneses, M. A. (2025). Antimicrobial activity of clove (*Syzygium aromaticum*) essential oil in meat and meat products: A systematic review. *Antibiotics, 14*(5), 494.

Van Asten, A. (2002). The importance of GC and GC-MS in perfume analysis. *Trends in Analytical Chemistry*, *21(9-10)*, 698-708.

Vaszilcsin, C. G., Putz, M. V., Kellenberger, A., Dan, M. L. (2023). On the evaluation of metal-corrosion inhibitor interactions by adsorption isotherms. *Journal of Molecular Structure*, *1286*, 13564.

Wadi, M. A., Ahmed, S., Al-Mahmoud, A., et al. (2025). Evaluation of antibacterial activity and chemical analysis of clove aqueous extracts (*Syzygium aromaticum*). *BMC Complementary Medicine and Therapies, 25*, 1.

Walczak, M.S., Morales-Gil, P., Lindsay, R. (2019). Determining Gibbs energies of adsorption from corrosion inhibition efficiencies: Is it a reliable approach? *Corrosion Science*, *155*, 182-185.

Zdravković, M., Grekulović, V., Suljagić, J., Stanković, D., Savić, S., Radovanović, M., Stamenković, U. (2023). Influence of blackberry leaf extract on the copper corrosion behaviour in 0.5 M NaCl. *Bioelectrochemistry*, *151*, 108401.

Zdravković, M., Grekulović, V., Suljagić, J., Štrbac, N., Marković, I., Gorgievski, M., Marković, M. (2024). The *Rubus fruticosus* Leaf Extract as an Eco-Friendly Copper Corrosion Inhibitor. *Protection of Metals and Physical Chemistry of Surfaces*, *60*, 544-553.

Summary/Sažetak

U ovoj studiji, izolovano je eterično ulje komercijalnog karanfilića (*Syzygium aromaticum* (L.) Merr. & L. M. Perry). Hemijski sastav eteričnog ulja klinčića (CEO) analiziran je GC-FID/MS metodom. Sposobnost redukcije analizirana je pomoću FRAP (Ferric Reducing Antioxidant Power) testa, dok je efikasnost neutralizacije slobodnih radikala testirana pomoću DPPH testa za uklanjanje slobodnih radikala. Antibakterijski skrining je ispitan na referentnim bakterijskim sojevima, korištenjem difuzijskog testa. Ispitivanje potencijalnog uticaja CEO kao inhibitora korozije bakra izvršeno je korištenjem elektrohemijske frekventne modulacije (EFM), uzimajući u obzir da jedinjenja koja imaju antibakterijski i antioksidativni učinak također imaju uticaj na koroziju metala. GC-FID/MS analiza potvrdila je visoku prisutnost eugenola (74,41%), (*Z*)-izoeugenol acetata (13,18%) i (*E*)-β-kariofilena (10,60%) u eteričnom ulju karanfilića. Sadržaj polifenola je izuzetno visok i korelira s rezultatima antioksidativne aktivnosti. Utvrđeno je da je eterično ulje veoma efikasno u inhibiranju rasta testiranih bakterijskih sojeva, pri testnim koncentracijama od 40 i 80 mg/mL. Zone inhibicije CEO bile su uglavnom veće od onih kod kontrolnih antibiotika. Rezultati EFM-a pokazuju da CEO djeluje kao efikasan inhibitor korozije bakra u 0,5 M rastvoru NaCl, gdje se adsorbira na površini fizisorpcijom prema Langmuirovom adsorpcionom izotermi.

INSTRUCTIONS FOR AUTHORS

GENERAL INFORMATION

Bulletin of the Chemists and Technologists of Bosnia and Herzegovina (Glasnik hemičara i tehnologa Bosne i Hercegovine) is a semiannual international journal publishing papers from all fields of chemistry and related disciplines.

Categories of Contributions

1. *Original Scientific Papers* – (about 10 typewritten pages) report original research which has not been published previously, except in a preliminary form. The paper should contain all the necessary information to enable reproducibility of the described work.
2. *Short Communications* – (about 5 typewritten pages) describing work that may be of a preliminary nature but which merits immediate publication.
3. *Notes* – (about 3 typewritten pages) report unpublished results of short, but complete, original research or describe original laboratory techniques.
4. *Reviews* – (about 30 typewritten pages) present a concise and critical survey of a specific research area. Generally, these are prepared by the invitation of the Editor.
5. *Book and Web Site Reviews* – (about 2 typewritten pages).
6. *Extended Abstracts* – (about 2 typewritten pages) of Lectures given at international meetings.

Reviewing the Manuscript

All contributors are evaluated according to the criteria of originality and quality of their scientific content, and only those deemed worthy will be accepted for publication. To facilitate the reviewing process, authors are encouraged to suggest three persons competent to review their manuscript. Such suggestions will be taken into consideration but not always accepted.

The Editor-In-Chief and Editors have the right to decline formal review of a manuscript when it is deemed that the manuscript is:

1. on a topic outside the scope of the Journal;
2. lacking technical merit;
3. of insufficient novelty for a wide international readership;
4. fragmentary and providing marginally incremental results; or
5. is poorly written.

Proofs

When a manuscript is ready for printing, the corresponding author will receive a PDF-formatted manuscript for proof reading, which should be returned to the journal within one week. Failure to do so will be taken as the authors are in agreement with any alteration which may have occurred during the preparation of the manuscript.

Copyright

Subscribers may reproduce tables of contents or prepare lists of articles including abstracts for internal circulation within their institutions. Permission of the Publisher is required for resale or distribution outside the institution and for all other derivative works, including compilations and translations.

Professional Ethics and Publication Policy

The journal expects the Editors, Referees and authors to adhere to the well-known standards of professional ethics. Authors are responsible for the factual accuracy of their contributions. Submission of the paper commits the author not to submit the same material elsewhere. Referees should act promptly. If certain circumstances preclude prompt attention to the manuscript at the time it is received, the non-received manuscript should be returned immediately to the Editor or the Referee should contact the Editor for possible delay of the report submission date. The Editor accepts full responsibility for his decisions on the manuscripts.

PREPARATION AND SUBMISSION OF MANUSCRIPT

Cover Letter

Manuscripts must be accompanied by a cover letter in which the type of the submitted manuscript. It should contain:

1. full name(s) of the author(s),
2. mailing address (address, phone and fax numbers, e-mail) of the author to whom correspondence should be addressed,
3. title of the paper (concise, without any abbreviations),
4. type of contribution,
5. a statement that the article is original and is currently not under consideration by any other journal or any other medium, including preprints, electronic journals and computer databases in the public domain, and
6. the names, full affiliation (department, institution, city and country), and
7. e-mail addresses of three potential Referees.

Contributors from Bosnia and Herzegovina should provide the name and full affiliation of at least one Referee from abroad.

Authors are fully encouraged to use ***Cover Letter Template*****.**

Manuscript preparation

The submitted articles must be prepared with Word for Windows. Manuscripts should be typed in English (either standard British or American English, but consistent throughout) with 1.5 spacing (12 points Times New Roman; Greek letters in the character font Symbol) in A4 format leaving 2.5 cm for margins. Authors are fully encouraged to use ***Manuscript Template***.

All contributions should be written in a style that addresses a wider audience than papers in more specialized journals. Manuscripts with grammar or vocabulary deficiencies are disadvantaged during the scientific review process and, even if accepted, may be returned to the author to be rewritten in idiomatic English. The authors are requested to seek the assistance of competent English language expert, if necessary, to ensure their English is of a reasonable standard. The journal maintains its policy and takes the liberty of correcting the English of manuscripts scientifically accepted for publication.

Tables and figures and/or schemes should not be embedded in the manuscript but their position in the text indicated. In electronic version (Word.doc document) tables and figures and/or schemes should follow the text, each on a separate page. Please number all pages of the manuscript including separate lists of references, tables and figures with their captions.

IUPAC and International Union of Biochemistry and Molecular Biology recommendations for the naming of compounds should be followed.

SI units, or other permissible units, should be employed. The designation of physical quantities should be in Times New Roman font. In text, graphs, and tables, brackets should be used to separate the designation of a physical quantity from the unit. Please do not use the axes of graphs for additional explanations; these should be mentioned in the figure captions and/or the manuscript (example: “pressure at the inlet of the system, kPa” should be avoided).

Percents and *per mills*, although not being units in the same sense as the units of dimensioned quantities, can be treated as such. Unit symbols should never be modified (for instance: w/w %, vol.%, mol.%) but the quantity measured has to be named, *e.g.* mass fraction, w=95 %; amount (mole) fraction, x=20 %.

Latin words, as well as the names of species, should be in *italic*, as for example: *i.e., e.g., in vivo, ibid, Artemisia annua* L., *etc*. The branching of organic compound should also be indicated in *italic*, for example, *n*-butanol, *tert*-butanol, *etc*.

Decimal numbers must have decimal points and not commas in the text (except in the Bosnian/Croatian/Serbian abstract), tables and axis labels in graphical presentations of results. Thousands are separated, if at all, by a comma and not a point.

Structure of the Manuscript

The manuscript must contain, each on a separate page, the title page, abstract in English, (abstract in Bosnian/Croatian/Serbian), graphical abstract (optional), main text, list of references, tables (each table separately), illustrations (each separately), and legends to illustrations (all on the same page).

1. ***Title page*** must contain: the title of the paper (bold letters), full name(s) of the author(s), full mailing addresses of all authors (italic), keywords (up to 6), the phone and fax numbers and the e-mail address of the corresponding author.
2. A one-paragraph ***abstract*** written of 150–200 words in an impersonal form indicating the aims of the work, the main results and conclusions should be given and clearly set off from the text. Domestic authors should also submit, on a separate page, a Summary/Sažetak. For authors outside Bosnia and Herzegovina, the Editorial Board will provide a Bosnian/Croatian/Serbian translation of their English abstract.
3. Authors are encouraged to submit a ***graphical abstract*** that describes the subject matter of the paper. It should contain the title of the paper, full name(s) of the author(s), and graphic that should be no larger than 11 cm wide by 5 cm tall. Authors are fully encouraged to use ***Graphical Abstract Template.***
4. ***Main text*** should have the following form:
   - ***Introduction***should include the aim of the research and a concise description of background information and related studies directly connected to the paper.
   - ***Experimental*** section should give the purity and source of all employed materials, as well as details of the instruments used. The employed methods should be described in sufficient detail to enable experienced persons to repeat them. Standard procedures should be referenced and only modifications described in detail.
   - ***Results and Discussion***should include concisely presented results and their significance discussed and compared to relevant literature data. The results and discussion may be combined or kept separate.
   - The inclusion of a ***Conclusion***section, which briefly summarizes the principal conclusions, is highly recommended.
   - ***Acknowledgement*** (optional).
   - Please ensure that every ***reference*** cited in the text is also present in the reference list (and *vice versa*). Unpublished results and personal communications are not recommended in the reference list, but may be mentioned in the text. If these references are included in the reference list they should follow the standard reference style of the journal and should include a substitution of the publication date with either "Unpublished results" or "Personal communication" Citation of a reference as "in press" implies that the item has been accepted for publication. As a minimum, the full URL should be given and the date when the reference was last accessed. Any further information, if known (DOI, author names, dates, reference to a source publication, etc.), should also be given. No more than 30 references should be cited in your manuscript.

     In the text refer to the author's name (without initials) and year of publication (e.g. "Steventon, Donald and Gladden (1994) studied the effects..." or "...similar to values reported by others (Anderson, Douglas, Morrison, *et al.*, 1990)..."). Type the names of the first three authors at first citation. At subsequent citations use first author *et al.* The list of references should be arranged alphabetically by

authors' names and should be as full as possible, listing all authors, the full title of articles and journals, publisher and year.

Examples of ***reference style***:

a) Reference to a journal publication:
Warren, J. J., Tronic, T. A., Mayer, J. M. (2010). Termochemistry of proton-coupled electron transfer reagents and its implications. *Chemical Reviews*, *110 (12)*, 6961-7001.

b) Reference to a book:
Corey, E. J., Kurti, L. (2010). *Enantioselective chemical synthesis*. (1st Ed.) Direct Book Publishing, LLC.

c) Reference to a chapter in an edited book:
Moody, J. R., Beck II, C. M. (1997). Sample preparation in analytical chemistry. In Setlle, F. A. (Ed.), *Handbook of instrumental techniques for analytical chemistry*. (p.p. 55-72). Prentice Hall.

d) Reference to a proceeding:
Seliskar, C. J., Heineman, W.R., Shi, Y., Slaterbeck, A.F., Aryal, S., Ridgway, T.H., Nevin, J.H. (1997). *New spectroelectrochemical sensor*, in Proceedings of 37th Conference of Analytical Chemistry in Energy and Technology, Gatlinburg, Tenesee, USA, p.p. 8-11.

e) Patents:
Healey, P.J., Wright, S.M., Viltro, L.J., (2004).*Method and apparatus for the selection of oral care chemistry*, The Procter & Gamble Company Intellectual Property Division, (No.US 2004/0018475 A1).

f) Chemical Abstracts:
Habeger, C. F., Linhart, R. V., Adair, J. H. (1995). Adhesion to model surfaces in a flow through system. *Chemical Abstracts,* CA 124:25135.

g) Standards:
ISO 4790:1992. (2008). *Glass-to-glass sealings - Determination of stresses*.

h) Websites:
Chemical Abstract Service, www.cas.org, (18/12/2010).

- ***Tables*** are part of the text but must be given on separate pages, together with their captions. The tables should be numbered consequently in Latin numbers. Quantities should be separated from units by brackets. Footnotes to tables, in size 10 font, are to be indicated consequently (line-by-line) in superscript letters. Tables should be prepared with the aid of the Word table function, without vertical lines. Table columns must not be formatted using multiple spaces. Table rows must not be formatted using Carriage returns (enter key; ↵ key). Tables should not be incorporated as graphical objects.
- ***Figures and/or Schemes*** (in high resolution) should follow the captions, each on a separate page of the manuscript. High resolution illustrations in TIF or EPS format (JPG format is acceptable for colour and greyscale photos, only) must be uploaded as a separate archived (.zip or .rar) file.

Figures and/or Schemes should be prepared according to the artwork instructions.

- ***Mathematical and chemical equations*** must be numbered, Arabic numbers, consecutively in parenthesis at the end of the line. All equations should be embedded in the text except when they contain graphical elements (tables, figures, schemes and formulae). Complex equations (fractions, inegrals, matrix…) should be prepared with the aid of the Word Equation editor.

Artwork Instructions

Journal accepts only TIF or EPS formats, as well as JPEG format (only for colour and greyscale photographs) for electronic artwork and graphic files. MS files (Word, PowerPoint, Excel, Visio) are NOT acceptable. Generally, scanned instrument data sheets should be avoided. Authors are responsible for the quality of their submitted artwork.

Image quality: keep figures as simple as possible for clarity - avoid unnecessary complexity, colouring and excessive detail. Images should be of sufficient quality for the printed version, i.e. 300 dpi minimum.

Image size: illustrations should be submitted at its *final size* (8 cm for single column width or 17 cm for double column width) so that neither reduction nor enlargement is required.

Photographs: please provide either high quality digital images (250 dpi resolution) or original prints. Computer print-outs or photocopies will not reproduce well enough for publication. Colour photographs rarely reproduce satisfactorily in black and white.

The facility exist for color reproduction, however the inclusion of color photographs in a paper must be agreed with Editor in advance.

Reporting analytical and spectral data

The following is the recommended style for analytical and spectral data presentation:

1. ***Melting and boiling points***:
   mp 163–165°C (lit. 166°C)
   mp 180°C dec.
   bp 98°C
   Abbreviations: mp, melting point; bp, boiling point; lit., literature value; dec, decomposition.
2. ***Specific Rotation***:
   $[a]^{23}_{D}$ –222 (*c* 0.35, MeOH).
   Abbreviations: a, specific rotation; D, the sodium D line or wavelength of light used for determination; the superscript number, temperature (°C) at which the determination was made; In parentheses: *c* stands for concentration; the number following *c* is the concentration in grams per 100 mL; followed by the solvent name or formula.

3. ***NMR Spectroscopy***:
   ^{1}H NMR (500 MHz, DMSO-d_6) d 0.85 (s, 3H, CH_3), 1.28–1.65 (m, 8H, 4´CH_2), 4.36–4.55 (m, 2H, H-1 and H-2), 7.41 (d, *J* 8.2 Hz, 1H, ArH), 7.76 (dd, *J* 6.0, 8.2 Hz, 1H, H-1'), 8.09 (br s, 1H, NH).
   ^{13}C NMR (125 MHz, $CDCl_3$) d 12.0, 14.4, 23.7, 26.0, 30.2, 32.5, 40.6 (C-3), 47.4 (C-2'), 79.9, 82.1, 120.0 (C-7), 123.7 (C-5), 126.2 (C-4).
   Abbreviations: d, chemical shift in parts per million (ppm) downfield from the standard; *J*, coupling constant in hertz; multiplicities s, singlet; d, doublet; t, triplet; q, quartet; and br, broadened. Detailed peak assignments should not be made unless these are supported by definitive experiments such as isotopic labelling, DEPT, or two-dimensional NMR experiments.
4. ***IR Spectroscopy***:
   IR (KBr) n 3236, 2957, 2924, 1666, 1528, 1348, 1097, 743 cm^{-1}.
   Abbreviation: n, wavenumber of maximum absorption peaks in reciprocal centimetres.
5. ***Mass Spectrometry***:
   MS *m/z* (relative intensity): 305 (M^+H, 100), 128 (25).
   HRMS–FAB (*m/z*): $[M+H]^+$calcd for $C_{21}H_{38}N_4O_6$, 442.2791; found, 442.2782.
   Abbreviations: *m/z*, mass-to-charge ratio; M, molecular weight of the molecule itself; M^+, molecular ion; HRMS, high-resolution mass spectrometry; FAB, fast atom bombardment.
6. ***UV–Visible Spectroscopy***:
   UV (CH_3OH) l_{max} (log e) 220 (3.10), 425 nm (3.26).
   Abbreviations: l_{max}, wavelength of maximum absorption in nanometres; e, extinction coefficient.
7. ***Quantitative analysis***:
   Anal.calcd for $C_{17}H_{24}N_2O_3$: C 67.08, H 7.95, N 9.20. Found: C 66.82, H 7.83, N 9.16.All values are given in percentages.
8. ***Enzymes and catalytic proteins relevant data:***
   Papers reporting enzymes and catalytic proteins relevant data should include the identity of the enzymes/proteins, preparation and criteria of purity, assay conditions, methodology, activity, and any other information relevant to judging the reproducibility of the results[1]. For more details check Beilstein Institut/STRENDA (standards for reporting enzymology data) commission Web site (http://www.strenda.org/documents.html).

Submission Checklist

The following list will be useful during the final checking of an article prior to sending it to the journal
for review:

- E-mail address for corresponding author,

[1] For all other data presentation not mentioned above please contact Editor for instructions.

- Full postal address,
- Telephone and fax numbers,
- All figure captions,
- All tables (including title, description, footnotes),
- Manuscript has been "spellchecked" and "grammar-checked",
- References are in the correct format for the journal,
- All references mentioned in the Reference list are cited in the text, and *vice versa*.

Submissions

Submissions should be directed to the Editor by e-mail: ***glasnik@pmf.unsa.ba***, or ***glasnikhtbh@gmail.com***. All manuscripts will be acknowledged on receipt (by e-mail) and given a reference number, which should be quoted in all subsequent correspondence.

Glasnik hemičara i tehnologa Bosne i Hercegovine

Bulletin of the Chemists and Technologists of Bosnia and Herzegovina

Print ISSN: 0367-4444
Online ISSN: 2232-7266

Zmaja od Bosne 33-35, BA-Sarajevo
Bosnia and Herzegovina
Phone: +387-33-279-918
Fax: +387-33-649-359
E-mail: glasnik@pmf.unsa.ba
glasnikhtbh@gmail.com

Sponsors

Glasnik hemičara i tehnologa Bosne i Hercegovine

Bulletin of the Chemists and Technologists of Bosnia and Herzegovina

Print ISSN: 0367-4444
Online ISSN: 2232-7266

Zmaja od Bosne 33-35, BA-Sarajevo
Bosnia and Herzegovina
Phone: +387-33-279-918
Fax: +387-33-649-359
E-mail: glasnik@pmf.unsa.ba
glasnikhtbh@gmail.com